

SYNTHESIS AND DEVELOPMENT OF NANOCOMPOSITES OF MAGNETIC
NANOPARTICLES-SILICA-MANNAN AS VACCINE ADJUVANTS



A Dissertation Submitted in Partial Fulfillment of the Requirements
for the Degree of Doctor of Philosophy in Chemistry

Department of Chemistry

FACULTY OF SCIENCE

Chulalongkorn University

Academic Year 2019

Copyright of Chulalongkorn University

การสังเคราะห์และพัฒนานาโนคอมพอสิตของอนุภาคนาโนแม่เหล็ก-ซิลิกา-แมนแนนเพื่อเป็นสาร
เสริมฤทธิ์วัคซีน



วิทยานิพนธ์นี้เป็นส่วนหนึ่งของการศึกษาตามหลักสูตรปริญญาวิทยาศาสตรดุษฎีบัณฑิต
สาขาวิชาเคมี ภาควิชาเคมี
คณะวิทยาศาสตร์ จุฬาลงกรณ์มหาวิทยาลัย
ปีการศึกษา 2562
ลิขสิทธิ์ของจุฬาลงกรณ์มหาวิทยาลัย

Thesis Title	SYNTHESIS AND DEVELOPMENT OF NANOCOMPOSITES OF MAGNETIC NANOPARTICLES-SILICA-MANNAN AS VACCINE ADJUVANTS
By	Miss Kamonlatth Rodponthukwaji
Field of Study	Chemistry
Thesis Advisor	Assistant Professor Numpon Insin, Ph.D.
Thesis Co Advisor	Assistant Professor PATCHAREE RITPRAJAK, D.D.S., Ph.D.

Accepted by the FACULTY OF SCIENCE, Chulalongkorn University in Partial Fulfillment of the Requirement for the Doctor of Philosophy

..... Dean of the FACULTY OF SCIENCE
(Professor POLKIT SANGVANICH, Ph.D.)

DISSERTATION COMMITTEE

..... Chairman
(Associate Professor VUDHICHAJ PARASUK, Ph.D.)

..... Thesis Advisor
(Assistant Professor Numpon Insin, Ph.D.)

..... Thesis Co-Advisor
(Assistant Professor PATCHAREE RITPRAJAK, D.D.S., Ph.D.)

..... Examiner
(Assistant Professor PANUWAT PADUNGROS, Ph.D.)

..... Examiner
(Assistant Professor Pannee Leeladee, Ph.D.)

..... External Examiner
(Associate Professor Dakrong Pissuwan, Ph.D.)

กมลสิทธิ์ รอดพันทุกข์วชิ : การสังเคราะห์และพัฒนานาโนคอมพอสิตของอนุภาคนาโนแม่เหล็ก-ซิลิกา-แมนแนนเพื่อเป็นสารเสริมฤทธิ์วัคซีน. (SYNTHESIS AND DEVELOPMENT OF NANOCOMPOSITES OF MAGNETIC NANOPARTICLES-SILICA-MANNAN AS VACCINE ADJUVANTS) อ.ที่ปรึกษาหลัก : ผศ. ดร.นำพล อินสิน , อ.ที่ปรึกษาร่วม : ผศ.ทญ. ดร.พัชรี ฤทธิ์ประจักษ์

ในช่วงหลายปีที่ผ่านมาวัคซีนได้รับการพิจารณาว่าเป็นวิธีในการรักษาโรคต่าง ๆ ที่มีประสิทธิภาพ แต่อย่างไรก็ตามก็การรักษาโรคด้วยการฉีดวัคซีนนั้นยังมีข้อบกพร่อง เช่น การตอบสนองของระบบภูมิคุ้มกันยังไม่มีประสิทธิภาพที่ดีพอ ดังนั้น การพัฒนาวัคซีนโดยการกระตุ้นการทำงานของเซลล์ภูมิคุ้มกันด้วยวัสดุระดับนาโนเมตรที่ใช้เป็นสารเสริมฤทธิ์วัคซีนจึงเป็นวิธีที่น่าสนใจ ในงานนี้ได้นำอนุภาคแม่เหล็กที่มีสมบัติซูเปอร์พาราแมกเนติกมาใช้เป็นตัวนำส่งอนุภาคไปยังเซลล์เดนไดรติก นอกจากนี้สารแมนแนนที่สกัดได้จาก *Saccharomyces cerevisiae* ได้ถูกนำมาใช้เป็นตัวจับกับตัวรับบนผิวของเซลล์เดนไดรติก อนุภาคระดับนาโนคอมพอสิตของซิลิกา แม่เหล็กและแมนแนนได้ถูกสังเคราะห์ขึ้นและนำไปวิเคราะห์เอกลักษณ์ด้วยวิธีต่าง ๆ เช่น FESEM TEM XRD VSM และ ICP-OES นอกจากนี้อนุภาคนาโนคอมพอสิตที่สังเคราะห์ได้ถูกนำไปศึกษาสมบัติทางชีวภาพ เช่น ความเป็นพิษต่อเซลล์ การกระตุ้นการทำงานของเซลล์ การกระตุ้นการหลั่งสารสื่อของเซลล์ การนำเข้าสู่เซลล์ภายใต้การเหนี่ยวนำด้วยสนามแม่เหล็กภายนอก จากการศึกษาพบว่าประจุบนผิวของอนุภาคนาโนคอมพอสิตมีความเป็นบวกมากขึ้น แสดงว่าการดัดแปรพื้นผิวด้วยสารแมนแนนประสบผลสำเร็จ นอกจากนี้ ด้วยการทำงานร่วมกันของอนุภาคแม่เหล็กและแมนแนนทำให้การเหนี่ยวนำอนุภาคและการเข้าไปยังเซลล์เป้าหมายได้ดีอย่างเห็นได้ชัดภายในเวลา 15 นาที ดังนั้น จึงสรุปได้ว่าการทำงานร่วมกันของอนุภาคแม่เหล็กและแมนแนนสามารถกระตุ้นการทำงานของเซลล์เดนไดรติกได้อย่างมีประสิทธิภาพ ทำให้อนุภาคที่สังเคราะห์ได้จากงานวิจัยนี้เหมาะสมที่จะต่อยอดการศึกษาในระดับ *in vivo* ต่อไปเพื่อใช้เป็นสารเสริมฤทธิ์วัคซีน

สาขาวิชา เคมี
ปีการศึกษา 2562

ลายมือชื่อนิสิต
ลายมือชื่อ อ.ที่ปรึกษาหลัก
ลายมือชื่อ อ.ที่ปรึกษาร่วม

5972804323 : MAJOR CHEMISTRY

KEYWORD: Superparamagnetic nanoparticle, Silica, Mannan, Adjuvant, Dendritic cell
Kamonlatth Rodponthukwaji : SYNTHESIS AND DEVELOPMENT OF
NANOCOMPOSITES OF MAGNETIC NANOPARTICLES-SILICA-MANNAN AS VACCINE
ADJUVANTS. Advisor: Asst. Prof. Numpon Insin, Ph.D. Co-advisor: Asst. Prof.
PATCHAREE RITPRAJAK, D.D.S., Ph.D.

Over the past years, vaccination has been considered as an effective treatment against a wide range of pathogens and diseases. Despite a promising outcome, the lack of strong immune response of some types of vaccines is still challenging. Therefore, targeting and activating dendritic cells (DCs) using nanomaterial-based vaccine adjuvant is of our interest. Herein, superparamagnetic iron oxide nanoparticles (SPIONs) have been exploited as directing agents to the targeted dendritic cells (DCs). In addition, mannan extracted from *Saccharomyces cerevisiae* was used as targeting molecules for targeting DCs. Nanocomposites of silica-magnetic nanoparticles-mannan (S-SPION-MN) were successfully fabricated. The synthesized particles were morphologically and physically characterized using FESEM, TEM, XRD, VSM and ICP-OES techniques. For biological studies, the synthesized materials were determined for cytotoxicity, DC maturation, cytokine production, and cellular uptake. As a result, alteration in surface charge from highly negative charge to slightly negative charge suggested the successful coating of mannan on nanocomposite surfaces. Under a magnetic induction, S-SPION-MN showed great enhancement of DCs targeting within 15 min due to the synergistic effect of mannan and magnetic nanoparticles. The co-existence of SPIONs and mannan significantly facilitated the DCs targeting ability and maturation of DCs. As a result, the nanocomposites from this work can be beneficial for further development *in vivo* study as a potential candidate in antigen delivery to targeted immune cells.

Field of Study: Chemistry

Student's Signature

Academic Year: 2019

Advisor's Signature

Co-advisor's Signature

ACKNOWLEDGEMENTS

First of all, I would like to express my sincere gratitude to my advisor Assistant Professor Dr. Numpon Insin who kindly supported and provided me fruitful knowledge throughout my Ph.D. studying. His intellection, patience and generosity have motivated me in doing research. In addition, I also would like to deeply thank my co-advisor, Assistant Professor Dr. Patcharee Ritprajak for guiding me and providing me biological knowledge. Without her guidance, I would not have gained any experiences in biological study.

Besides, I would like to give special thanks to my thesis committee: Associate Professor Dr. Vudhichai Parasuk, Assistant Professor Dr. Dakrong Pissuwan, Assistant Professor Dr. Panuwat Padungros, and Dr. Pannee Leeladee for their insightful suggestion, kindness and encouragement.

Kamonlatth Rodponthukwaji

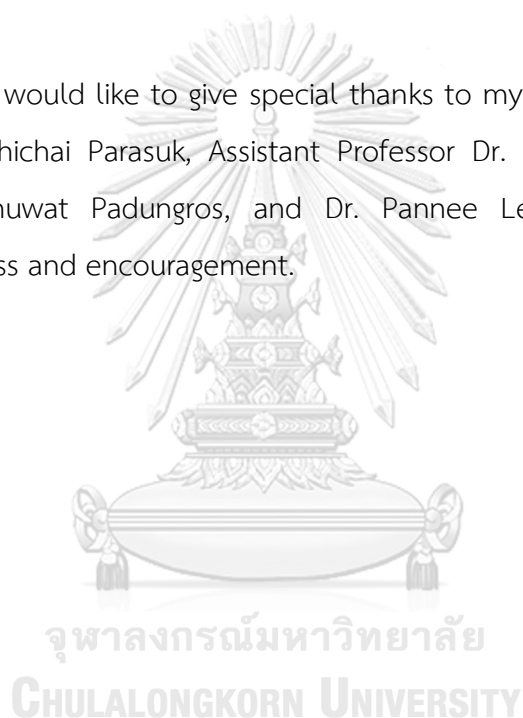


TABLE OF CONTENTS

	Page
.....	iii
ABSTRACT (THAI).....	iii
.....	iv
ABSTRACT (ENGLISH).....	iv
ACKNOWLEDGEMENTS.....	v
TABLE OF CONTENTS.....	vi
TABLE OF FIGURES.....	x
TABLE OF TABLES.....	xvi
CHAPTER I INTRODUCTION.....	1
1.1 Statement of problem.....	1
1.2 The objectives of this thesis.....	2
1.2.1 To synthesize nanocomposites of silica-superparamagnetic iron oxide nanoparticles-mannan (S-SPION-MN).....	2
1.2.2 To biologically study the synthesized S-SPION-MN nanocomposites and develop them for being used as vaccine adjuvants.....	2
1.3 Scope of this thesis.....	2
CHAPTER II THEORIES AND LITERATURE REVIEWS.....	4
2.1 Principles of vaccines and immune systems.....	4
2.1.1 Background and development of vaccines.....	4
2.1.2 Role of immune system.....	8
2.1.3 Techniques used in biological study.....	12
2.1.3.1 Principle of MTT assay.....	12

2.1.3.2 Principle of ELISA	13
2.1.3.3 Principle of flow cytometry.....	14
2.2 Nanomaterials used in immunological application	16
2.2.1 Types of nanoparticles and their fates in medical applications	16
2.2.2 Silica-based particles	18
2.2.3 Magnetic nanoparticles.....	19
2.2.3.1 Magnetic behaviors.....	19
2.2.3.2 Iron oxide nanoparticles and their magnetic property	20
2.2.3.3 Synthesis of superparamagnetic nanoparticles	22
2.3 Literature reviews.....	24
2.3.1 Mannan and its potential in targeting and maturation of dendritic cells (DCs).....	24
2.3.2 Silica nanoparticles and biocompatibility study	28
2.3.1 Superparamagnetic nanoparticles used in biomedical applications.....	33
CHAPTER III EXPERIMENTS.....	39
3.1 Lists of instruments, chemical and biological reagents used in this study.....	39
3.2 Synthesis of nanocomposites	42
3.2.1 Synthesis of nanocomposites of silica-superparamagnetic nanoparticles (S-SPION).....	42
3.2.2 Preparation of nanocomposites of S-SPION and mannan (S-SPION-MN) ..	43
3.3 Materials characterizations and biological studies of synthesized S-SPION, and S-SPION-MN nanocomposites	45
3.3.1 Physical characterizations.....	45
3.3.2 SPIONs and mannan loading content.....	45
3.3.3 Cell culture	46

3.3.4 Cytotoxicity	46
3.3.5 Cellular internalization	47
3.3.6 Induction of dendritic cell maturation and cytokine secretion.....	47
CHAPTER IV RESULTS AND DISCUSSION	49
4.1 Materials characterizations.....	49
4.1.1 Characterization of silica nanoparticles (SiNPs) and silica-magnetic nanoparticles (S-SPION) by FESEM and TEM.....	49
4.1.2 Characterization of silica nanoparticles (SiNPs) and silica-magnetic nanoparticles (S-SPION) by XRD.....	52
4.1.3 Magnetic characterization of silica-magnetic nanoparticles (S-SPION) by VSM.....	53
4.1.4 Functionalization of silica-magnetic nanoparticles with mannan (S-SPION-MN)	54
4.1.5 Magnetic characterization of silica-magnetic nanoparticles-mannan (S-SPION-MN) using a VSM	56
4.1.6 Characterization of silica-magnetic nanoparticles-mannan (S-SPION-MN) by hydrodynamic size, zeta potential and ICP-OES.....	57
4.2 Biological activities.....	58
4.2.1 Cytotoxicity study.....	58
4.2.2 DC maturation.....	60
4.2.3 Cytokine assessment	62
4.2.4 Cellular internalization	63
4.2.4.1 Cellular uptake visualized by a confocal microscope	63
4.2.4.2 Cellular uptake assessed by flow cytometry	67
CHAPTER V CONCLUSION.....	69

APPENDIX..... 71

REFERENCES 73

VITA..... 82



TABLE OF FIGURES

Figure 2.1 Illustration of timeline of vaccine development [9].	5
Figure 2.2 Illustration of innate immune cells and adaptive immune cells [31].	9
Figure 2.3 Pathogen recognition of dendritic cell through receptors [32].	10
Figure 2.4 The functions of B and T lymphocytes in adaptive immunity [34].	11
Figure 2.5 Overview of the interaction of innate immunity and adaptive immunity [35].	12
Figure 2.6 Chemical reaction of transforming MTT into formazan crystals.	13
Figure 2.7 Schematic depiction of sandwich ELISA method. The protocol is composed of 5 steps. Step 1: capture antibody is coated on the plate. Step 2: Sample is added and the antigen is bound to the presented antibody. Step 3: A biotin labeled detection antibody is added and subsequently bound to the captured antigen. Step 4: Avidin-HRPO is added to bind with the labeled detection antibody. Step 5: TMB substrate is added and transformed into a detectable form, expressing color. [38].	14
Figure 2.8 Illustration of a) flow cytometer and b) Dot plot obtained from FSC and SSC detectors [39].	15
Figure 2.9 Illustration of fluorescence measurement a) fluorescence intensity single stained cell showing negative (low intensity) positive (high intensity) cells. b) fluorescence signaling of double cell staining [39].	15
Figure 2.10 Examples of nanoparticles applied in immunology [42].	16
Figure 2.11 Graphical illustration of the modification of nanoparticles to improve immunogenicity [43].	17
Figure 2.12 Graphical illustration of multifunctional silica-based nanoparticles [48].	18
Figure 2.13 Mechanism of silica formation by Stöber method.	19
Figure 2.14 Crystal structures of three different types of iron oxide nanoparticles [52].	20

Figure 2.15 The correlation of nanoparticles size and magnetic domains [53].	21
Figure 2.16 Magnetization curves of superparamagnetic, ferromagnetic and paramagnetic materials [54].	22
Figure 2.17 The possible ways to attain monodispersed nanoparticles. Curve I: involving single step of nucleation and growth, Curve II: involving in nanoparticles aggregation, and curve III: involving in Ostwald ripening reaction [58].	23
Figure 2.18 Scheme representation of SPIONs formation by thermal decomposition method [60].	24
Figure 2.19 Gene expression results from macrophages stimulated by different particles, lipofectamine-DNA, SLN-DNA, and Man-SLN-DNA [63].	25
Figure 2.20 Cellular uptake assessed by a) flow cytometry b) confocal microscopy of mannan-coated PLGA nanoparticles via physical adsorption and covalent interactions [64].	26
Figure 2.21 DC-histograms showing the effect of mannan formulations to the upregulation degrees of DC maturation markers a) CD86 and b) CD40. The expression of surface markers was assessed by flow cytometry [29].	27
Figure 2. 22 Cell viability of A549, Hela, Caco-2, Jurkat, and U937 cells incubated with 25 nm silica nanoparticles with different charges (negative and positive charges) and concentrations (S1: 2.5 pM, S2: 25 pM, S3: 250 pM, S4: 2500 pM) at 48h and 96h.	29
Figure 2.23 Cell viability of MCF-7 cells incubated with different sizes (160, 240, and 330 nm) and doses (1.5, 3, and 5 mg/mL) of plain and PEGylated silica nanoparticles at various times (24, 48, and 72 h).	30
Figure 2.24 The results of a) cell proliferation, and b) cell viability of Caco-2 cells incubated with nanocomposites of silica and magnetic nanoparticles at 24, 48, 72, 96 h and 7 days at different concentrations (i.e. 10, 50, 100 µg/mL).	31
Figure 2.25 Cell viability of RAW 264.7 macrophages incubated with increasing doses of plain and amino-functionalized silica nanoparticles with different degrees coverage of amino groups in a) the absence of serum and b) in the presence of serum.	32

Figure 2.26 Depiction of surface coating of SPIONs by a) inorganic materials, b) organic materials and encapsulation of SPIONs inside c) nanospheres, d) nanocapsules [74].33	
Figure 2.27 Schematic representation of a) the synthesis of nanocomposites of water-dispersible SPIONs and b) the aid of an external magnetic field in targeting cancer cells [75].	34
Figure 2.28 Confocal microscopy images of MCF-7 incubated with different particles for 1 h a) free DOX, b) incubating cell with free FA prior to the addition of DOX@FA-SPIONs, c) DOX@FA-SPIONs without magnetically aid, d) DOX@FA-SPIONs with magnetically aid [75].	35
Figure 2.29 Cellular uptake of RAW264.7 and DCs incubated with different types of nanoparticles for 3 h in the absence and presence of magnetic field [72].	36
Figure 2.30 Schematic representation of the synthesis of hyaluronic acid-conjugated mesoporous silica-SPIONs and its application in targeted drug delivery [76].	37
Figure 3.1 Depiction of the synthesis of S-SPION nanocomposites.	42
Figure 3.2 Temperature program used to fabricate S-SPION nanocomposites.	43
Figure 3.3 Schematic representation of the synthesis of S-SPION-MN nanocomposites.	43
Figure 3.4 Mannan structures in fungal cell wall [84].	44
Figure 4.1 Schematic representation of the synthesis of S-SPION-MN and its benefit of magnetically aid in biological study.	49
Figure 4.2 FESEM images of fabricated silica nanoparticles with a) small and b) large sizes.	50
Figure 4.3 FESEM images of S-SPION synthesized with a) 10 mg, b) 20 mg, c) 60 mg, and d) 180 mg of Fe(acac) ₃ .	51
Figure 4.4 a) SEM image and b) TEM image of large S-SPION synthesized with 10 mg of Fe(acac) ₃ .	52

Figure 4.5 XRD patterns of the synthesized nanoparticles (i.e. S-SPION (S), S-SPION (L), and S-SPION_180Fe) compared to a magnetite reference (JCPDS:19-0629) and bare SiNPs.	53
Figure 4.6 Magnetization-magnetic field (M-H) curves of S-SPION (S) and S-SPION (L) nanocomposites.	54
Figure 4.7 Magnetization curves of coated nanocomposite (S-SPION-MN) compared to the uncoated sample (S-SPION).	57
Figure 4.8 Cytotoxicity of the synthesized particles in BMDCs. Cell viability was assessed by MTT assay and presented as optical density (O.D. at 570 nm). BMDCs were incubated with the tested particles at a) 6 h, b) 12 h, c) 24 h, and d) 48 h. * indicates the statistically significant difference between samples, as determined by One-way ANOVA with Tukey HSD (n = 3) at $p < 0.05$	59
Figure 4.9 Effects of the particulate mannan on DC maturation. BMDCs were incubated with tested particles at various concentrations as indicated for (a) 24 h and (b) 48 h. The expression of DC markers, CD80, CD86 and MHC class II, was assessed by flow cytometric analysis. DCs were identified by gating on CD11c ⁺ fraction. Then the expression levels of the maturation markers were assessed using histogram analysis (Appendix: Figure A3), and presented in geometric mean fluorescence intensity (MFI). * indicates the statistically significant difference between the two samples, as determined by One-way ANOVA with Tukey HSD (n = 3) at $p < 0.05$	61
Figure 4.10 The percentage of mature DCs. BMDCs were incubated with tested particles at various concentrations as indicated for (a) 24 h and (b) 48 h. DCs were identified by gating on CD11c ⁺ fraction. Then the percentage of CD80, CD86 and MHC class II positive cells were assessed by dot plot analysis. * indicates the statistically significant difference between the two samples, as determined by One-way ANOVA with Tukey HSD (n = 3) at $p < 0.05$	62
Figure 4.11 Cytokine production from stimulated BMDCs. BMDCs were incubated with the tested particles at different concentrations as indicated for (a) 24 h and (b) 48 h. Cytokine production was assessed by ELISA method. * indicates the statistically	

significant difference between the two samples, as determined by One-way ANOVA with Tukey HSD (n = 3) at $p < 0.05$	64
Figure 4.12 Internalization of particulate mannan by BMDCs. BMDCs were incubated with particulate mannan (S-SPION-MN) for 15 min and 3 h with and without a 260 mT magnetic field, and the internalization of the particles was observed under confocal microscopy. Representative confocal images of BMDCs (blue for nuclei and red for plasma membrane) and fluorescent S-SPION-MN particles (green) are displayed.....	66
Figure 4.13 Internalization of S-SPION by BMDCs. BMDCs were incubated with particles for 15 min and 3 h with and without a 260 mT magnetic field, and the internalization of the particles was observed under confocal microscopy. Representative confocal images of BMDCs (blue for nuclei and red for plasma membrane) and fluorescent S-SPION particles (green) are displayed.....	67
Figure 4.14 Flow cytometric analysis of BMDC internalization. BMDCs were incubated with particulate mannan (S-SPION-MN) for 15 min and 3 h with and without a 260 mT magnetic field. The percentage of cellular uptake was evaluated using histogram analysis. * indicates the statistically significant difference between the two samples, as determined by One-way ANOVA Tukey HSD (n = 3) at $p < 0.05$	68
Figure A1 Picture demonstration of the synthesized S-SPION nanocomposite a) without and b) with an induction of an external magnetic field.....	71
Figure A2 Colorimetric assay of sulfuric acid-phenol method confirming the presence of mannan in S-SPION nanocomposite.	71
Figure A3 Flow cytometric analysis of DC maturation. BMDCs were stimulated with particulate mannan (S-SPION-MN). The dot plot analysis of BMDC was first shown using side scatter (SSC) and forward scatter (FSC), and the live cells were gated. (a) DCs were identified by gating on CD11c ⁺ population. The left panel is the control staining, and the right panel is the control staining with anti-mouse CD11c mAb. The number shown in the panels represented the percentage of CD11c ⁺ cells. (b) Histogram analysis of DCs markers (i.e. CD80, CD86 and MHC class II expression on	

CD11c+ cells). The numbers indicated the geometric mean fluorescence intensity (MFI). 72



TABLE OF TABLES

Table 3.1 List of instruments	39
Table 3.2 List of chemicals	40
Table 3.3 Biological reagents	41
Table 4.1 Zeta potential and coated mannan content	55
Table 4.2 Properties of synthesized particles	58



CHAPTER I

INTRODUCTION

1.1 Statement of problem

Over the past decades, vaccination has been well-known and widely used as an effective treatment against infectious diseases and malignancies. Principally, a relatively small dose of mild form of interested pathogen is administrated into a body and subsequently allows the immune cells to undergo a protective immunity against presented antigen [1]. Once a patient is infected and then recovers from the infection, the immunity of the body will be able to remember that disease for long. Therefore, when the body receives the same pathogen, the body immunity will rapidly attack the specific antigen resulted in an efficient protection [2]. Although vaccination has shown a promising outcome, some types of vaccine (e.g. live-attenuated vaccines) are of concern for safety uses. Therefore, other types of vaccines (killed and inactivated vaccines) were alternatively emerged. However, lack of strong induction of immune responses regarding to the use of inactivated vaccines leads to a poor host defense [3].

Interestingly, vaccine adjuvant has thus received much attention. Adjuvants are substances used in combination with vaccines to boost immune responses. However, there are only a few acceptable adjuvants for clinical treatment, thus the development of vaccine adjuvants has become a popular issue over the past years. Among various types of adjuvants, mannan is considered as one of the effective adjuvants due to a large number of mannose receptors on immune cells enabling it to serve as a targeting molecule [4, 5]. Although mannan has shown a potency as vaccine adjuvants, soluble mannan has demonstrated unsatisfactory results. Therefore, synthesis of particulate mannan is of our interest.

Nanoparticles have received much attention in many applications due to the variation in size and shape, and the diversity of surface functionalization. In recent years, silica nanoparticles, ones of the most common materials used in various works, have been widely applied in the field of biomedicine since they are

biocompatible and easily functionalized. Moreover, superparamagnetic iron oxide nanoparticles (SPIONs) have also drawn much attention due to their unique superparamagnetic property. SPIONs will exhibit magnetic property under an induction of an external magnetic field and become colloidal solution in the absence of an external magnetic field.

Herein, we hypothesized that the synthesis of particulate mannan would enhance the immune responses, making it a promising adjuvant. Therefore, silica nanoparticles were synthesized as a based material along with a large quantity of SPIONs coating on silica nanoparticles surface. The nanocomposites were then coated with extracted mannan on the outermost layer. Apart from the benefit of mannan as a targeting moiety, having SPIONs incorporated in the synthesized material would also lead to an enhancement of cellular uptake under an external magnetic field. Once the nanocomposites were engulfed by immune cells, the nanocomposites were also assumed to enhance the cell stimulation and maturation. The capability of eliciting strong immune responses by the nanocomposites of silica-SPION-mannan studied *in vitro* would make them a promising adjuvant and worth investigating *in vivo* in the future.

1.2 The objectives of this thesis

- 1.2.1 To synthesize nanocomposites of silica-superparamagnetic iron oxide nanoparticles-mannan (S-SPION-MN)
- 1.2.2 To biologically study the synthesized S-SPION-MN nanocomposites and develop them for being used as vaccine adjuvants

1.3 Scope of this thesis

This research focused on the synthesis of silica-superparamagnetic iron oxide nanoparticles-mannan (S-SPION-MN). Firstly, silica nanoparticles were synthesized using Stöber method, producing nanoparticles size of about 500 nm. Next, thermal decomposition method was chosen to synthesize nanocomposites of silica-superparamagnetic iron oxide (S-SPION) nanoparticles. The morphology and structure of nanocomposites were then determined using Transmission electron microscopy

(TEM) and X-ray power diffraction (XRD), respectively. Inductively coupled plasma optical emission spectrometer (ICP-OES) was used for elemental analysis. Mannan was subsequently coated on the S-SPION surface using EDC/NSH coupling reagents. The confirmation of mannan attachment was revealed by a colorimetric assay using the phenol-sulfuric acid method. Also, the change of zeta potentials of synthesized materials revealed the success of mannan coating. In addition, characteristic of superparamagnetic property of before and after surface modification of S-SPION was confirmed using a vibrating-sample magnetometer (VSM). To reveal an efficacy of S-SPION-MN as vaccine adjuvant, the synthesized nanocomposites were later biologically studied including cytotoxicity test, cytokine release assessment, maturation of cells and cellular internalization. In this case, bone marrow-derived dendritic cells (BM-DCs) were represented as interested antigen presenting cells (MPCs). For cytotoxicity test, MTT (3-(4,5-dimethylthiazol-2-yl)-2,5-diphenyltetrazolium bromide) cell viability assay was used to observe cell viability. Released cytokines from stimulated cells were assessed by ELISA method. To observe cellular uptake, confocal laser scanning microscope and flow cytometer were used. Lastly, flow cytometric analysis was chosen for determination of DCs' maturation.

CHAPTER II

THEORIES AND LITERATURE REVIEWS

2.1 Principles of vaccines and immune systems

2.1.1 Background and development of vaccines

Vaccination has gained its reputation as an effective treatment against a variety of infectious diseases and malignancies [6]. Notably, in 1796, it was a momentous time as Edward Jenner used a cowpox material as a vaccine against smallpox. His vaccine's creation became practical and has been developed over 200 years. The first vaccine development in laboratories was done by Louis Pasteur for chicken cholera protection in 1879. Later, he successfully created a vaccine against rabies in 1885. He was the person who firstly to use the word "vaccinate" to demonstrate the performance of inoculation in chicken and later became worldwide use. Then, there was a rapid development in vaccine research leading to achievement in producing vaccines against various diseases, such as polio, measles, mumps, and rubella through the 1930s [7, 8]. Figure 2.1 demonstrated a timeline of vaccine development over the past years [9].

Vaccines have been categorized into three types (e.g. live attenuated, inactivated, and subunit vaccines) according to the protocol for vaccine preparation [10]. Live attenuated vaccines (LAVs) are prepared from weakened viruses or bacteria. LAVs have demonstrated promising outcomes against viral diseases, such as smallpox, polio, measles and so on. Even though LAVs are very effective as they can elicit strong immune responses, the vaccines have not been used practically due to safety uses. For example, LAVs can cause a reversion to wild-type virulence [11]. Thanks to an advanced technology that can improve vaccine's preparation, vaccine could be produced with a large scale of concentrated and purified with non-destroyed immune activity. Due to the improved vaccine's preparation, killed and inactivated vaccines were then introduced and rapidly developed. Inactivated vaccines are basically acquired by growing wild viruses or bacteria in culture media and inactivating them by chemical or physical means before used. This type of vaccine has been reported as a safe modality of treatment as viruses and bacteria cannot replicate themselves once administered in a body. For example, in 1994, Bruce *et al.* [12] reported the safety use of a new inactivated vaccine against *Hepatitis A. Influenza A (H5N1)*, a pathogen for severe disease causing a large number of deaths. In 2006, John *et al.* assessed the safety and immune response of using inactivated subvirion influenza A (H5N1) vaccines. The study revealed that the vaccine did not cause adverse effects and might be effective use against the disease in human [13]. Despite its safety use, inactivated vaccines have still shown a downside effect as they elicit inadequate immune responses compared to an equivalent dose of live attenuated vaccines [14, 15]. Moreover, subunit vaccines have received significant attention as modern vaccines (i.e. more intact treatment and less undesirable side effects). Subunit vaccines are composed of some fragments of pathogens, normally surface proteins, which are exploited to target immune cells and subsequently stimulate immunogenicity [16]. Other than their ease in manufacture and less adverse effects, the subunit vaccines can also induce broad immune responses [17]. Despite safety uses, subunit vaccine has remained an issue hindering the success of vaccination due to poor immunogenicity [18]. Therefore, providing a stronger induction signal of subunit vaccine is of concerned.

Typically, there are two ways to improve the efficacy of vaccines. One is to increase vaccine's dose. The other one is to add substances which are able to help vaccine elicit strong immune responses [19]. These boosters are termed as adjuvants. Adjuvants have been recognized as additional components to enhance the therapeutic capability of vaccine antigens [20]. The incorporation of vaccine and adjuvants, substances used in combination with vaccines to enhance immune response of vaccines, has become an efficient alternative for subunit vaccination.

Since adjuvants have drawn a great attention in vaccine development, researchers have focused on the studies related to the synthesis and improvement of natural adjuvants. Adjuvants are presented in various types based on their sources, for instance, aluminum-based adjuvants, liposome adjuvants, adjuvants emulsions, carbohydrate adjuvants and so on [21]. However, only certain types of adjuvants have been approved for human use, including alum-based adjuvants and oil in water emulsions (MF59, AS03) [22].

Among different types of adjuvants, carbohydrates, which can be found naturally, have attracted much interest due to high biocompatibility and low toxicity. Some carbohydrate structures have been considered as one of the most promising adjuvants as they are biodegradable and biocompatible [23]. Besides, carbohydrates can be recognized by C-type lectin receptors overexpressed on antigen presenting cells (APCs) (i.e. dendritic cells (DCs) and macrophages) [24]. Once the binding of carbohydrates and receptors occurs, this interaction will result in the activation and cytokine production of APCs. The released cytokines will further enhance the activation of antigen-specific T- and B-cell responses [23]. Mannan, a polysaccharide of mannose units, has been reported as a good adjuvant due to strong affinity between mannan and mannose receptors on DCs membrane [4]. In this regard, mannan is of our interest as an effective targeting molecule. Sheng *et al.* [25] reported the use of mannan and its derivatives (oxidized and reduced mannan) to perform a tumor antigen carrying into DCs. The results showed that mannan and its derivatives could potentially stimulate the secretion of inflammatory cytokines, interleukin-1 β and tumor necrosis factor- α , and differential T helper 1 (Th1)/Th2 cytokines, making them potential as vaccine adjuvants. Besides, Nguyen *et al.* [26]

studied the role of mannan extracted from candida's cell wall in controlling immune response pathway. The results showed that mannan with different structures would provide different degrees of immune responses. In the case of using targeting ligands, however, it has been reported that particulate delivery along with targeting TLR-4 ligand exhibited higher degree of DCs activation and maturation compared to a soluble formulation [27]. In order to improve immunogenicity, a particulate form of adjuvant is thus highly required. Over the past years, there are many studies related to mannan-coated biocompatible materials, such as cationic solid lipid nanoparticles [28], poly(lactic-co-glycolic acid) (PLGA) [29], chitosan [30], have been investigated. Regardless of the type of biocompatible materials, the outcomes are similar in terms of the improvement in cellular uptake and cell maturation. Significantly, the enhancement of immune responses was attributed to the presence of mannan leading to specifically targeting antigen presenting cells (APCs). However, incorporation of mannan and inorganic materials have not been well studied yet. Therefore, we were interested in using the benefit of inorganic materials, ease of manufacture and variation in size and shape, combining with specific targeting ability of mannan molecules.

2.1.2 Role of immune system

When our body receives pathogens (e.g. bacteria, viruses or infectious agents which can cause disease), the protective system, also known as immune system, of the body plays an important role in protecting the body from infection thereby attacking the invaders. Principally, the immune system is composed of two compartments (i.e. innate and adaptive immunity). These two components are functionally connected. Figure 2.2 shows the immune cells involved in innate and adaptive immune systems.

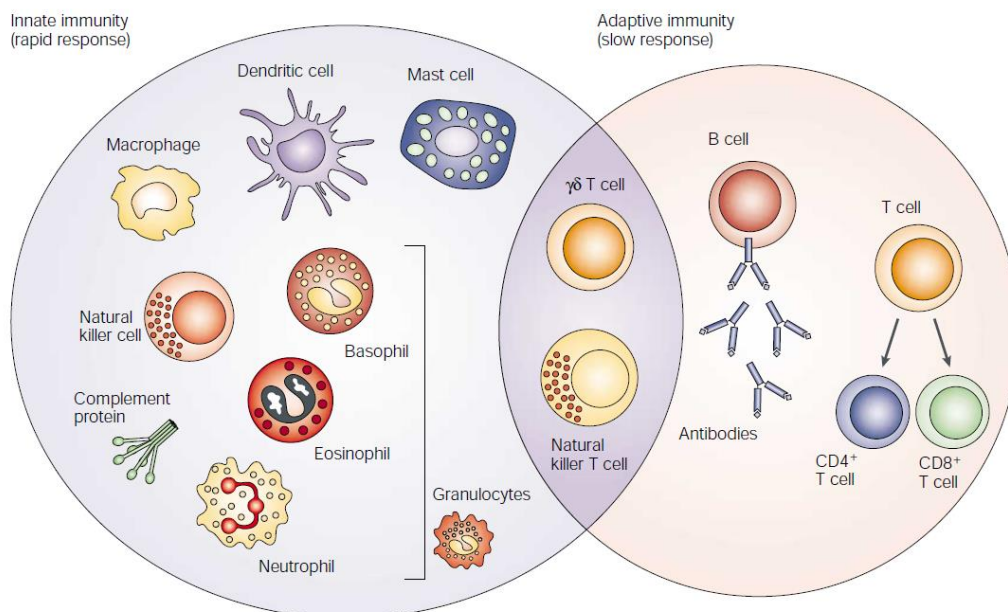


Figure 2.2 Illustration of innate immune cells and adaptive immune cells [31].

Innate immunity is the first barrier to attack pathogens which exhibits a quick response to the invaders but no specificity. It is composed of various types of immune cells, for example macrophage, dendritic cell, neutrophil, and so on. Among those cells, dendritic cells (DCs) always play an important role as mediators in initiating and regulating the immune response of innate and adaptive immunities. Basically, DCs are capable of recognizing infectious agents through host-pathogen interaction. As DCs contain a large number of receptors (e.g. Toll-like receptors (TLRs), RIG-I-like receptors (RLRs), NOD-like receptors (NLRs), etc.) on their surface membrane as shown in Figure 2.3 [32], this makes DCs promising immune cells as they can recognize a broad range of antigens. These receptors have specific encoded pattern recognition receptors (PRRs) which can recognize the pathogen via pathogen-associated molecular patterns (PAMPs). Therefore, the pathogen that conserves PAMPs structure can be engulfed by DCs through this interaction [33].

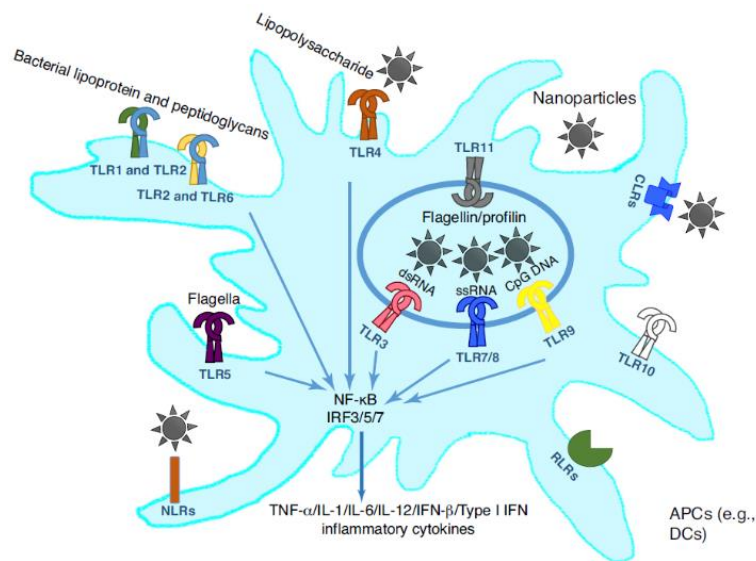


Figure 2.3 Pathogen recognition of dendritic cell through receptors [32].

Adaptive immunity is divided into two systems (humoral and cellular systems). In contrast to innate immunity, adaptive immunity takes a longer time to respond to the entered pathogens but more specific to the presented disease. In this system, B and T lymphocytes are the major components. Although these two lymphocytes have different pathways to attack antigens, two cells receive the signal from the antigen via the same procedure called antigen presentation. B cells or B lymphocytes are involved in humoral immunity producing antibodies against specific antigens, while T lymphocytes are related to cell-mediated system. In this system, T cells can recognize antigen, which is presented on the surface of infected cells. Figure 2.4 displays different roles of B cells and T cells in terms of immune responses [34].

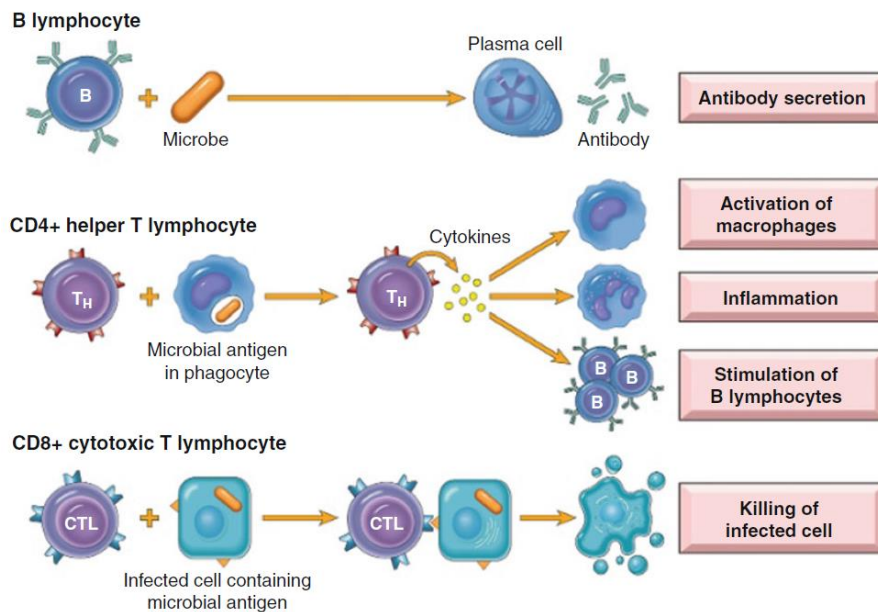


Figure 2.4 The functions of B and T lymphocytes in adaptive immunity [34].

To understand the process of immune response, Figure 2.5 depicts the collaboration of innate immune cell (i.e. dendritic cell as antigen presenting cell (APC)) and adaptive immune cell (naïve T cell) after bacterial infection. Briefly, entered pathogen can be initially recognized by APCs and subsequently proceeded through antigen presentation process giving rise to the expression of that antigen on APCs surface membrane via receptors called Major Histocompatibility Complex (MHC) molecules. Subsequently, the presented antigen is subjected to naïve T cell in order to activate it into an active form. The activated T cell is consequently ready to proceed for further immune response involving production of antibodies, memory B cells, and effector T cells [35]. Once the body produces antibodies, recurrence of infection with the same type of antigen will be readily responded by the specifically produced antibody in a fast manner. This rapid and effective action of the immune system significantly decreases a large amount of death.

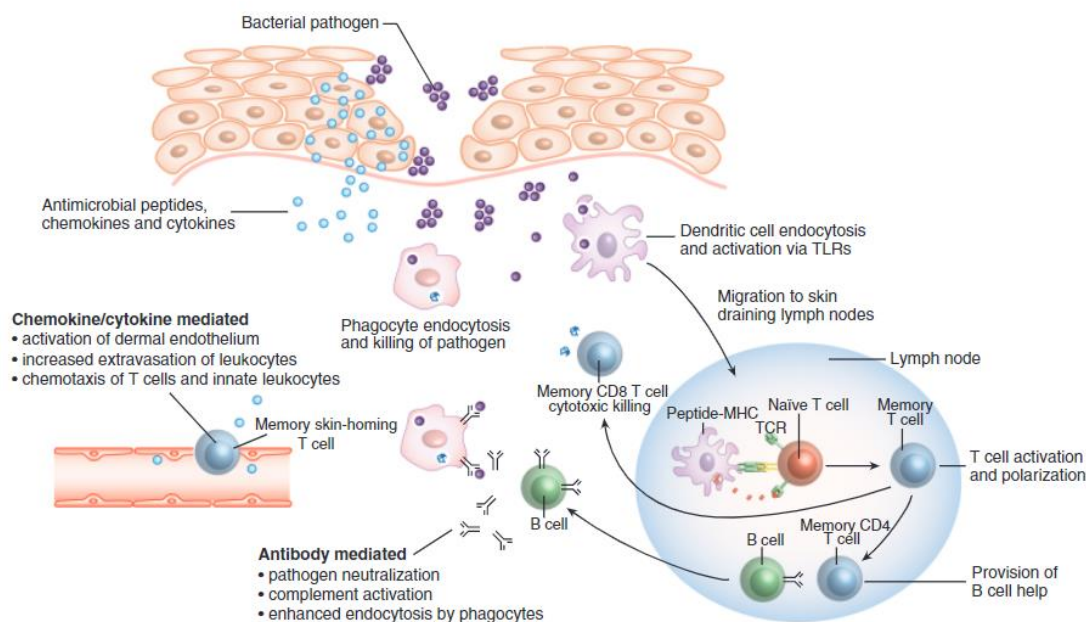


Figure 2.5 Overview of the interaction of innate immunity and adaptive immunity [35].

As abovementioned, immune system plays a crucial role in protecting life from severe infection. Therefore, it is worthy of studying in the development of immunotherapy. However, to achieve an effective immune response, first step in acquiring an effective antigen mediator must be greatly considered. In this regard, stimulation and maturation of DCs is the primary aim for immunology.

2.1.3 Techniques used in biological study

2.1.3.1 Principle of MTT assay

This MTT assay is a colorimetric method which has been widely used to determine cell viability, cytotoxicity and activity regardless of cell types. According to an advanced technology, nanoparticles have been comprehensively applied in biomedicine application as drug carriers, vaccine adjuvants, theranostic agents and so on. Therefore, biocompatibility of nanoparticles of interest must be of primary consideration. A compound named (3-(4,5-dimethylthiazol-2-yl)-2,5-diphenyltetrazolium bromide or MTT is a common chemical used in testing cell metabolic activity. Principally, the active cells contain NAD(P)H-dependent

oxidoreductase enzymes which can reduce the MTT (yellow solution) to insoluble formazan (purple crystals). The chemical reaction is shown in Figure 2.6. The produced formazan crystals are indirectly reflected to the number of viable cells. For quantitatively analysis, dimethyl sulfoxide (DMSO) is firstly used to dissolve formazan crystals into soluble form. Then, the absorbance of colored solution can be measured using a multi-well spectrometer at 570 nm. The darker colored solution implies the higher numbers of live cells [36].

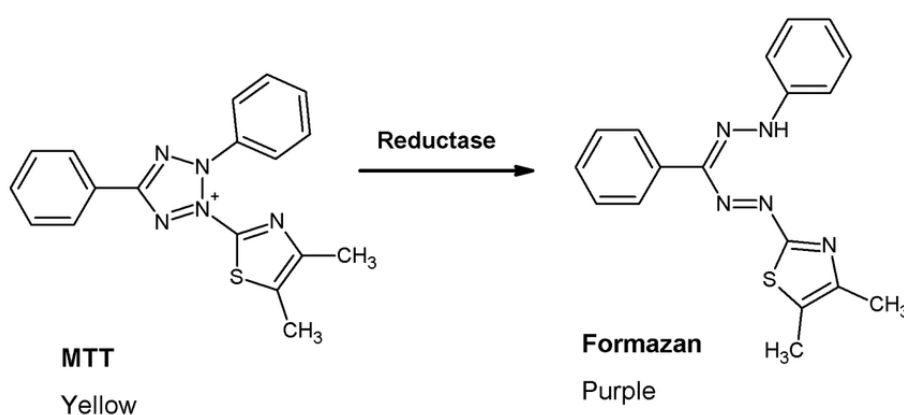


Figure 2.6 Chemical reaction of transforming MTT into formazan crystals.

2.1.3.2 Principle of ELISA

Cytokine assessment is one of standard biological studies. The produced cytokine from stimulated cells is normally verified by ELISA assay. ELISA stands for enzyme-linked immunosorbent assay. The basic principle of sandwich ELISA is based on the detection of interested antigen by a specific antibody via specific antibody-antigen interaction. Schematic illustration in Figure 2.7 displays the process of the targeted antigen detection. Briefly, capture antibody is firstly coated on a well. This capture antibody is utilized to immobilize a targeted antigen. Next, captured antigen can be recognized by a specific biotin labelled detection antibody. The presented biotin can be readily interacted with substrate enabling arrested antigen detectable. If the conjugation between antigen and detection antibody takes place, it can be measurable by determining the absorbance of colored solution. The colored solution is acquired by converting the attached substrate to a detectable form [37].

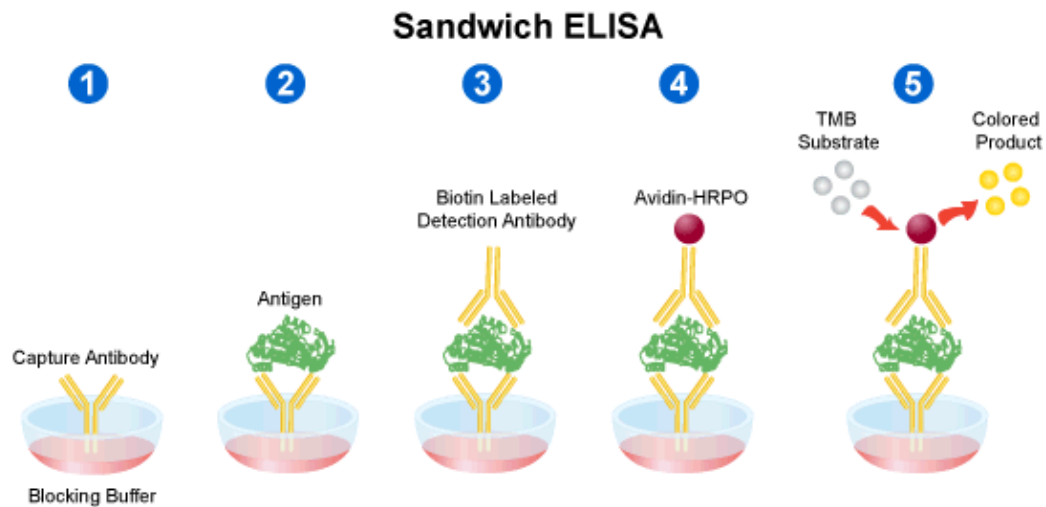


Figure 2.7 Schematic depiction of sandwich ELISA method. The protocol is composed of 5 steps. Step 1: capture antibody is coated on the plate. Step 2: Sample is added and the antigen is bound to the presented antibody. Step 3: A biotin labeled detection antibody is added and subsequently bound to the captured antigen. Step 4: Avidin-HRPO is added to bind with the labeled detection antibody. Step 5: TMB substrate is added and transformed into a detectable form, expressing color. [38].

2.1.3.3 Principle of flow cytometry

Flow cytometry is a laser-based technique used for determination of cell number, cell type, and cellular components especially proteins. Depiction in Figure 2.8a describes the setup of flow cytometer machine. Fundamentally, a heterogeneous sample of cell suspension passes through in liquid stream. The detectors, such as forward scatter (FSC) and side scatter (SSC), are in perpendicular places to determine the component and number of cells. FSC detector is used to assess the size and shape of interested cells, while SSC detector indicates fluorescence and granularity of cells. Figure 2.8b shows the dot plot obtained from FSC and SSC detectors. The position of dots refers to complexity, component, and type of scattered cells.

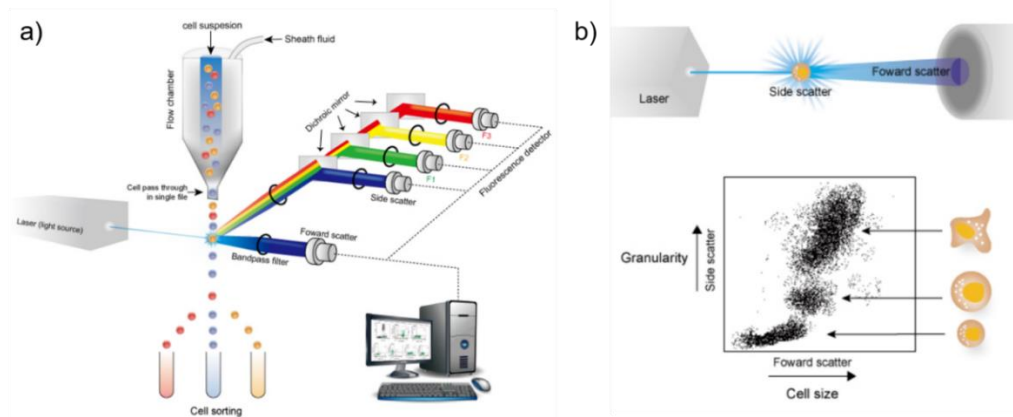


Figure 2.8 Illustration of a) flow cytometer and b) Dot plot obtained from FSC and SSC detectors [39].

Moreover, this technique allows us to understand the phenotyping of cell by labelling the surface markers on cell surface with fluorescent antibodies. The fluorescence detectors can measure the fluorescence intensity which reflects the number of interested components through fluorescence intensity. Figure 2.9 exhibits fluorescence signal obtained from dyed cells with single or multiple staining.

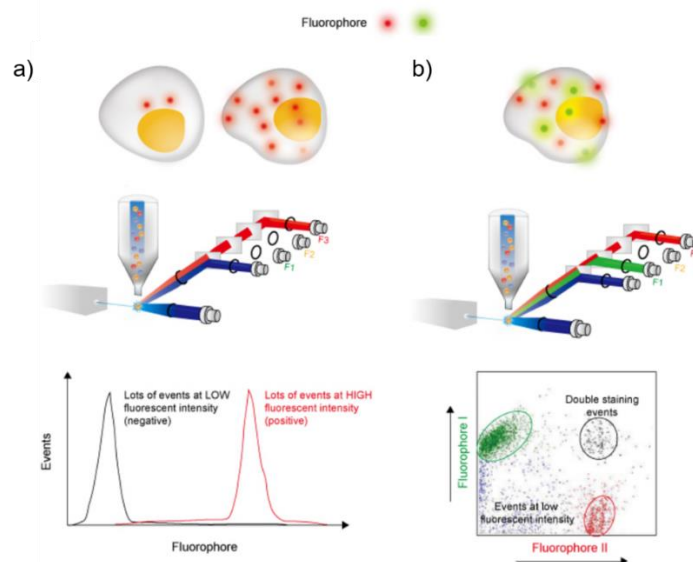


Figure 2.9 Illustration of fluorescence measurement a) fluorescence intensity single stained cell showing negative (low intensity) positive (high intensity) cells. b) fluorescence signaling of double cell staining [39].

2.2 Nanomaterials used in immunological application

2.2.1 Types of nanoparticles and their fates in medical applications

Nanotechnology has played a crucial role over the past decades as an innovative platform. Therefore, nanoparticles have been comprehensively studied in various fields. Particularly, they have gained much interest in biomedical applications (e.g. drug or vaccine delivery, diagnostics, therapeutics, theranostics) as they can be readily engineered in order to achieve biological requirements [40].

In immunotherapy, it has been known that effective immunogenicity requires enough antigen for immune stimulation, adequate immune induction, suitably specific antigen [41]. In this aspect, stimulation of APCs (i.e. dendritic cells) is the primary goal. Therefore, exploiting nanoparticles in immunotherapy has become more popular in recent years. There are a variety of nanoparticles used as nanoparticles-based vaccine delivery system and vaccine adjuvants. Figure 2.10 shows examples of nanoparticles applied in immunological study, such as dendrimer, liposome, micelle, virus-like particle and so forth [42]. Although organic materials (e.g. polymers, liposomes, etc.) have been intensively investigated due to their biodegradability and biocompatibility, some inorganic nanoparticles, such as silica nanoparticles, gold nanoparticles, iron oxide nanoparticles, have been applied in this field as antigen carriers and theranostic agents as well.

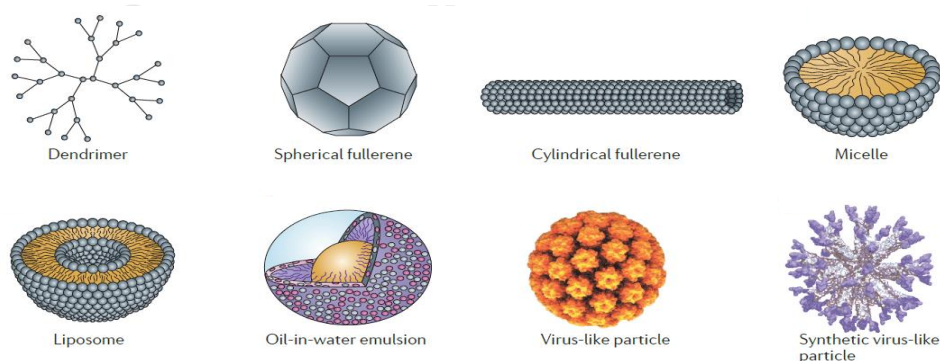


Figure 2.10 Examples of nanoparticles applied in immunology [42].

Regardless of types of nanoparticles, modification of nanoparticles is a key factor that makes nanoparticles a distinctive delivery system. The ease of manufacture and versatile modification provides a variety of nanoparticle-based therapeutic agents. There are different ways to engineer nanoparticles with distinguish formulations as shown in Figure 2.11 [43]. For example, surface of nanoparticles can be functionalized with cell targeting moiety, enhancing high specific targeting ability and consequently providing deeper cell penetration [44]. Heterogeneous porosity of nanoparticles is beneficial in obtaining high antigen loading capacity [45]. In addition, nanoparticles can be tuned to have either positive or negative surface charges depending on the purpose of the study (e.g. increasing the interaction between cell and nanoparticles) [46]. Due to physical and chemical tunability of nanoparticles, requirement in prolonged circulation time, enhanced biocompatibility and avoiding non-specific recognition from phagocytes has given rise to a new regime of nanoparticle-based therapeutic agents. Synthesis of nanoparticles camouflaged with red blood cell membrane has emerged as a promising way to disguise nanoparticles from scavengers [47]. Furthermore, the design of nanoparticles which can be responsive to external stimuli, such as light, pH, magnetic field, is also in the front line of biomaterial development nowadays.

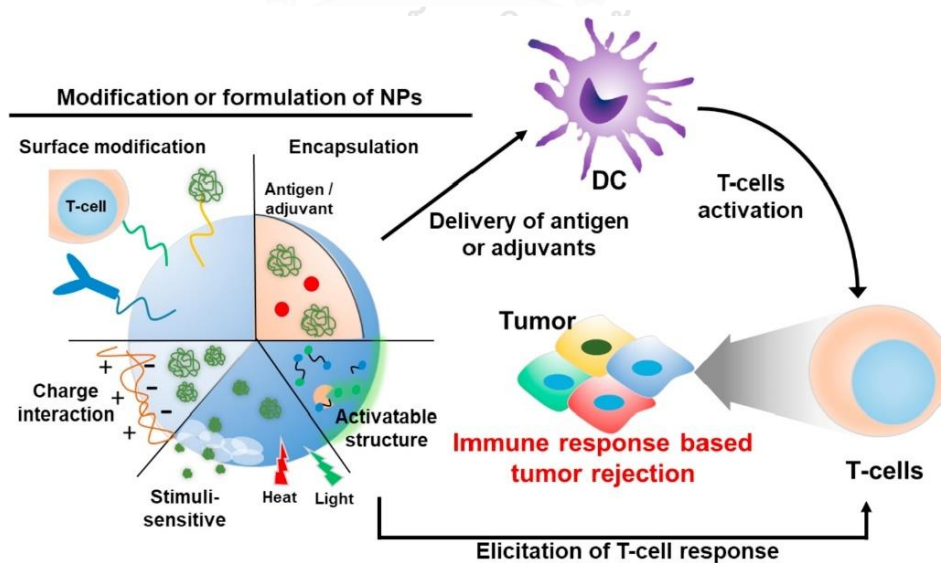


Figure 2.11 Graphical illustration of the modification of nanoparticles to improve immunogenicity [43].

In this work, we therefore focused on the utilization of magnetically responsive-inorganic materials accompanied with natural components as vaccine adjuvants owing to their high stability, biocompatibility, ease of fabrication and modification.

2.2.2 Silica-based particles

Among diversity of inorganic materials, silica-based particles have shown a potential in biomedical application over decades owing to its biocompatibility and multifunctionality. Since silica framework can be readily modified with other components, silica-based materials can provide multi-tasks in a single modality, for instance, a drug carrier with enhancing specifically targeting ability [48]. Figure 2.12 displays a graphical depiction of multifunctional mesoporous silica nanoparticles. Liu and coworkers fabricated dual-functionalized Janus mesoporous particles for tumor targeting enhancement. The synthesized mesoporous silica can be modified with other compounds via covalent bonding between amino group on mesoporous silica surface and carboxyl group of tumor targeting ligand (HA) and pH responsive polymer (DMMA), making nanoparticles possess two different functionalities [49].

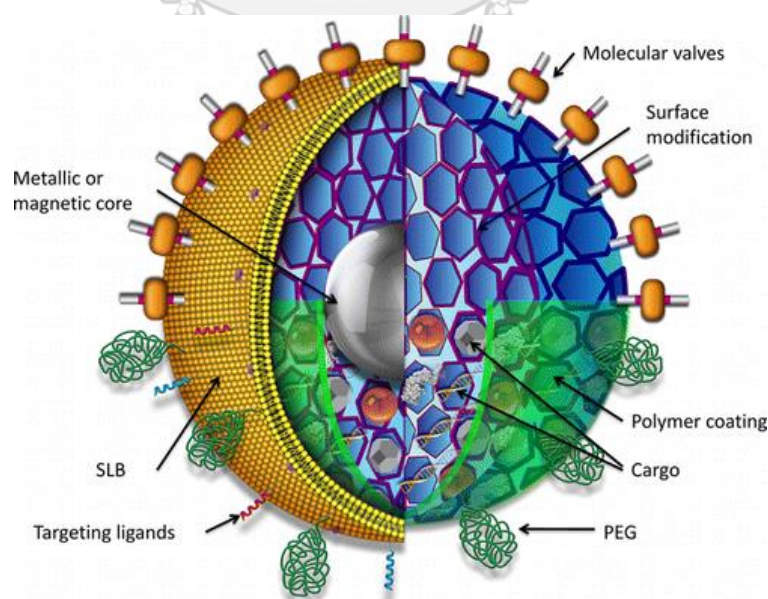


Figure 2.12 Graphical illustration of multifunctional silica-based nanoparticles [48].

Other than surface functionalization, alteration in size of silica nanoparticles is also achievable by a modified Stöber method. Synthesis of silica nanoparticles adopting Stöber protocol has been a common route to produce controlled spherical silica nanoparticles. Principally, silica formation is involving hydrolysis and condensation of silica source, typically tetraethyl orthosilicate (TEOS) in the existing of water and ammonia solution [50]. Firstly, silica source (TEOS) is hydrolyzed in alcoholic solution containing ammonia as a catalyst. Secondly, the reaction produces a mixture of ethoxysilanols, which can further condense with other TEOS or silanols, leading to crosslinking of silica frameworks [51]. The mechanism of silica formation is presented in Figure 2.13.

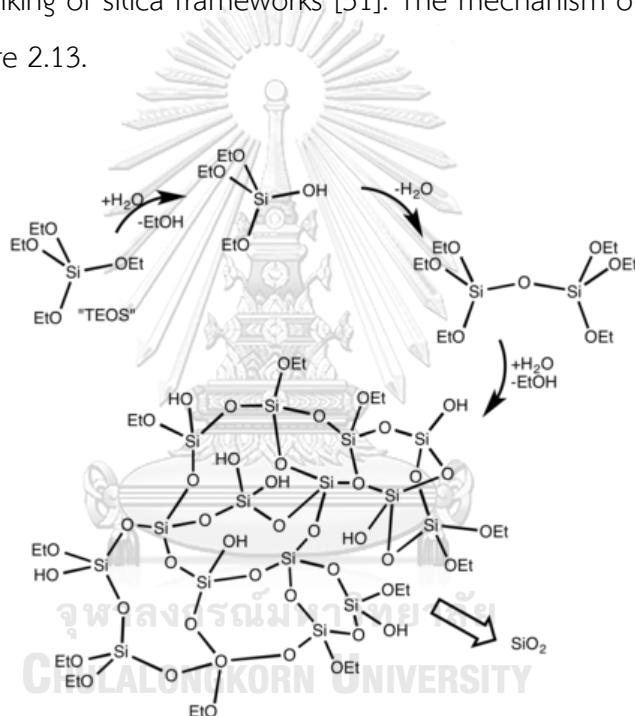


Figure 2.13 Mechanism of silica formation by Stöber method.

2.2.3 Magnetic nanoparticles

2.2.3.1 Magnetic behaviors

Magnetic nanoparticles have received much interest in recent years as they can be controlled by an external magnetic field, resulting in a great possibility in biomedical applications as a non-invasive treatment method. Referring to its magnetic property, materials can be generally classified into five different types of magnetism (i.e. diamagnetism, paramagnetism, ferromagnetism, ferrimagnetism, and

antiferromagnetism). Diamagnetic materials have weak repulsion with an external magnetic field due to the filled electronic subshells. In contrast, paramagnetic materials can be slightly attracted to magnetic fields due to the unpaired electrons in subshells. However, paramagnetism of the materials will disappear when the applied field is removed. For ferromagnetic materials, the magnetic moments align in the same direction with equal magnitude when the magnetic field is applied, while antiferromagnetism possesses equal magnitude of magnetic moments with antiparallel direction. Materials containing ferrimagnetism have unequal magnitude of antiparallel magnetic moments.

2.2.3.2 Iron oxide nanoparticles and their magnetic property

In this case, unpaired electrons of Fe^{2+} and Fe^{3+} in 3d shell can cause three different states (ferromagnetic, ferrimagnetic and antiferromagnetic forms) when crystal structures are formed. Commonly, iron oxide nanoparticles have three main different structures (namely Hematite, Magnetite, and Maghemite). Figure 2.14 displays their crystal structures [52]. Among those structures, nanostructures of magnetite (Fe_3O_4) and maghemite ($\gamma\text{-Fe}_2\text{O}_3$) have gained tremendous interest from researchers worldwide as they possess strong unique magnetic property, called superparamagnetic property.

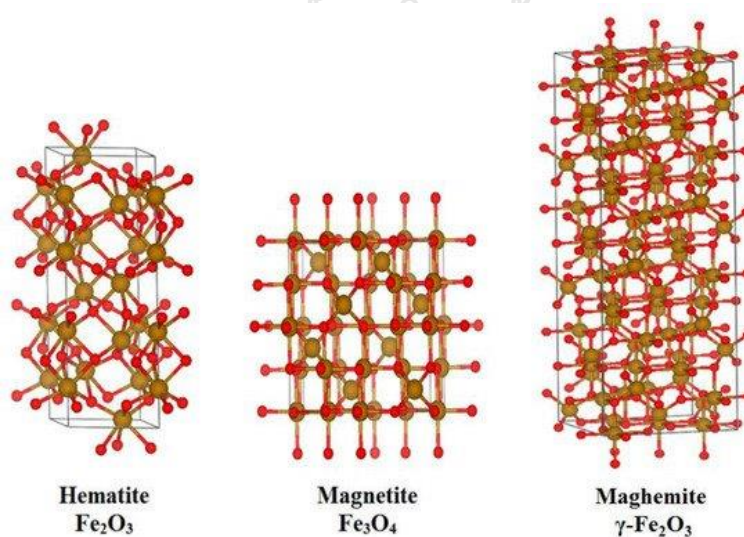


Figure 2.14 Crystal structures of three different types of iron oxide nanoparticles [52].

Superparamagnetic materials are differentiated from ferromagnetic materials by the concept of magnetic domain. Magnetic domain is composed of a number of magnetic moments which are aligned in the same direction. A number of domains depends on the particle's size. Ferromagnetic nanoparticles contain multi-domains with different magnitudes and directions of magnetization. When an external magnetic field is applied, the magnetic moments in multi-domain respond to the external field in the same direction. Once the applied field is removed, the magnetism is remained. When the size of nanoparticles is reduced, the magnetic domain becomes smaller. At below critical size, multi-domains are turned into single domain. In this regard, no net magnetization is maintained in the absence of an external magnetic field due to thermal fluctuation effect. The relation between nanoparticles diameter and magnetic domain is presented in Figure 2.15 [53].

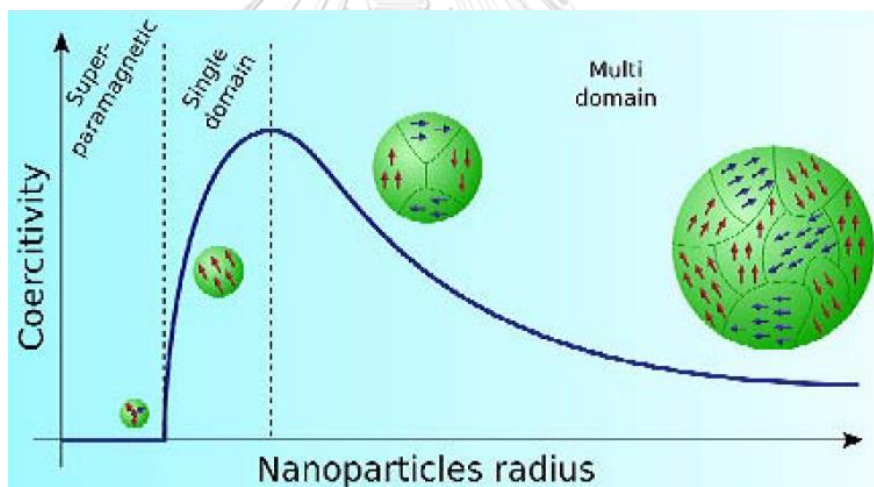


Figure 2.15 The correlation of nanoparticles size and magnetic domains [53].

Characteristics of ferromagnetic and superparamagnetic materials can be displayed in terms of magnetization curve as shown in Figure 2.16. The graph shows the correlation between an applied magnetic field and the magnitude of magnetization. There are two important terms, called remanence and coercivity, which can describe magnetic characters of the materials. Remanence refers to the remaining magnetization after a magnetic field is removed. Coercivity shows magnetic resistance in ferromagnetic materials through the requirement of magnetic field

intensity in the opposite direction to demagnetize the magnetism of the materials. It can be seen in the graph below that different types of magnetic materials possess different characteristic curves. The presence of hysteresis loop is ascribed to ferromagnetic materials as the materials can maintain magnetization in the absence of applied magnetic field. In contrast, superparamagnetic and paramagnetic materials exhibit no hysteresis loop. In another word, coercivity is zero when the applied magnetic field is removed, showing no net magnetization [54].

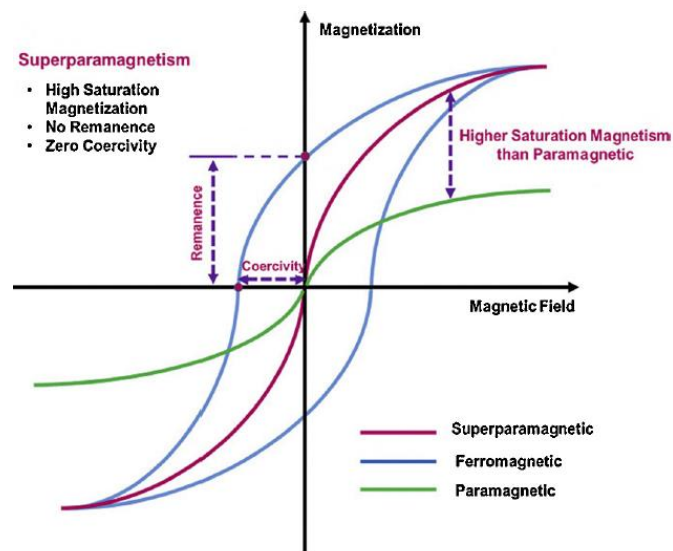


Figure 2.16 Magnetization curves of superparamagnetic, ferromagnetic and paramagnetic materials [54].

2.2.3.3 Synthesis of superparamagnetic nanoparticles

Superparamagnetic iron oxide nanoparticles (SPIONs) can be synthesized by several facile methods, for instance coprecipitation [55], microemulsion [56], and thermal decomposition [57]. In theory, for precipitation method, monodispersed nanoparticles can be obtained via separation of nucleation and growth stages following LaMer and Dinegar's model as shown in Figure 2.17 (Curve I). According to the proposed graphs, there are three possible ways to achieve monodispersed nanoparticles. For Curve I, single nucleation and growth step from diffusion occur. In

Curve II, the aggregation of small nanoparticles is performed. Finally, for Curve III, Ostwald ripening growth step is involved [58].

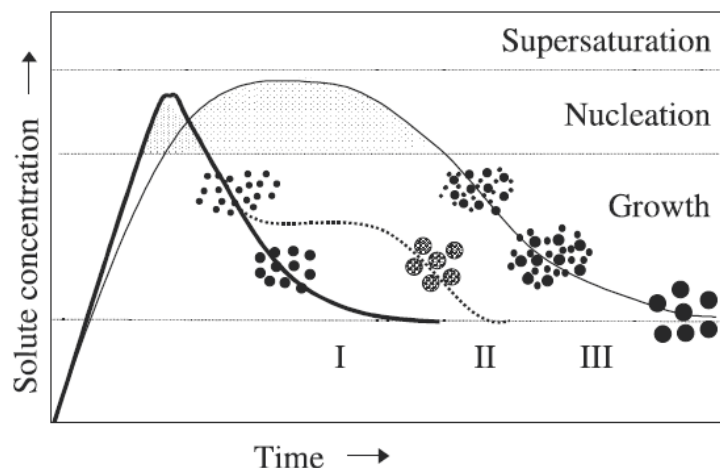


Figure 2.17 The possible ways to attain monodispersed nanoparticles. Curve I: involving single step of nucleation and growth, Curve II: involving in nanoparticles aggregation, and curve III: involving in Ostwald ripening reaction [58].

Among various synthetic methods, thermal decomposition is widely used to fabricate SPIONs. Although coprecipitation approach is considered to be a convenient method to produce SPIONs, thermal decomposition, which is more complicated, can provide a narrow distribution of nanoparticles size due to the effectiveness in separation of nucleation and growth steps [57]. Moreover, this method is environmentally friendly (i.e. use non-toxic chemicals). This method also offers flexibility in producing different sizes and shapes by controlling synthesis temperature, concentration of stabilizers and types of solvents.

The mechanism of SPIONs formation can be described in Figure 2.18. Briefly, iron precursor, commonly iron(III) oleate, is firstly decomposed and capped by an excess surfactant (e.g. oleic acid) presented in the organic solution. Notably, excess surfactant allows slower nucleation period and growth time, producing monodispersed nanoparticles [59]. It should be noted that this step is normally carried out under the absence of air. Then, the rapid nucleation occurs when it

reaches to nucleation temperature. After the growth step performs afterward at higher temperature [60].

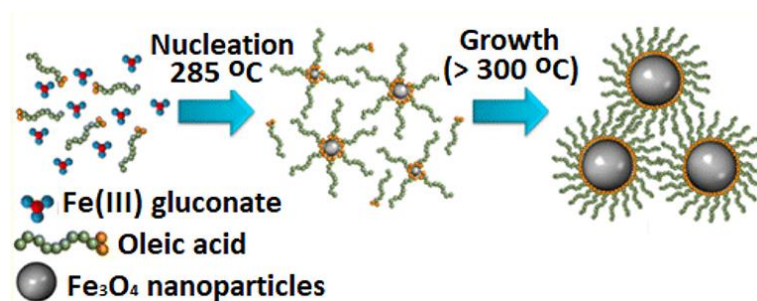


Figure 2.18 Scheme representation of SPIONs formation by thermal decomposition method [60].

However, this method is suitable for SPIONs dispersed in organic solvent. In order to make water-soluble SPIONs, an extra step for phase transfer is required.

2.3 Literature reviews

2.3.1 Mannan and its potential in targeting and maturation of dendritic cells (DCs)

In recent years, researches involving vaccine delivery and targeting dendritic cells (DCs) have gained much attention. It has been well-known that DCs play an important role as mediators between innate and adaptive immunity. In connection with DC-based vaccine, DCs have been the most effective antigen presenting cells (APCs) for specific stimulation prime naïve T cells in accordance with the presented antigen [61]. However, the drawback of DC-based vaccines is the insufficiency of stimulation and maturation of DCs. Therefore, targeting DCs should be firstly focused.

Comprehensive studies in targeting DCs have been devoted in the past years. As immature DCs membrane is composed of several types of receptors, such as C-type lectin receptors (CLRs), mannose receptor (MR), Dec-205 receptor, etc., exploring substances used as a specific targeting moiety to one of those receptors is a necessity [62]. One of the most interesting compounds is carbohydrate which can be specifically recognized by CLRs. Carbohydrate adjuvants have become more popular

as they can be found naturally. In 2010, Yu and co-workers [63] demonstrated the role of mannan used as targeting molecules. In this work, cationic solid lipid nanoparticles (SLNs) were used as a DNA cargo. However, DNA-loaded SLNs lacked DCs targeting ability. Therefore, mannan-grafted L- α -phosphatidylethanolamine (mannan-grafted PE) was synthesized and utilized as a targeting moiety. It should be noted that mannan in this work was not obtained from natural resources. Figure 2.19 exhibits percentage of gene expression of macrophages stimulated by different particles. As a result, mannan-coated SLN-DNA expressed high percentage due to the targeting ability of grafted mannan coated on nanoparticles surface.

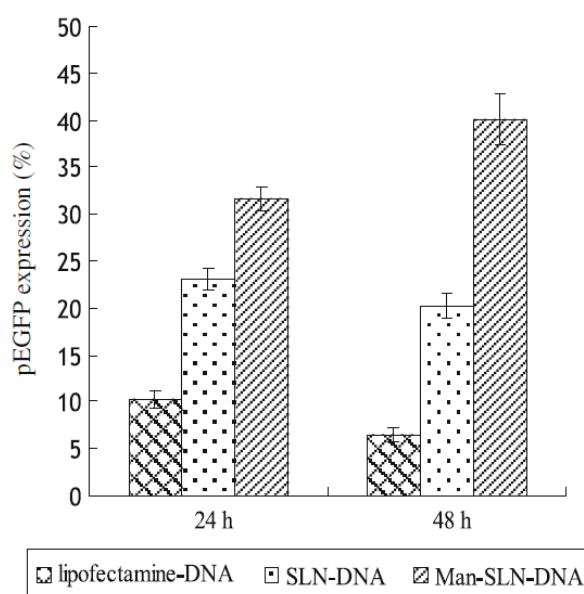


Figure 2.19 Gene expression results from macrophages stimulated by different particles, lipofectamine-DNA, SLN-DNA, and Man-SLN-DNA [63].

In 2011, mannan-decorated PLGA particles through covalent and physisorption interactions were prepared, and the degree of cellular uptake according to different attachment strategies of mannan was determined by Ghotbi's group [64]. The cellular uptake results were under evaluation by flow cytometry and confocal microscopy as shown in Figure 2.20a and 2.20b, respectively. From the results, it can be concluded that the high degree of cellular uptake can be acquired by both covalent and physical adsorption interactions of mannan and PLGA particles.

However, there was higher content of mannan covered on PLGA surface via covalent bond than physical adsorption. Nonetheless, this work also suggested the benefit of using mannan to specifically target DCs, irrespective of mannan attachment methods.

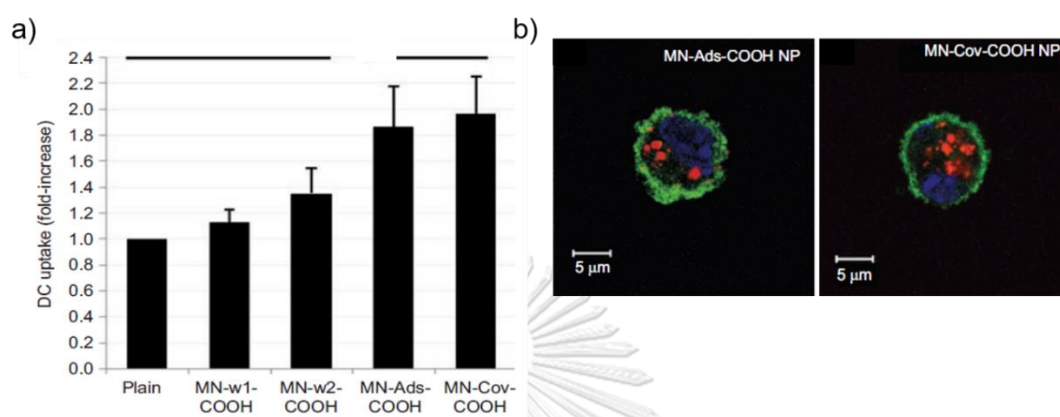


Figure 2.20 Cellular uptake assessed by a) flow cytometry b) confocal microscopy of mannan-coated PLGA nanoparticles via physical adsorption and covalent interactions [64].

Other than the advantage of using mannan as a targeting moiety, some reports have demonstrated that mannan can also induce maturation of DCs. Maturation of DCs can be determined by the upregulation of surface maturation markers (i.e. CD40, CD86). In 2014, Haddadi and co-workers [29] synthesized mannan-coated PLGA nanoparticles. Different terminated functional groups of PLGAs, ester and carboxylic groups, were used to modify with mannan through physical adsorption and covalent conjugation. The surface markers of DC maturation were assessed using a flow cytometry. Figure 2.21a and 2.21b display the DC-histograms showing the upregulation of CD86 and CD40, respectively. As a result, conjugated mannan via covalent bond with COOH-PLGAs provided the highest surface markers content in both CD86 and CD40 compared to the rest particles. Comparably, mannan-coated particles through physical adsorption (MN-Ads-COOH) also gave comparable amount of upregulated surface markers to covalent one (MN-Cov-COOH). Notably, in this work, soluble mannan was also compared to particulate formulations. As a result, particulate mannan (MN-Cov-COOH) containing 6.9 μg/mL of mannan can upregulate

43% of CD86, while only 32.6% can be expressed by the stimulation of soluble mannan at high concentration (150 $\mu\text{g}/\text{mL}$). This outcome strongly suggested that particulate mannan outperformed soluble form of mannan.

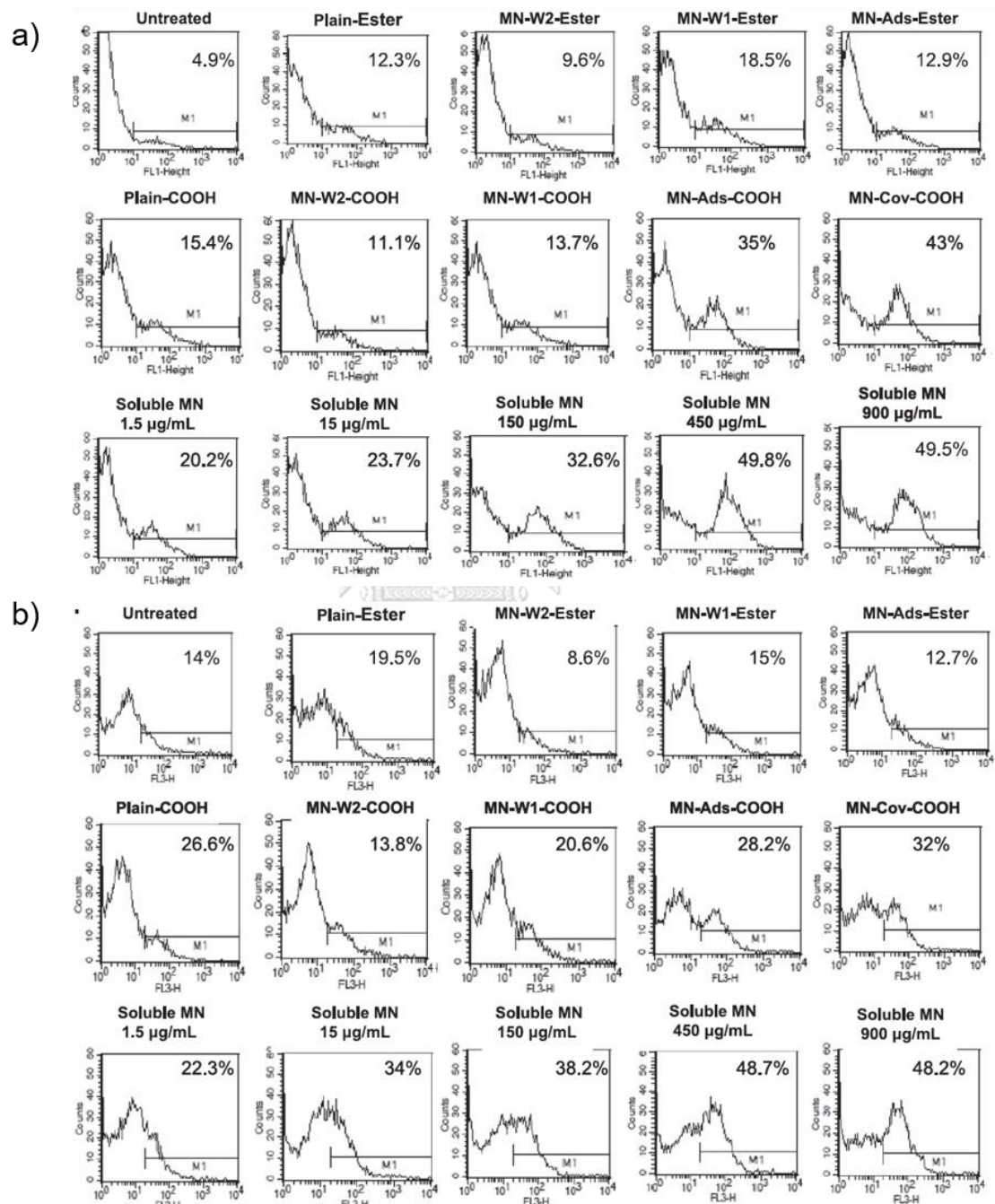


Figure 2.21 DC-histograms showing the effect of mannan formulations to the upregulation degrees of DC maturation markers a) CD86 and b) CD40. The expression of surface markers was assessed by flow cytometry [29].

As abovementioned, DCs are key factors in stimulating and regulating immune responses. Therefore, researches focusing on targeting and maturation of DCs are of great interest. Mannan, classified as carbohydrates, can be found naturally. It is one of interesting substances which can play a significant role in improvement of DCs targeting ability. Also, some works have already demonstrated that mannan is a good adjuvant by improving DCs maturation. However, soluble form of mannan has not shown a satisfactory result compared to the particulate one. Therefore, fabricating particulate mannan has become our interest. In this regard, there are many works synthesizing nanocomposites of mannan and organic materials, for instance, PLGAs, chitosan, solid lipid nanoparticles. Although organic materials are shown to be biocompatible, physical stability and ability to control size and shape are still of concern. Consequently, establishment of an efficient particulate mannan by incorporation of inorganic substances for targeting and maturing DCs is our purpose.

2.3.2 Silica nanoparticles and biocompatibility study

When nanomaterials are applied in biomedicine application, biocompatibility of such nanoparticles is one of the most important factors which must be primely obtained attention. Once nanoparticles are administered into a body, the nanoparticles are non-specifically subjected to biological environments. The non-specific interactions between biological systems and foreign nanoparticles can hinder efficacy of therapeutic agents.

For over decades, silica-based nanoparticles have been chosen as one of the most popular nanomaterials used in biomedical applications as they are non-toxic and biocompatible nanomaterials. There are several studies assessing the biocompatibility of silica-based nanoparticles. For instance, in 2012, Malvindi and co-workers [65] investigated the size and charge effects of silica nanoparticles towards cell viability. In this work, three different sizes of 25, 60, and 115 nm silica nanoparticles with negative and positive charges were proven to be non-toxic towards five types of cells line (i.e. A549, Hela, Caco-2, Jurkat, and U937 cells) at 48 h and 96 h. The bar graphs in Figure 2.22 demonstrated the cell viability of stimulated cells with 25 nm silica nanoparticles containing different surface charges and

concentrations. As a result, there is no significance of cell death regarding to charges and concentrations. It should be noted that the result from silica particles of other sizes (not shown) also demonstrated the same outcome in cell viability test. Therefore, this work suggested that silica nanoparticles are biocompatible and safe to use in biological field.

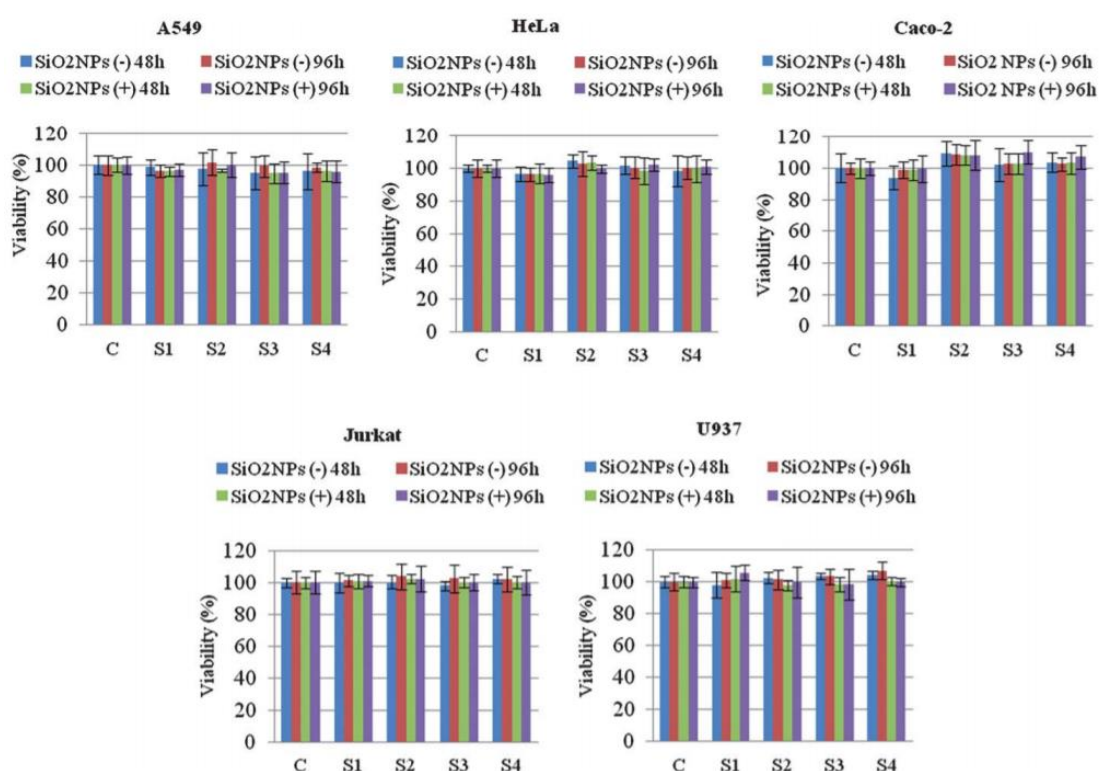


Figure 2. 22 Cell viability of A549, Hela, Caco-2, Jurkat, and U937 cells incubated with 25 nm silica nanoparticles with different charges (negative and positive charges) and concentrations (S1: 2.5 pM, S2: 25 pM, S3: 250 pM, S4: 2500 pM) at 48h and 96h.

Although some studies suggested that silica nanoparticles are safe to use in biological applications, there are some controversial works. For example, in 2013, Chiriaco and co-workers [66] demonstrated that biocompatibility of silica nanoparticles was dependent of doses, sizes and exposure time. The study of cell viability of MCF-7 cells via MTT assay showed that cell viability percentage was significantly decreased according to the increasing doses, sizes and exposure times

(Figure 2.23a - 2.23c). However, biocompatibility of silica nanoparticles could be improved by PEGylated silica nanoparticles as shown in Figure 2.23d. As a result, this work suggested the possibility to reduce toxicity of silica nanoparticles which could be achieved by coating silica surface with biocompatible substances.

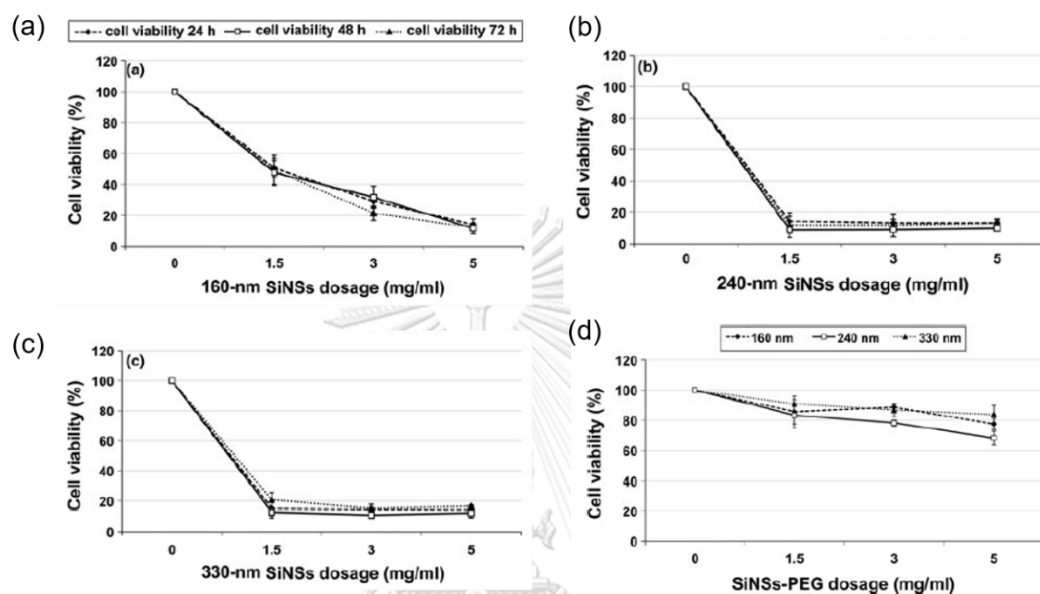


Figure 2.23 Cell viability of MCF-7 cells incubated with different sizes (160, 240, and 330 nm) and doses (1.5, 3, and 5 mg/mL) of plain and PEGylated silica nanoparticles at various times (24, 48, and 72 h).

Moreover, in 2017, biocompatibility of nanocomposites of silica and magnetic iron oxide was also investigated by Foglia and co-workers [67]. Magnetic iron oxide with size of 3 nm was firstly prepared and consecutively coated with silica shell. Then, fluorescence dye FITC was covalently attached on the silica shell. The biocompatibility of the nanocomposites was evaluated by assessing cell proliferation and cell viability of Caco-2 cells through BrdU incorporation assay and WST metabolic activity, respectively. The cells were incubated with the nanocomposites at different concentrations and various time points. The results are shown here in Figure 2.24. The researchers found that the nanocomposites of silica and magnetic nanoparticles were biocompatible. For cell proliferation result, the proliferation rate of all concentrations was constantly increased in the same manner as a control

group. The result of cell viability was also consistent with cell proliferation outcome as there was no significant cell death observed in all concentrations of nanocomposites compared to the control one. Therefore, the researchers concluded that their synthesized nanocomposites of silica and magnetic nanoparticles attached with fluorescence FITC dye were non-toxic and suitable for used in biomedicine applications.

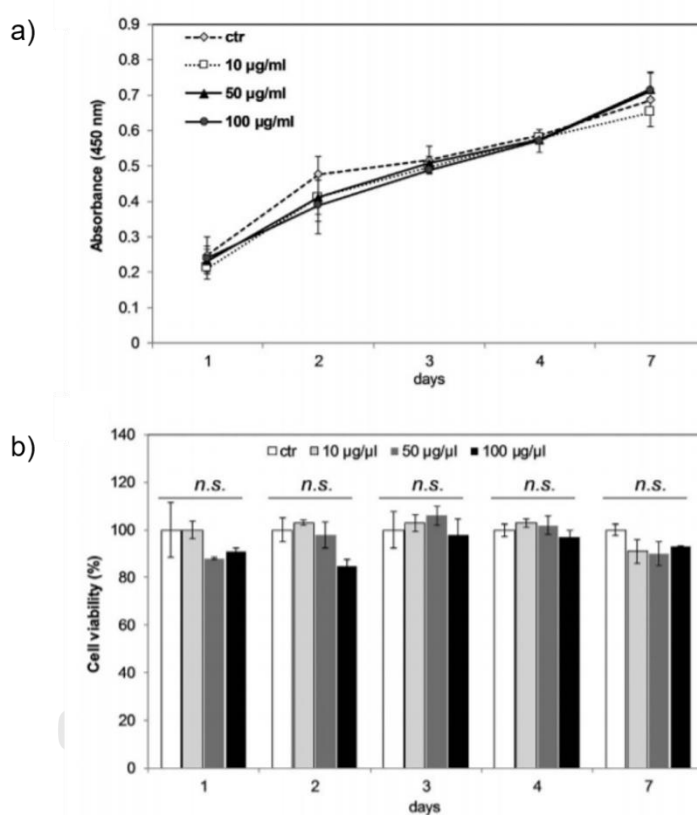


Figure 2.24 The results of a) cell proliferation, and b) cell viability of Caco-2 cells incubated with nanocomposites of silica and magnetic nanoparticles at 24, 48, 72, 96 h and 7 days at different concentrations (i.e. 10, 50, 100 µg/mL).

It is well-known that silica nanoparticles can be easily tuned in sizes and readily functionalized with other chemicals to provide multifunctional silica nanoparticles. Amino-functionalized silica nanoparticles are ones of the most desirable products as they can be further covalently coupled to other substances containing carboxylic groups, such as proteins, polymers, carbohydrates, through

amide bond formation. Therefore, in 2019, biocompatibility of plain and amino-functionalized silica nanoparticles with different degrees of amino group coverage were systemically investigated by Hsiao's group [68]. In addition to the effect of surface functionalization of silica nanoparticles, the researchers also studied the effect of serum protein to the biocompatibility of modified silica nanoparticles because the nanoparticles will be administered into bloodstream *in vivo* study. Thus, the impact of serum to the fate of nanoparticles should be of concern. In this work, they found that both plain and functionalized silica nanoparticles caused cell death dependent on doses in the absence of serum as shown in Figure 2.25a. This incident was due to strong cellular membrane interaction between nanoparticles and cell membrane. However, in the presence of serum, the cell viability (shown in Figure 2.25b) was significantly risen. The formation of protein corona can diminish cellular interaction and the nanoparticles can subsequently be internalized without causing cell membrane rupture. These findings implied that exposing amino or silanol groups to cells could be an issue in biocompatibility. Therefore, to avoid such a problem, further functionalization via amide bond formation could be an alternative way to reduce toxicity.

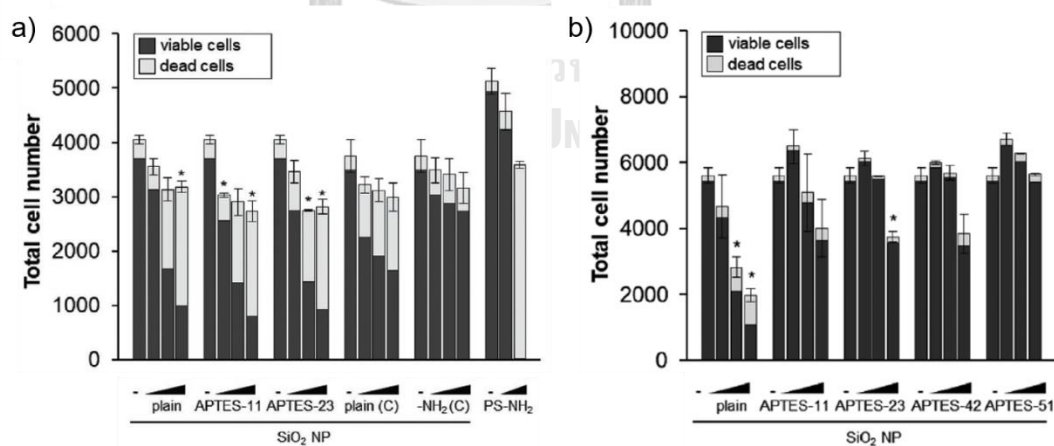


Figure 2.25 Cell viability of RAW 264.7 macrophages incubated with increasing doses of plain and amino-functionalized silica nanoparticles with different degrees coverage of amino groups in a) the absence of serum and b) in the presence of serum.

2.3.1 Superparamagnetic nanoparticles used in biomedical applications

In recent years, superparamagnetic nanoparticles (SPIONs) have been widely applied in biological applications, such as hyperthermia treatment, diagnostic agents, and therapeutic delivery platform [69-72], owing to their favorable biocompatibility and biodegradability.

Despite the advantage of superparamagnetism, the assembly of magnetic nanoparticles can be a burden. Small SPIONs possess high surface energies causing the aggregation and consequently loss of superparamagnetism [73]. Thus, stabilizing SPIONs with other biocompatible materials can be an alternative way to protect magnetic property and make them biocompatible. SPIONs can be incorporated with other materials in different manners, such as surface coating with inorganic and organic materials, encapsulating inside polymer shell, as displayed in Figure 2.26 [74].

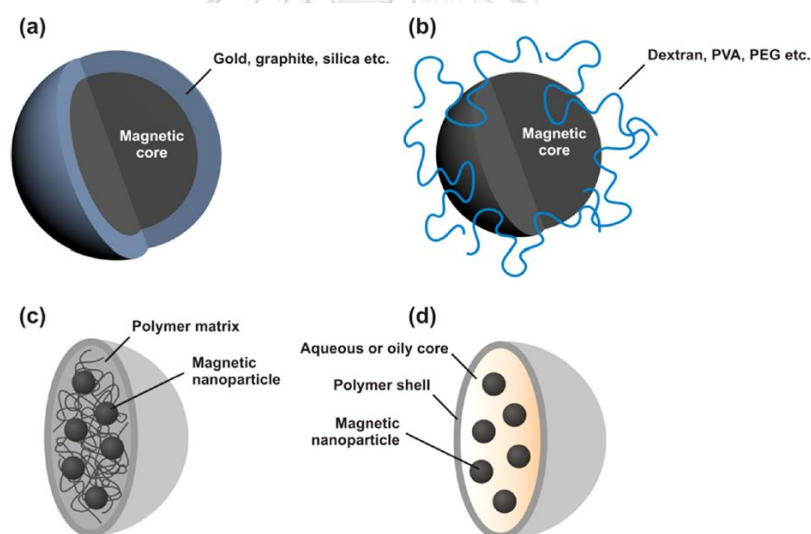


Figure 2.26 Depiction of surface coating of SPIONs by a) inorganic materials, b) organic materials and encapsulation of SPIONs inside c) nanospheres, d) nanocapsules [74].

Due to remarkably superparamagnetic character, SPIONs have been widely exploited in biomedicine as a non-invasive method. Herein, enhancement of cells targeting by SPIONs nanocomposites will be focused. For example, in 2017, Huang and co-workers [75] synthesized water-dispersible SPIONs nanocomposites

conjugated with folic acid (FA) for cancer cells targeting. FA was used as a targeting motif. Schematic representation of the synthesis of SPIONs co-conjugated with poly(ethylene glycol) (PEG) and polyethylenimine (PEI) nanocomposites were shown in Figure 2.27a. Figure 2.27b displayed the scheme showing magnetically targeting aid of SPIONs nanocomposites by an induction of an external magnetic field. Under the induction of a magnetic field, the fabricated nanocomposites showed an enhancement of targeting ability compared to the particles without using an external magnet. However, only confocal microscopy images were used to explain the improvement of targeting ability (Figure 2.28). In another word, particles with magnetically aid in drug delivery (DOX@FA-SPIONs + MF) from confocal images might not show a clear result compared to the particles in the absence of an external magnet (DOX@FA-SPIONs). Thus, statistical data of cellular uptake may be required.

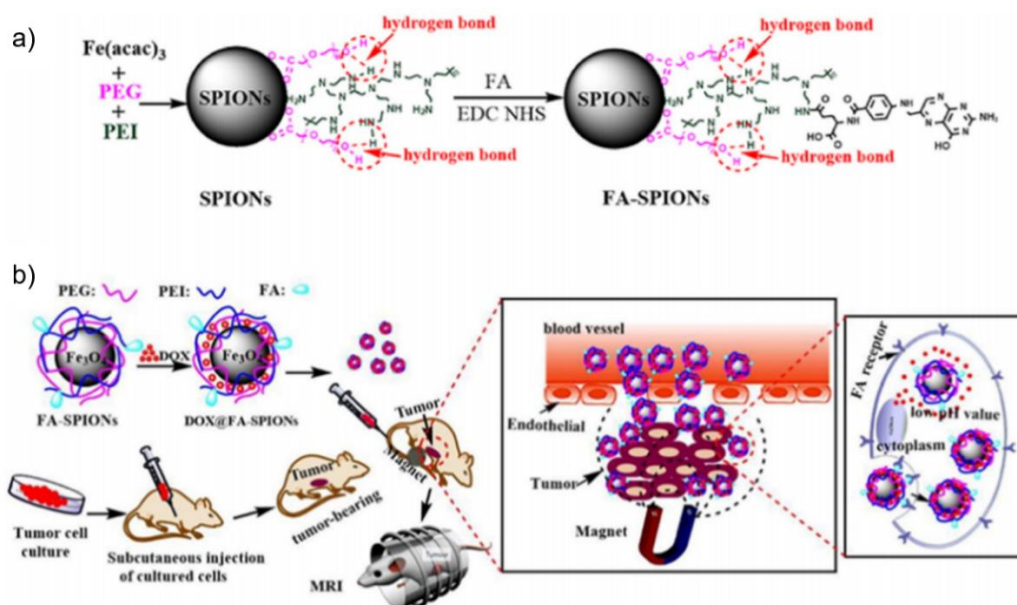


Figure 2.27 Schematic representation of a) the synthesis of nanocomposites of water-dispersible SPIONs and b) the aid of an external magnetic field in targeting cancer cells [75].

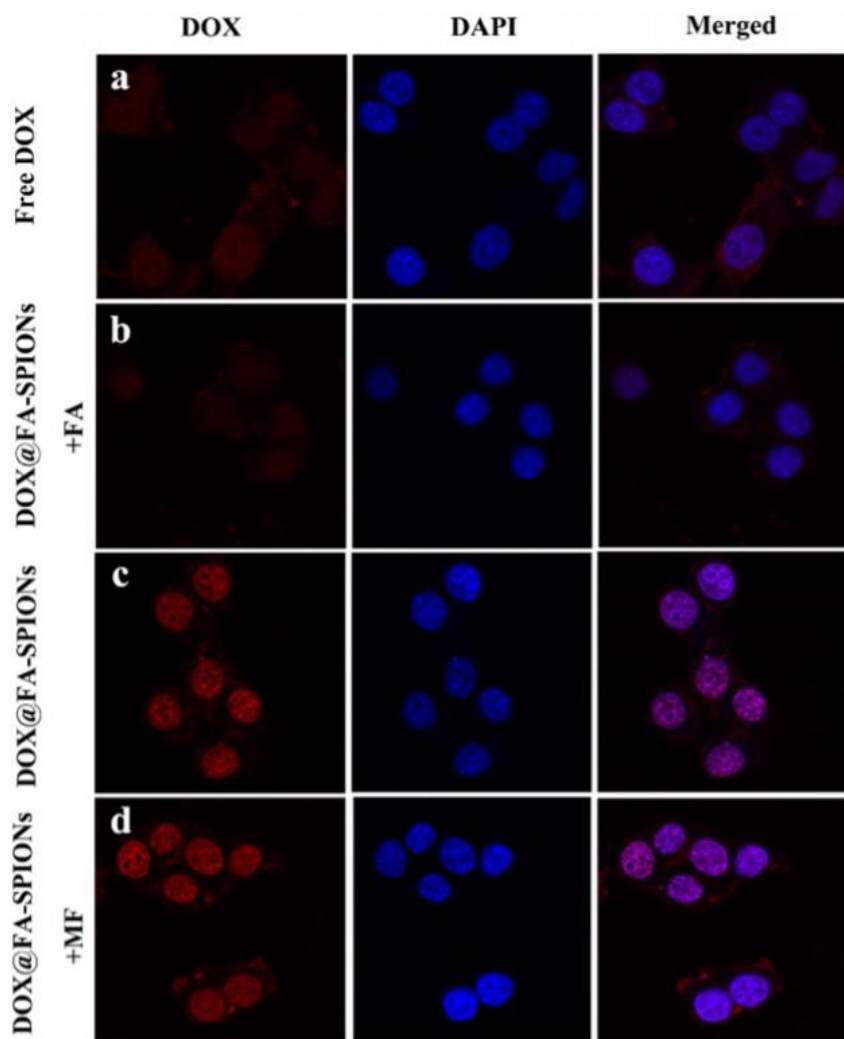


Figure 2.28 Confocal microscopy images of MCF-7 incubated with different particles for 1 h a) free DOX, b) incubating cell with free FA prior to the addition of DOX@FA-SPIONs, c) DOX@FA-SPIONs without magnetically aid, d) DOX@FA-SPIONs with magnetically aid [75].

In addition, reaching targeted DCs under an external magnetic field is achievable. Chalathan and co-workers [72] demonstrated the benefit of using superparamagnetic nanoparticles as an important tool for cell targeting. In this work, the researchers produced composites of PLGAs and SPIONs with two different sizes (300 nm and 500 nm) as an antigen delivery platform. Bovine serum albumin was used as a model antigen. As expected, the magnetized composites were well internalized by macrophages RAW264.7 and DCs, regardless of cell types, as shown in

Figure 2.29. Notably, large size of nanocomposites could be taken up by both cells more than small size nanocomposites as observed in confocal images shown below.

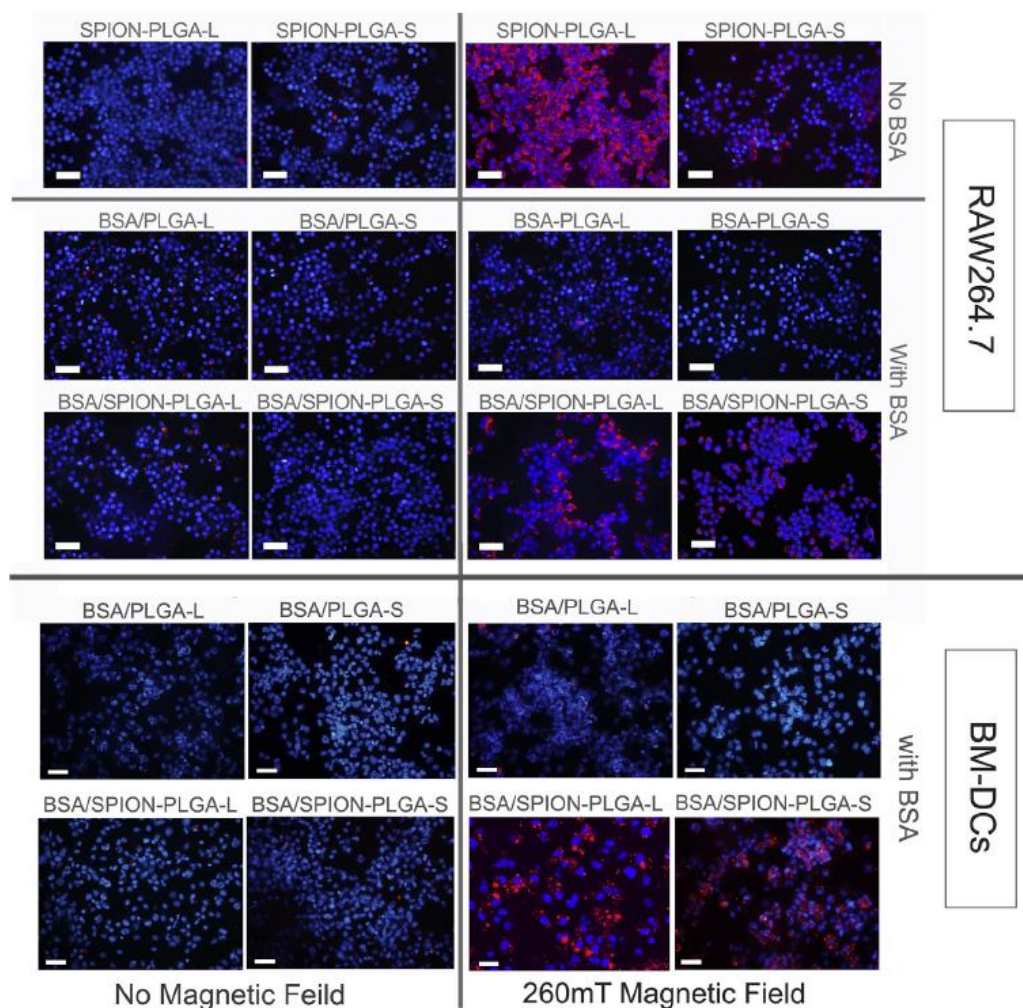


Figure 2.29 Cellular uptake of RAW264.7 and DCs incubated with different types of nanoparticles for 3 h in the absence and presence of magnetic field [72].

Recently, in 2019, using SPIONs in biomedical purpose has still maintain its reputation. Fang and co-workers [76] produced nanocomposites of inorganic materials, mesoporous silica and SPIONs, as a targeted drug delivery platform. Besides, hyaluronic acid was conjugated as a cancer cell targeting molecule. The scheme in Figure 2.30 exhibits the outlook of this work. The purpose of using SPIONs in this work is slightly different from others. Under an induction of external magnetic

field, the retention of magnetic nanocomposites in tumor microenvironment could be prolonged, rendering nanocomposites increase their therapeutic efficacy.

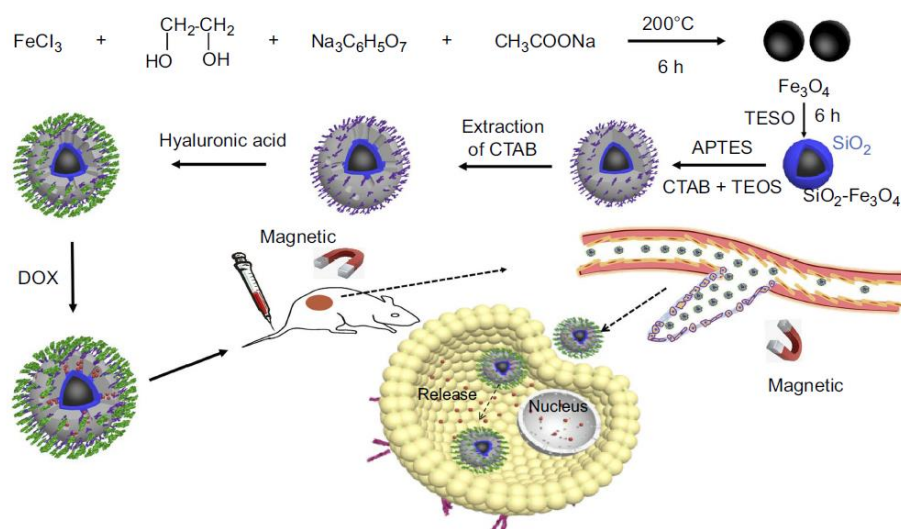


Figure 2.30 Schematic representation of the synthesis of hyaluronic acid-conjugated mesoporous silica-SPIONs and its application in targeted drug delivery [76].

As shown in literature reviews, SPIONs can be applicable in different purposes (e.g. cell targeting, maintaining therapeutic agents at specific sites, etc.). Therefore, some factors, such as biocompatibility, size and targeting capability of magnetic-based nanocomposites, must be considered in order to reach high efficacy.

In this thesis, the researcher focused on fabricating nanocomposites which can enhance DCs targeting ability and the degree of DCs maturation as it can be a valuable candidate in vaccine adjuvants. Thus, favorable size for DCs uptake must be firstly taken into account to achieve an efficient cellular internalization. Reportedly, the size of 500 nm or below is desirable for DCs uptake [77]. Hence, nanomaterials with size tunability in concerted with capacity to provide high stability for small SPIONs are assumed to be a good candidate for the targeting and activation of DCs.

According to literature reviews, one of the most versatile materials used in biological studies, which shows potential in preventing the aggregation of magnetic nanoparticles, is silica nanoparticle. As support materials, silica nanoparticles have

been well-known for their biocompatibility, low toxicity, ease of fabrication with tunability in sizes, and variety in surface functionalization [78]. Thanks to those features, silica nanoparticles have been extensively reported as silica-based nanostructures for a wide range of biomedical applications [79-81].

Therefore, herein, I am interested in the synthesis of multifunctional nanocomposites of silica-magnetic nanoparticles-mannan (S-SPION-MN) as an adjuvant. The nanocomposites of silica and SPIONs are assumed to be collectively stable. In concerted with mannan modification, the synthesized nanocomposites would be biocompatible. Moreover, incorporation of mannan and SPIONs would synergistically enhance targeting ability of the particles and subsequently be able to elicit strong immune responses of the targeted DCs.



CHAPTER III

EXPERIMENTS

According to the experimental studies, the experiments are categorized into three sections. The first section shows the list of chemical and biological reagents used in this work. All instruments are also listed in this topic. In the second part, the synthesis of nanocomposites of silica-SPIONs-mannan (S-SPION-MN) is described. Finally, the last section is composed of characterizations and biological studies of the synthesized particles.

3.1 Lists of instruments, chemical and biological reagents used in this study

All instruments involved in characterizations and investigations of the synthesized S-SPION-MN nanocomposites are listed below in Table 3.1.

Table 3.1 List of instruments

Instruments	Model
X-ray Powder Diffraction Spectrometer (XRD)	DMAX2200/Ultima ⁺ (Rigaku)
Transmission Electron Microscope (TEM)	Tecnai F20 (Philips Electron Optics)
Inductively Coupled Plasma-Optical Emission Spectrometer (ICP-OES)	Perkin Elmer Optima 2100
Field-Emission Scanning Electron Microscope (FESEM)	JSM7610F (JEOL)
Centrifuge	Centaur 2 (Sanyo)
Magnetic Stirrer	MS 101 (Gem)
Vibrating-Sample Magnetometer (VSM)	LakeShore Model 7404
Particle Size Distribution Analyzer (ZSP)	Malvern, Instruments Ltd, UK
Microplate Reader	Epoch 2 Microplate Reader, VT, USA
Fluorescence Microscope	BX50 (Olympus)
Flow Cytometric Analysis (FACS)	FACS Calibur TM (BD Bioscience)

For the synthesis of nanocomposites of S-SPION, SPION-MN, the chemicals used in the syntheses and biological studies are listed in Table 3.2.

Table 3.2 List of chemicals

Chemicals	Suppliers
Tetraethyl orthosilicate (TEOS, 98%)	Aldrich
ammonium hydroxide (NH ₄ OH; 25%)	Merck
ethanol (EtOH, AR grade)	RCI Labscan
3-aminopropyltriethoxysilane (APTES, ≥ 98%)	Aldrich
iron (III) acetylacetonate (Fe(acac) ₃ , 97%)	Aldrich
N-hydroxysuccinimide (NHS, 98%)	Aldrich
N-(3-Dimethylaminopropyl)-N'-ethylcarbodiimide hydrochloride (EDC, ≥ 98%)	Sigma-Aldrich
fluorescein isothiocyanate (FITC, > 90%)	Sigma
hexane (AR grade)	RCI Labscan
sulfuric acid (H ₂ SO ₄ , 98%)	RCI Labscan
phenol (≥ 96%)	Sigma-Aldrich
Tetraethylene glycol (TEG, > 95%)	TCL
Dimethyl Sulfoxide (DMSO, 99.9%)	VWR Amresco
Bovine serum albumin (BSA. Fraction V, protease-free grade)	VWR international
4',6-Diamidine-2'-phenylindole dihydrochloride (DAPI, > 90%)	Sigma
CellMask Deep Red Plasma Membrane Stain	Invitrogen
Poly-L-lysine hydrobromide (cell culture grade)	Sigma
Paraformaldehyde (95%)	Sigma
<i>Saccharomyces cerevisiae</i> mannan	Research Unit in Integrative Immuno-

	Microbial Biochemistry and Bioresponsive Nanomaterials, Chulalongkorn University
--	--

Biological reagents used in cell studies, including cell culture, cytotoxicity test, cellular internalization, cell stimulation and maturation, are included in Table 3.3.

Table 3.3 Biological reagents

Biological reagents	Suppliers
Roswell Park Memorial Institute medium (RPMI 1640)	Gibco™ Life Technologies
Sodium pyruvate	Gibco™ Life Technologies
Glutamax	Gibco™ Life Technologies
Fetal bovine serum (FBS)	Gibco™ Life Technologies
Penicillin-streptomycin	Gibco™ Life Technologies
ELISA kits	Biologend
Purified anti-mouse CD16/32 monoclonal antibody (mAb)	Biologend
PerCP/Cy5.5-labeled anti-mouse I-A/I-E mAb	Biologend
FITC- labeled anti-mouse CD80 mAb	Biologend
APC- labeled anti-mouse CD11c mAb	Biologend
PE- labeled anti-mouse CD86 mAb	eBioscience
TWEEN® 20 for molecular biology	VWR Amresco
(3-(4,5-Dimethylthiazol-2-yl)-2,5-diphenyltetrazolium bromide) (MTT)	Invitrogen

3.2 Synthesis of nanocomposites

3.2.1 Synthesis of nanocomposites of silica-superparamagnetic nanoparticles (S-SPION)

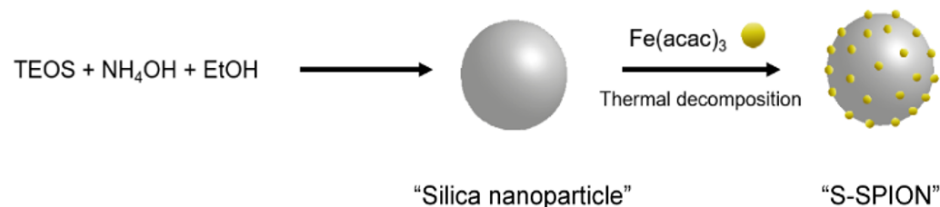


Figure 3.1 Depiction of the synthesis of S-SPION nanocomposites.

Figure 3.1 displayed the schematic representation of the synthesis of S-SPION nanocomposites. Firstly, silica nanoparticles were fabricated following Stöber method as reported by Nozawa and co-workers [82]. Briefly, EtOH (50 mL) and NH_4OH (9.5 mL) were mixed and designated as Solution A. Then, Solution B was prepared by mixing TEOS (5 mL) and EtOH (30 mL). Subsequently, Solution B was added dropwise into a stirring Solution A with the dropping rate of 1 mL/min. The colorless mixture was then turned white and turbid. The reaction mixture was continuously stirred at room temperature for 24 h. The product was washed with EtOH until the pH reached 7 and collected by centrifugation (8000 rpm, 5 min). Then, the materials were dried overnight in a 60°C oven.

Secondly, the nanocomposites of silica-superparamagnetic nanoparticles (S-SPION) were *in situ* synthesized following a procedure previously reported [83]. The obtained silica nanoparticles (200 mg) were dispersed in deionized (DI) water by sonication before added into a 250 mL round-bottom flask containing x mg of Fe(acac)_3 (x = 10, 20, 60, and 180 mg) and TEG (10 g). Subsequently, temperature program was performed following to the diagram in Figure 3.2. The mixture was heated to 110 °C under vacuum for 1 h to remove small traces of water, and it was then heated up to 210 °C under N_2 atmosphere for 2 h. This step allows the formation of nuclei and subsequent growth of nanoparticles. Next, the temperature was increased to 300 °C under air for 1 h to allow produced nanoparticles partially oxidized and then cooled down to room temperature. Finally, the mixture was

washed with acetone to remove unbound magnetic nanoparticles. The water dispersible product was then obtained. The synthesized nanocomposite was designated as S-SPION.

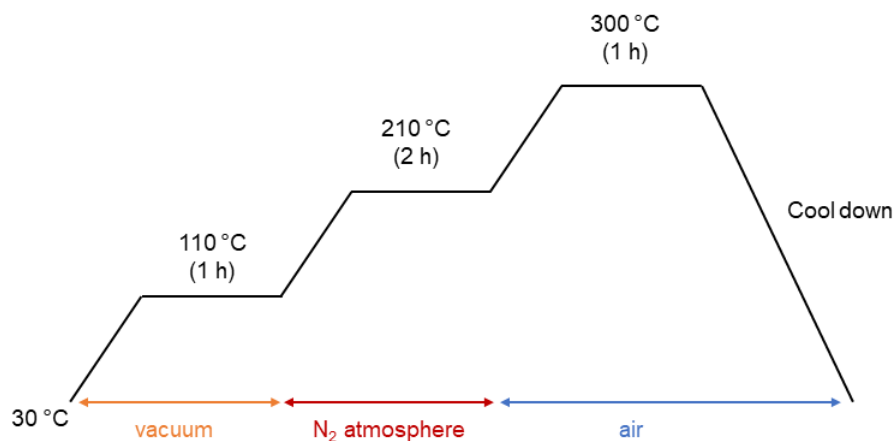


Figure 3.2 Temperature program used to fabricate S-SPION nanocomposites.

3.2.2 Preparation of nanocomposites of S-SPION and mannan (S-SPION-MN)

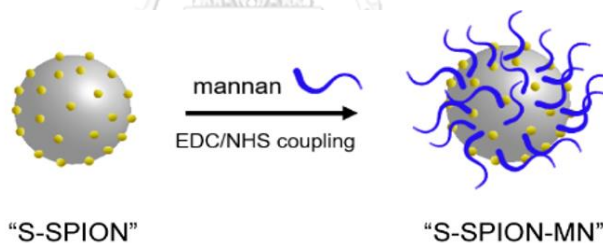


Figure 3.3 Schematic representation of the synthesis of S-SPION-MN nanocomposites.

The overview of the synthesis of S-SPION-MN is presented in Figure 3.3. Amino-functionalization surface was firstly done as followed. S-SPION (150 mg) was sonicated in hexane (10 mL) for 10 min. Then, APTES (200 μ L) was added into the solution of S-SPION and further sonicated for 1 h. S-SPION-NH₂ was then obtained. Secondly, S-SPION-NH₂ (100 mg) was dispersed in DI water (8 mL) and subsequently added into a mixture of solution containing mannan (30 mg of extracted mannan/ 2 mL of DI water), EDC (50 mg), and NHS (40 mg). The mixture was vigorously stirred at room temperature for 24 h. It was then washed with DI water, and the supernatant

was collected and kept at 4 °C for mannan loading assessment. The final product of S-SPION-MN was kept at 4 °C.

It is noteworthy that mannan in this work was naturally obtained from the extraction of *Saccharomyces cerevisiae*. The extraction protocol was followed by published work by Nguyen and co-workers [26]. Assumedly, the structure of extracted mannan is likely to have the same structure as MNN1 shown in Figure 3.4. In addition, the extracted mannan possesses molecular weight of 10kDa according to the previous published work [26].

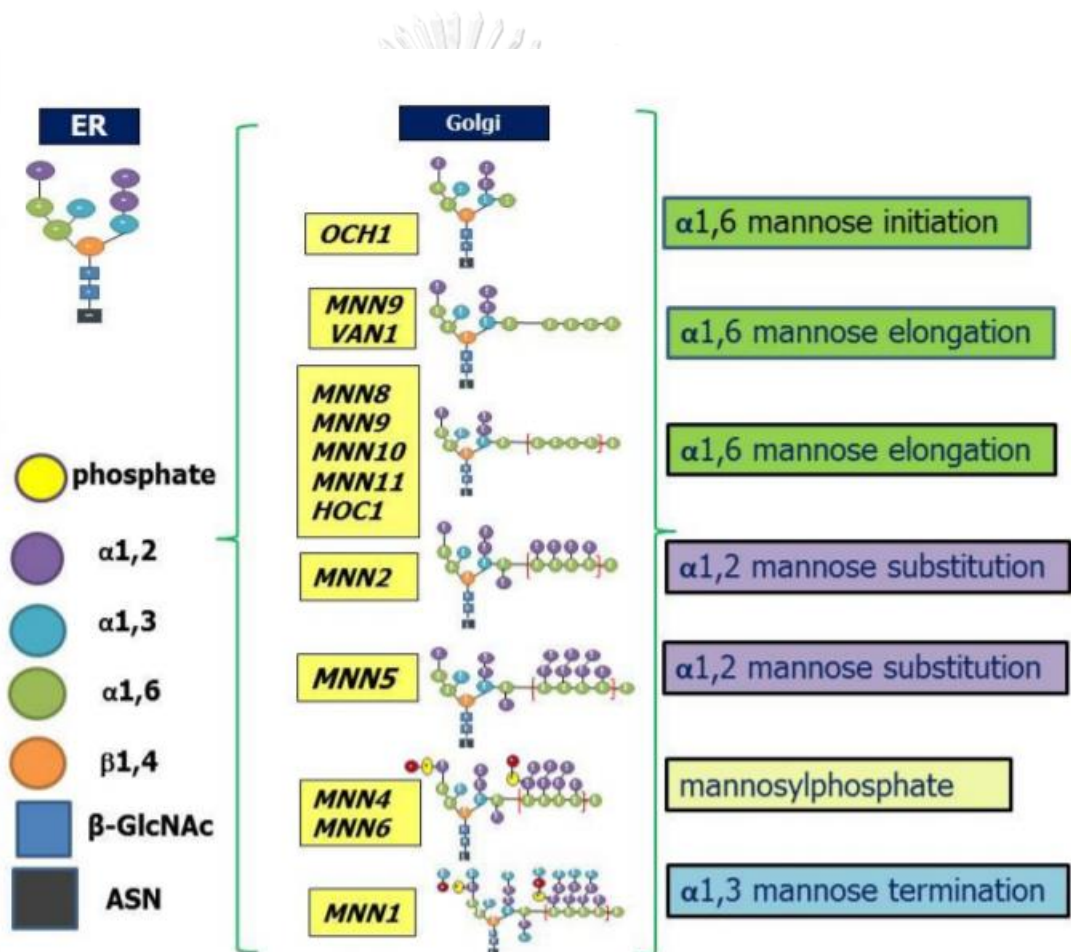


Figure 3.4 Mannan structures in fungal cell wall [84].

3.3 Materials characterizations and biological studies of synthesized S-SPION, and S-SPION-MN nanocomposites

3.3.1 Physical characterizations

Morphology of prepared nanocomposites was characterized using a field emission scanning electron microscope (FESEM) (JSM7610F, JEOL, Japan). The magnetite character was also verified using x-ray powder diffraction spectrometer (XRD) (DMAX2200/Ultima-plus instrument, Rigaku, Japan). In addition, the magnetic response was evaluated at room temperature using an in-house developed vibrating sample magnetometer (VSM) (Lakeshore, USA). To measure the amount of iron in nanocomposites of S-SPION, an inductively-coupled plasma optical emission spectrometer (ICP-OES) (Perkin Elmer Optima 2100) was applied. Moreover, mannan attachment was also confirmed by a zetasizer (Malvern, Instruments Ltd, UK) to evaluate the zeta potential and size distribution of the modified particles, S-SPION-MN.

3.3.2 SPIONs and mannan loading content

Iron-loading content of the synthesized S-SPION particles was determined by an inductively-coupled plasma optical emission spectrometer (ICP-OES) (Perkin Elmer Optima 2100). For the sample preparation, the sample was firstly dissolved in 37% hydrochloric acid for 15 min. Then, it was diluted with DI water and subsequently filtrated with 0.2 μm nylon syringe filter (VertiClean™).

The attached mannan was investigated using a colorimetric assay of sulfuric acid-phenol method [64]. Principally, H_2SO_4 could digest mannan into monosaccharides and later reacted with phenol producing a furfural compound, which provided a yellowish-brown color mixture. Thus, a direct determination of mannan on S-SPION particles would be a problem due to interfering color from the digested iron. For solving this problem, measurement of unattached mannan in supernatant was performed. The total amount of attached mannan on particles can be estimated from the difference in concentration of mannan in supernatant before and after loading. Briefly, concentrated H_2SO_4 (300 μL) was rapidly added in a collected supernatant (150 μL) and followed with the addition of 5% phenol (60 μL).

The mixture was then heated at 90 °C for 5 min to allow for color development. Then, the absorbance at 490 nm was measured using a microplate reader (Epoch 2 Microplate Reader, VT, USA). Notably, mannan with high molecular weight might not be completely digested. Thus, in this work, serial dilution was performed. In addition, glucose solution with different concentrations was chosen as a standard solution so the content of digested mannan could be directly evaluated from the standard solution.

3.3.3 Cell culture

Murine bone marrow-derived dendritic cells (BMDCs) were prepared following previous reports [72, 85]. All animal procedures were approved by an Institutional Animal Care and Use Committee (IACUC) of Faculty of medicine, Chulalongkorn University (021/2562). Briefly, bone marrow cells were isolated from femurs and tibias of 6-week old BALB/c female mice and seeded at the concentration of 1×10^6 cells in 24-wells plates. The bone marrow cells were cultured in RPMI supplemented with 10% FBS, 100 U/ml penicillin and 100 mg/mL streptomycin, 0.2 mM Glutamax, 10 ng/mL recombinant murine GM-CSF (Peprotech, NJ, USA) and 10 ng/mL recombinant murine IL-4 (Peprotech, NJ, USA). The cells were cultured at 37 °C incubator with 5% CO₂ for 7 days.

3.3.4 Cytotoxicity

Synthesized particles were tested for cytotoxicity using MTT assay. Briefly, BMDCs were seeded in a 96-well plate with the concentration of 2×10^5 cells/well in RPMI media. The cells were exposed to the prepared particles and soluble mannan with different concentrations at various times. Then, 12 mM MTT (3-(4,5-dimethylthiazol-2-yl)-2,5-diphenyltriazolium bromide) (Invitrogen, CA, USA) was added into the culture, and were then incubated at 37 °C for 2 h. Finally, the cells were washed with PBS, and DMSO was added to the cells to dissolve the formazan crystal. Subsequently, the optical density of the mixture was determined at 570 nm using a microplate spectrophotometer (Epoch, Biotek, VT, USA).

3.3.5 Cellular internalization

Firstly, S-SPION and S-SPION-MN particles were tagged with FITC. Briefly, FITC (1 mg) was dissolved in EtOH (2 mL). Synthesized particles (50 mg) were dispersed in DI water. Then, solution of FITC (200 μ L) was added to the mixture of prepared particles and continuously stirred for 24 h. The mixture was washed with DI water until fluorescence dye disappeared from the supernatant. At the end, the labelled particles were obtained.

For cells preparation, cover slips were coated with poly-L-lysine for 18 h in 12-well plates. Before adding BMDCs, coated cover slips were washed with PBS. Then, the cells, which were cultured in RPMI media, were added into a well with the concentration of 1×10^6 cells/mL. Subsequently, prepared particles were added into the cells and incubated for 15 min and 3 h. Then, the cells were washed with PBS and cell plasma membrane were stained with CellMask Deep Red (Invitrogen, CA, USA) for 5 min. The cells were fixed using 4% paraformaldehyde for 30 min at 4 °C. Nuclei were later stained with 30 nm DAPI (Invitrogen, CA, USA) for 5 min. Lastly, the stained cells were washed with PBS before they were observed under a fluorescence microscope (BX50 Olympus, Japan) with the $\lambda_{\text{ex/emit}}$ of 330/385 nm, 649/666 nm, and 522/535 nm for DAPI, CellMask Deep Red, and FITC, respectively.

3.3.6 Induction of dendritic cell maturation and cytokine secretion

BMDCs were stimulated with synthesized particles and soluble mannan with different concentrations under an external magnetic field for 3 h. After the magnetic field was removed, the cells were continuously incubated for the additional 24 h and 48 h. Then, BMDCs were collected and supernatants were kept for cytokine investigation. Maturation of the collected cells was evaluated by first blocking the cellular Fc receptor with anti-mouse CD16/32 mAbs, and then staining with fluorescence dye-labeled antibodies against murine CD11c, CD80, CD86 and MHC II. Unstimulated cells were used as a control. All stained cells were then subjected to a flow cytometric analysis (CytoFLEX, Beckman Coulter Inc., CA, USA), and analyzed by Kaluza analysis version 1.5a software (Beckman Coulter Inc., CA, USA).

For cytokine assessment, the levels of interleukin (IL)-6, IL1- β , interferon-gamma (IFN- γ), and tumor necrosis factor-alpha (TNF- α) in the collected supernatants were determined by ELISA method following to the Biolegend's protocol. The sandwich ELISA was performed using cytokine-specific capture and detection antibodies with streptavidin-horseradish peroxidase system. 3,3',5,5'-Tetramethyl benzidine (TMB) was used as a substrate. The absorbance was measured at 450 nm using a microplate spectrophotometer.



CHAPTER IV

RESULTS AND DISCUSSION

The production and biological assessment of nanocomposites that have a potential as good adjuvants were systemically studied, and the overall perspective of this work is graphically illustrated in Figure 4.1.

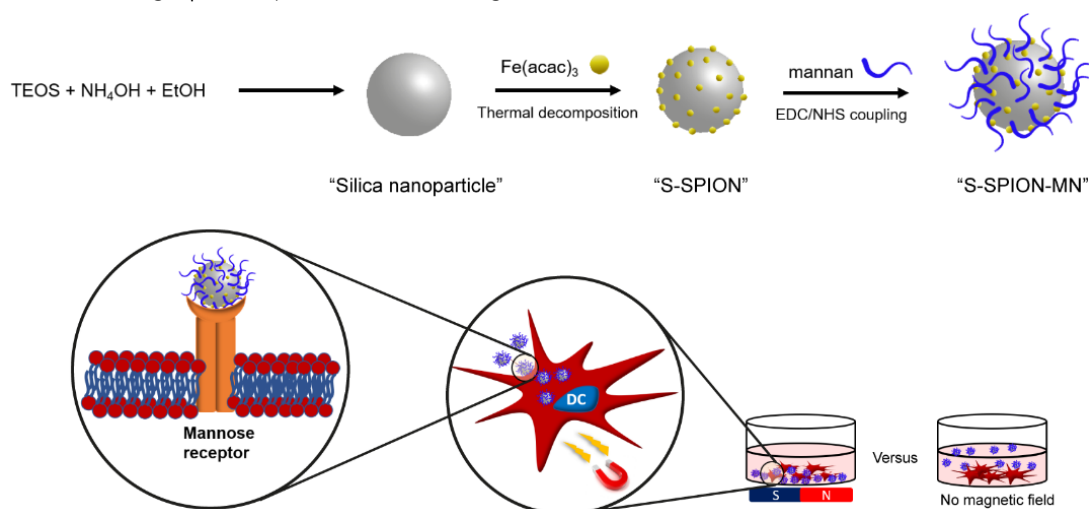


Figure 4.1 Schematic representation of the synthesis of S-SPION-MN and its benefit of magnetically aid in biological study.

Thus, all the results from materials characterizations and biological activities, such as cytotoxicity, cellular internalization, cell activation and maturation, of the synthesized nanocomposites are included in this chapter. Therefore, the following content in this chapter is divided into two sections (i.e. materials characterizations and biological activities). The discussion of the obtained results is also included.

4.1 Materials characterizations

4.1.1 Characterization of silica nanoparticles (SiNPs) and silica-magnetic nanoparticles (S-SPION) by FESEM and TEM

Firstly, silica nanoparticles (SiNPs) were synthesized following Stöber method. In order to study the effect of the size of the nanocomposites, silica nanoparticles with two different sizes were compared. Figure 4.2a and Figure 4.2b show FESEM

images of the synthesized silica nanoparticles with sizes of 198 ± 8.3 nm and 461 ± 33.3 nm, respectively. Both sizes of the produced SiNPs as characterized using FESEM exhibits spherical shape with a narrow size distribution and smooth surface.

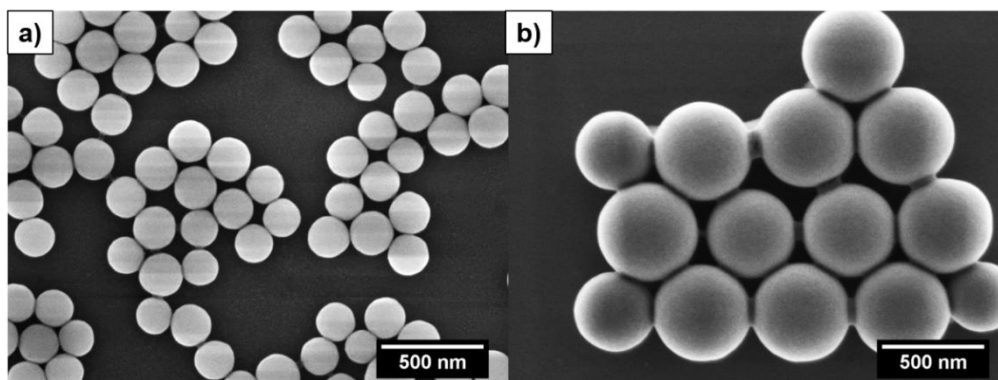


Figure 4.2 FESEM images of fabricated silica nanoparticles with a) small and b) large sizes.

Secondly, nanocomposites of silica and magnetic nanoparticles (S-SPION) were subsequently synthesized via thermal decomposition approach. Different amounts of iron precursor ($\text{Fe}(\text{acac})_3$) (i.e. 10, 20, 60, and 180 mg) were used for synthesizing S-SPION. It should be noted that small size of silica nanoparticles was used to investigate the effect of precursor amount. From FESEM images in Figure 4.3, it clearly exhibited the impact of $\text{Fe}(\text{acac})_3$ content on the obtained nanocomposite's morphology. As a result, the degree of surface coverage of silica nanoparticles is dependent of $\text{Fe}(\text{acac})_3$ content. The higher amount of precursor used, the larger surface area occupied. As silica nanoparticles were used as support materials and were further modified with mannan, silica nanoparticles with partially covered surface is desirable. Herein, S-SPION with 10 mg of $\text{Fe}(\text{acac})_3$ (Figure 4.3a) was chosen to be a candidate for further studies as it provided a large amount of free space for surface functionalization. Although only small amount of $\text{Fe}(\text{acac})_3$ was applied, the obtained S-SPION nanocomposite still possessed superparamagnetic character. Notably, magnetic nanoparticles are likely to deposit on silica particles' surface by physical adsorption.

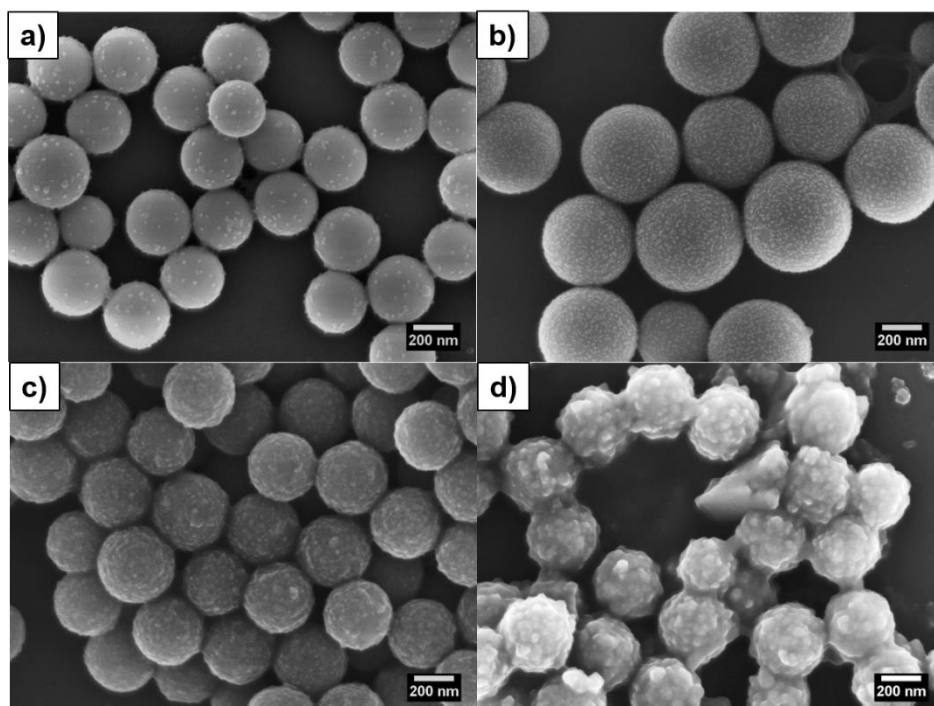


Figure 4.3 FESEM images of S-SPION synthesized with a) 10 mg, b) 20 mg, c) 60 mg, and d) 180 mg of $\text{Fe}(\text{acac})_3$

In addition, silica nanoparticles with large size (i.e. 461 ± 33.3 nm) were also fabricated with 10 mg of $\text{Fe}(\text{acac})_3$. As a result, the obtained large S-SPION nanocomposite showed similar result to the small S-SPION, providing large available surface on silica surface with small magnetic nanoparticles deposited on silica's surface (shown in Figure 4.4a and 4.4b as SEM and TEM images, respectively). Therefore, it can be claimed that this method is a versatile approach for the synthesis of S-SPION nanocomposites, regardless of the size of SiNPs.

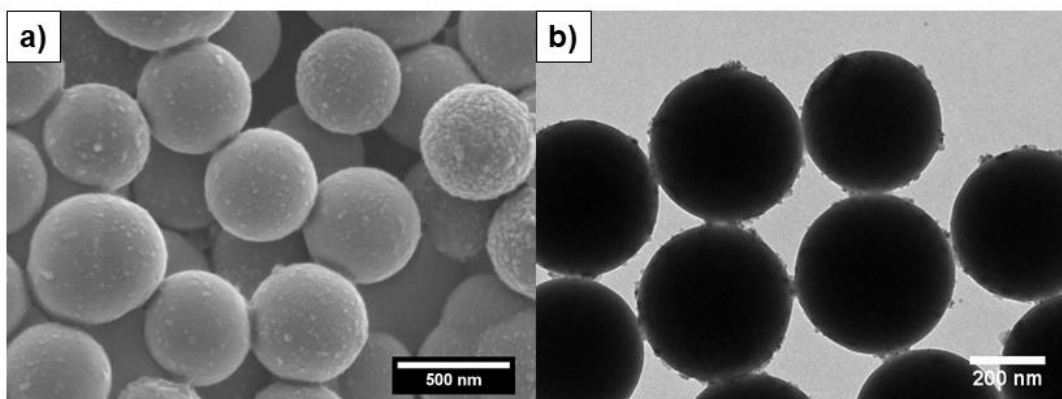


Figure 4.4 a) SEM image and b) TEM image of large S-SPION synthesized with 10 mg of $\text{Fe}(\text{acac})_3$

4.1.2 Characterization of silica nanoparticles (SiNPs) and silica-magnetic nanoparticles (S-SPION) by XRD

In addition, X-ray diffraction (XRD) was used to determine the structures of the synthesized SiNPs and S-SPION nanocomposites. For comparison, the structure of magnetite nanoparticles (JCPDS:19-0629) was used as a reference. Notably, S-SPION(S) and S-SPION(L) represented magnetic nanocomposites fabricated using small and large size of silica nanoparticles, respectively. According to XRD patterns in Figure 4.5, the characteristic peaks of magnetite nanoparticles from both sizes of magnetic nanocomposites cannot be clearly observed compared to the reference. The XRD patterns of S-SPION (S) and S-SPION (L) exhibit dominant characteristic peaks of amorphous silica. However, S-SPION nanocomposites, which were synthesized using the highest amount of iron precursor (i.e. 180 mg of $\text{Fe}(\text{acac})_3$), revealed magnetite characters as shown in the XRD pattern of S-SPION-180Fe. The obtained results suggested that the number of magnetic nanoparticles presented in the S-SPION nanocomposites plays a significant role in XRD patterns. Thus, other evidence is required to confirm the presence of magnetic nanoparticles as XRD patterns of S-SPION do not clearly provide significant peaks of presented magnetic nanoparticles. This observation is consistent with the published work by Ding *et al.* [86]. Nanocomposite of silica beads and quantum dots was synthesized and characterized by XRD. The XRD pattern of the synthesized nanocomposite showed very faint peaks

of quantum dots, predominantly occupied by amorphous character of silica. Therefore, to confirm the presence of magnetic materials, magnetic responses of S-SPION nanocomposites were further assessed.

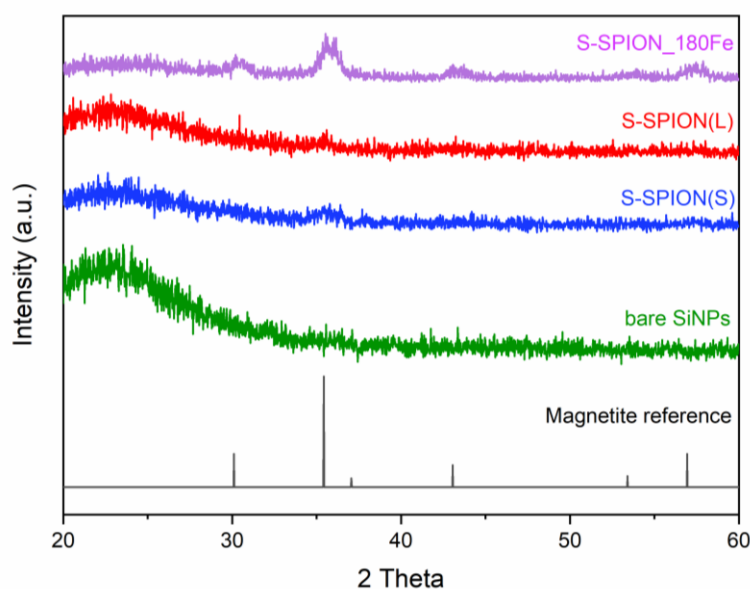


Figure 4.5 XRD patterns of the synthesized nanoparticles (i.e. S-SPION (S), S-SPION (L), and S-SPION_180Fe) compared to a magnetite reference (JCPDS:19-0629) and bare SiNPs.

4.1.3 Magnetic characterization of silica-magnetic nanoparticles (S-SPION) by VSM

To confirm the presence of magnetic property, magnetic response of the synthesized nanocomposite was simply determined using a permanent magnet. Under an induction of an external magnetic field, the synthesized nanocomposites were attracted to an external magnet as shown in Appendix: Figure A1. In addition, magnetic response was also assessed using a VSM. Figure 4.6 shows the magnetization-magnetic field (M-H) curves of S-SPION(S) and S-SPION (L) nanocomposites. From the M-H curves, S-SPION (S) and S-SPION (L) nanocomposites exhibited superparamagnetic character showing no hysteresis loop with the saturation magnetization of ~ 2.7 emu/g and ~ 0.6 emu/g, respectively. As a result, S-SPION (S) exhibited stronger magnetic response to an external magnetic field than S-

SPION (L). This observation implied that, at the same weight of nanocomposite, small size of nanocomposite contained higher surface area than the bigger particle, suggesting a larger number of magnetic nanoparticles deposited on silica surface.

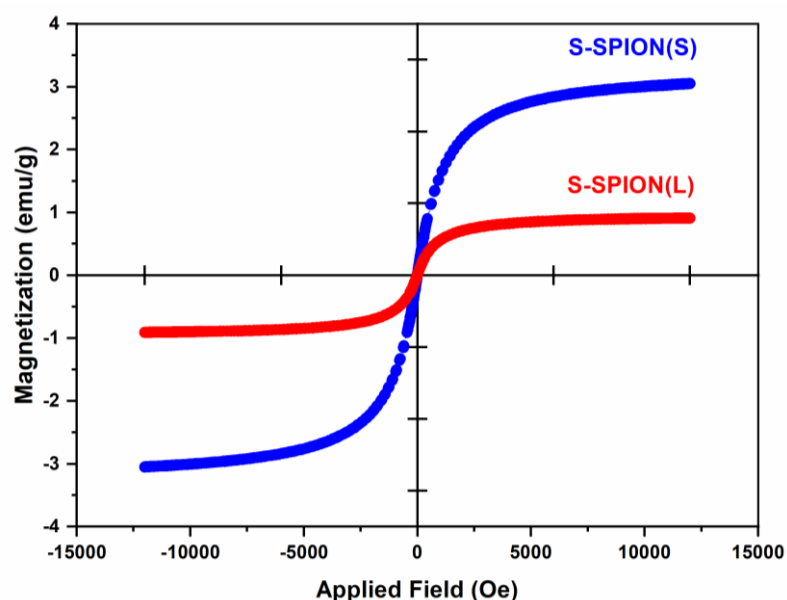


Figure 4.6 Magnetization-magnetic field (M-H) curves of S-SPION (S) and S-SPION (L) nanocomposites.

4.1.4 Functionalization of silica-magnetic nanoparticles with mannan (S-SPION-MN)

Mannan extracted from *Saccharomyces cerevisiae* cell wall contained characteristics of carbohydrate and protein in its structure. Thus, it was assumed that the extracted mannan was composed of protein residues [84]. Consequently, surface functionalization of S-SPION with APTES was firstly conducted. The obtained product designated as S-SPION-NH₂ was consisted of amino groups on S-SPION's surface. The success of amino surface functionalization could be confirmed by measuring zeta potential. The zeta potential result is shown in Table 4.1. Prior to surface modification, both sizes of S-SPION nanocomposite exhibited highly negative charge due to the abundance of silanol groups on nanocomposite's surface. After APTES was applied, some of silanol groups were replaced by positively charged amino groups as it can be observed that S-SPION-NH₂ nanocomposites are more positively

charged than the unmodified nanocomposite (S-SPION), regardless of particles size. For instance, zeta potential of S-SPION (S) was -29.80 ± 1.04 mV, while amino-modified particle (S-SPION-NH₂) exhibited less negativity (i.e. -22.60 ± 0.88 mV). For the large size of nanocomposite, the same trend of particles' charge was attained as well. However, the slight difference in charge after APTES modification might be due to the use of low concentration of APTES. If higher concentration of APTES had been used, higher positivity would have noticed. The effect of APTES concentrations to the zeta potential changes has been studied elsewhere [87].

Table 4.1 Zeta potential and coated mannan content

Samples		Zeta potential (mV) ^a	Mannan concentration (µg/ mg particle) ^b
Small	S-SPION (S)	-29.80 ± 1.04	N/A
	S-SPION (S)-NH ₂	-22.60 ± 0.88	N/A
	S-SPION (S)-MN	-2.92 ± 0.35	13.4
Large	S-SPION (L)	-39.17 ± 2.33	N/A
	S-SPION (L)-NH ₂	-20.16 ± 0.68	N/A
	S-SPION (L)-MN	-3.88 ± 0.13	4.69

^a Zeta potential measured by a Zetasizer

^b Mannan content measured using sulfuric acid-phenol colorimetric assay

N/A not applicable

Next, S-SPION-NH₂ was presumed to further functionalize with mannan through amide bond formation. EDC/NHS coupling reagent was applied in the reaction to activate carboxylic groups on mannan chain. The presence of mannan on nanocomposite's surface could be verified by measuring zeta potential as shown in Table 4.1. As a result, the zeta potential of both sizes of nanocomposites (i.e. S-SPION (S)-MN and S-SPION (L)-MN) exhibited less negativity (-2.92 ± 0.35 and $-3.88 \pm$

0.13 mV) than amino-functionalized ones (-22.60 ± 0.88 and -20.16 ± 0.68 mV). This result is ascribed to the charge neutralization of the coated mannan. This change in surface charge is consistent with the work reported by Walters and co-workers [88]. However, due to an obvious change of surface charge, mannan is thus likely to be coated through physical adsorption due to the little amount of protein residue existing in extracted mannan. Therefore, the consumption that mannan attached to silica particle via covalent bond might not be accurate.

Moreover, the existence of mannan could also be confirmed by colorimetric assay of sulfuric acid-phenol method. Principally, mannan is firstly broken down into monosaccharides by sulfuric acid. Then it was further dehydrated into furfural compounds and subsequently reacted with phenol, producing yellowish-brown solution. As shown in Appendix: Figure A2, the solution of S-SPION-MN nanocomposites of both sizes turned into yellowish-brown solution, while the solution of S-SPION nanocomposite still maintained pale yellow. In accordance with the result, it was clearly confirmed that mannan was successfully coated on S-SPION nanocomposite. Moreover, the concentration of coated mannan could be calculated from the observed absorbance. However, the interference of the color of iron nanoparticles deposited on silica nanoparticles might be an issue. Thus, the concentration of coated mannan is indirectly evaluated from the concentration of mannan before and after loading. Calculated concentration of coated mannan is shown in Table 4.2. As a result, S-SPION (S)-MN contained mannan with the concentration of $13.4 \mu\text{g}/\text{mg}$ particle, while S-SPION (L)-MN possessed less amount of mannan (i.e. $4.69 \mu\text{g}/\text{mg}$ particle). This outcome can be described as small nanoparticles provide higher surface area for mannan functionalization than the surface area acquired by bigger nanoparticles.

4.1.5 Magnetic characterization of silica-magnetic nanoparticles-mannan (S-SPION-MN) using a VSM

Magnetization of mannan-coated magnetic nanocomposite could be determined using a VSM. The magnetization curve of S-SPION-MN is shown in Figure 4.7 compared to the uncoated one. Noted, S-SPION (L) was chosen for further

investigations, instead of using small nanocomposite, even though smaller nanocomposite possessed superior magnetic property. This is likely due to the preferred size of DCs uptake (about 500 nm) [72]. As a result, the presence of mannan does not affect the character of superparamagnetic property by showing no hysteresis loop. The observed magnetization of S-SPION-MN was ~ 0.4 emu/g which was similar to the counterpart S-SPION (i.e. ~ 0.6 emu/g). As S-SPION-MN nanocomposite still contains superparamagnetism, it is suitable for further investigation in biological studies.

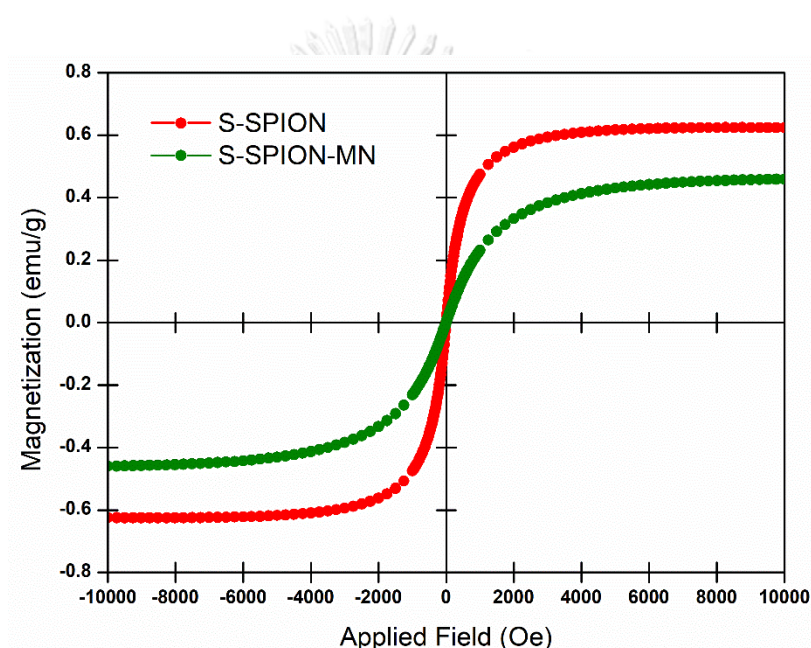


Figure 4.7 Magnetization curves of coated nanocomposite (S-SPION-MN) compared to the uncoated sample (S-SPION).

4.1.6 Characterization of silica-magnetic nanoparticles-mannan (S-SPION-MN) by hydrodynamic size, zeta potential and ICP-OES

Hydrodynamic size can be an alternative way to prove the existence of mannan on the magnetic nanocomposite. Table 4.2 shows the hydrodynamic size of uncoated and coated nanocomposites obtained by a zeta sizer. As a result, coated particles clearly demonstrated larger hydrodynamic size than the uncoated ones, assuring the presence of mannan. Moreover, zeta potential values of both

nanocomposites also confirmed the presence of mannan on particle surface, thereby neutralizing particle surface charge.

Following to all above results, it implied that mannan could be coated through physical adsorption. However, the content of iron nanoparticles before and after mannan attachment process has not been mentioned yet. Thus, ICP-OES was used to measure the amount of iron coated on nanocomposites. As shown in Table 4.2, the amount of Fe of both S-SPION (3.95 $\mu\text{g}/\text{mg}$ particle) and S-SPION-MN (4.07 $\mu\text{g}/\text{mg}$ particle) is comparable. Therefore, it can be implied that the protocol used to attach mannan does not affect the starting material's characteristics.

Table 4.2 Properties of synthesized particles

Samples	Size (nm) ^a	PDI ^a	Zeta potential (mV) ^a	Amount of Fe ($\mu\text{g}/\text{mg}$ particle) ^b
S-SPION	693.23 \pm 25.62	0.157 \pm 0.085	-39.17 \pm 2.33	3.95
S-SPION-MN	930.70 \pm 37.77	0.395 \pm 0.077	-3.88 \pm 0.13	4.07

^a Hydrodynamic size, PDI, and zeta potential measured by a Zetasizer

^b Iron content determined by ICP-OES analysis

4.2 Biological activities

4.2.1 Cytotoxicity study

In terms of biocompatibility, MTT assay was chosen as a reliable common method to study toxicity of the synthesized particles, S-SPION and S-SPION-MN. Therefore, cytotoxicity of the synthesized particles was tested by incubating the particles with DCs for different times (6 h, 12 h, 24 h, and 48 h). The results of cell viability are shown as O.D. value displayed in Figure 4.8. Particulate mannan (S-SPION-MN) and unmodified counterpart (S-SPION) with different concentrations (0.01, 0.10, and 1.00 ng particles/cell) were incubated with DCs. The assessment was compared to non-incubated cell (negative control), solution form of mannan and 0.5 $\mu\text{g}/\text{mL}$ of LPS. The cell viability is inversely proportional to the particle

concentrations. From the results, it can be observed that mannan in its solution form showed higher viability of cells compared to the particulate form. This phenomenon might be ascribed to the high stimulation of DCs by mannan in particulate formulation, since the high activation of DC can lead to the cell death [89, 90]. To confirm the effect of the presenting mannan, unmodified particles, S-SPION, demonstrated more survival of cells than the cells incubated with S-SPION-MN, especially at high concentration. According to the result, the existing mannan in particulate form showed greatly impact to the cell activity.

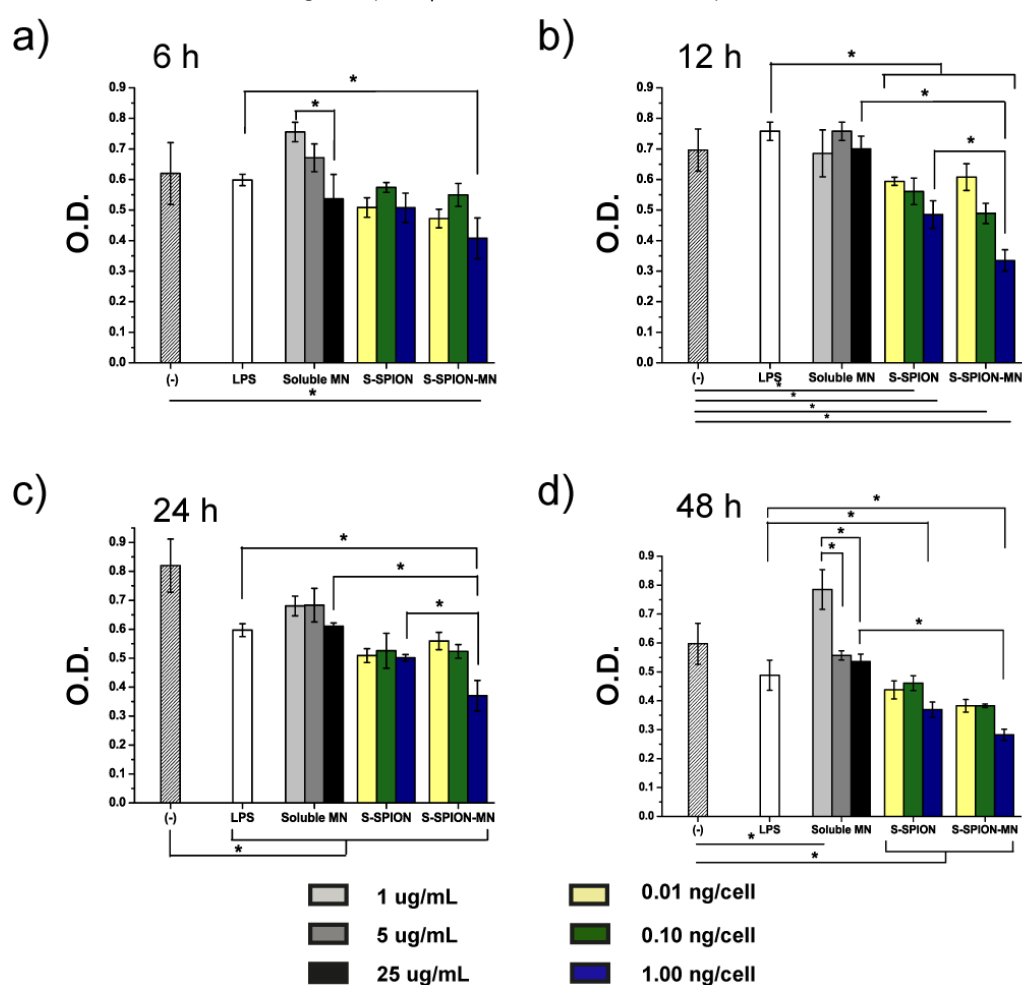


Figure 4.8 Cytotoxicity of the synthesized particles in BMDCs. Cell viability was assessed by MTT assay and presented as optical density (O.D. at 570 nm). BMDCs were incubated with the tested particles at a) 6 h, b) 12 h, c) 24 h, and d) 48 h. * indicates the statistically significant difference between samples, as determined by One-way ANOVA with Tukey HSD (n = 3) at $p < 0.05$.

4.2.2 DC maturation

To confirm the benefit of mannan in its particulate form, DC maturation was then investigated. As we have known that mature DCs play an important role in the induction of an effective T cell immunity [91]. Therefore, enhancement of DC maturation should be considered. In addition, from cytotoxicity study in the previous section, the result has primarily shown that the presence of mannan, particularly in the particulate form, might affect DC activation and maturation. To confirm our hypothesis, DC maturation was further determined. To assess DC maturation, three markers, CD80, CD86, and MHC class II, were used as indicators of matured DCs [92]. Figure 4.9 exhibited quantitative analysis showing mean fluorescence intensity (MFI) of DCs stimulated with different types of particles for 24 h (Figure 4.9a) and 48 h (Figure 4.9b). The fluorescence intensity is contributed to up-regulated expression of the markers on DCs, referring to the degree of DC maturation. According to the results obtained at 24 h and 48 h, only S-SPION and S-SPION-MN (at the concentration of 1 ng/cell) demonstrated high up-regulation of DCs markers compared to the unstimulated DCs (negative control) and soluble mannan. In comparison with S-SPION, S-SPION-MN exhibited significantly higher degree of DC maturation, confirming the important role of mannan in DC activation. From this result, it can be claimed that mannan plays an important role in DC activation. In addition, particulate form of mannan displayed a better immunogenicity than the soluble mannan in terms of DC activation and maturation even though high concentration of soluble mannan (25 $\mu\text{g}/\text{mL}$) was applied in comparison with particulate form of mannan, S-SPION-MN (at mannan concentration of less than 5 $\mu\text{g}/\text{mL}$). The detail of flow cytometric analysis comparing between soluble mannan and S-SPION-MN is shown in Appendix: Figure A3. Also, the percentage of positive cells analyzed from flow cytometry is presented in Figure 4.10. As a result, S-SPION-MN could be a potent candidate as an effective adjuvant.

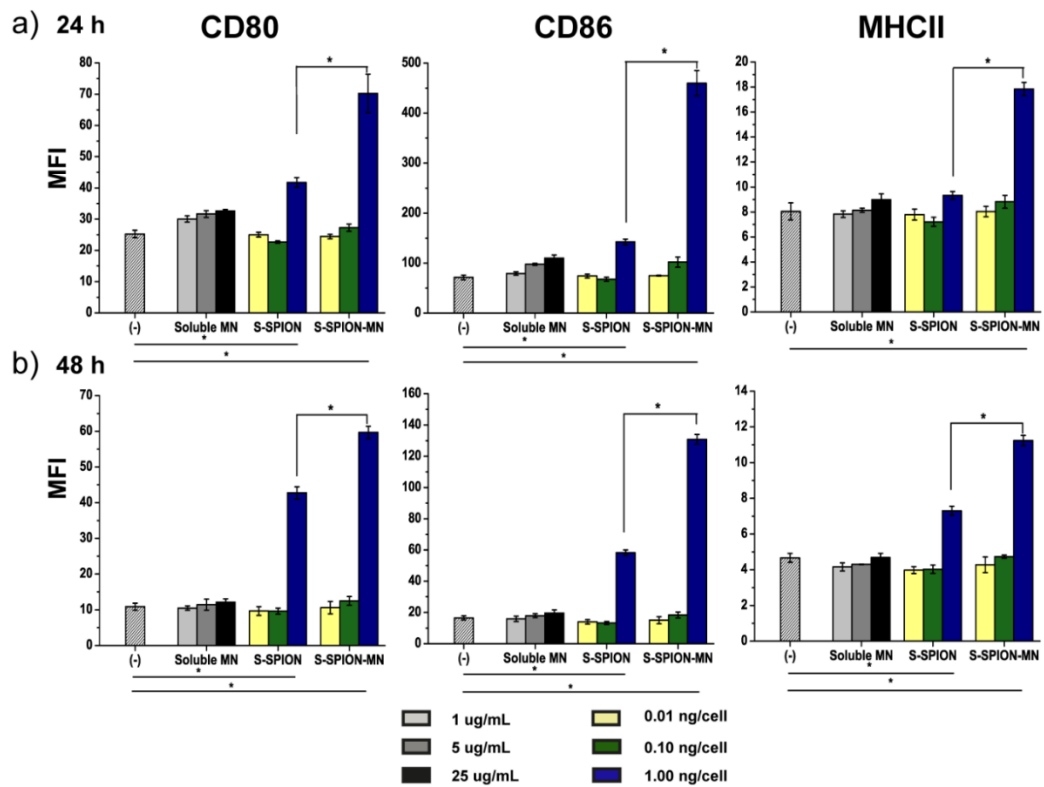


Figure 4.9 Effects of the particulate mannan on DC maturation. BMDCs were incubated with tested particles at various concentrations as indicated for (a) 24 h and (b) 48 h. The expression of DC markers, CD80, CD86 and MHC class II, was assessed by flow cytometric analysis. DCs were identified by gating on CD11c⁺ fraction. Then the expression levels of the maturation markers were assessed using histogram analysis (Appendix: Figure A3), and presented in geometric mean fluorescence intensity (MFI). * indicates the statistically significant difference between the two samples, as determined by One-way ANOVA with Tukey HSD (n = 3) at $p < 0.05$.

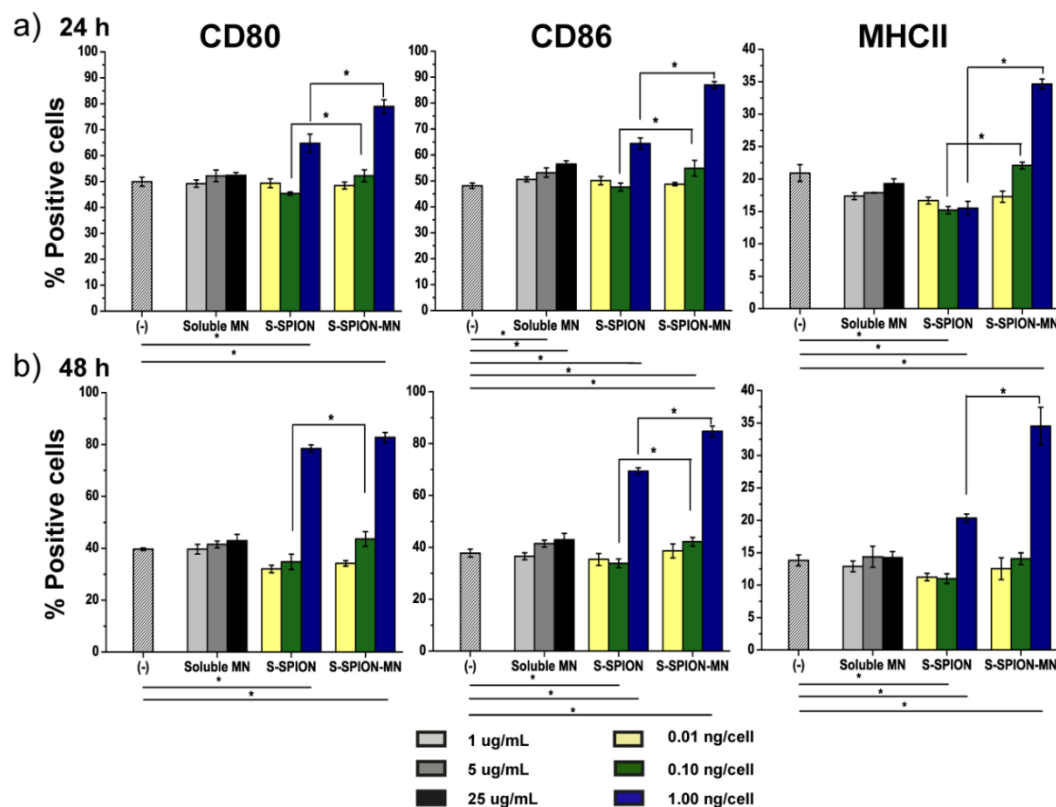


Figure 4.10 The percentage of mature DCs. BMDCs were incubated with tested particles at various concentrations as indicated for (a) 24 h and (b) 48 h. DCs were identified by gating on CD11c⁺ fraction. Then the percentage of CD80, CD86 and MHC class II positive cells were assessed by dot plot analysis. * indicates the statistically significant difference between the two samples, as determined by One-way ANOVA with Tukey HSD ($n = 3$) at $p < 0.05$.

4.2.3 Cytokine assessment

Generally, when DCs are stimulated, small proteins called cytokines are subsequently released. These secreted cytokines are involved in cell interactions and communications. Therefore, it is necessary to study the DCs activation by assessing the released cytokines. Herein, cytokine secretion was studied after the stimulation of DCs by the synthesized particles (e.g. S-SPION, particulate mannan (S-SPION-MN), and soluble form of mannan) at various concentrations. The cytokine investigation was conducted using ELISA method. The results are shown in Figure 4.11 that both 24 h and 48 h studies resulted in similar cytokine profiles. For instance, at the same

concentration of 1.0 ng particles/cell, S-SPION-MN obviously exhibited higher DC activation than those activated using S-SPION as high released amounts of proinflammatory cytokines (e.g. TNF- α , IL1- β , IL-6, and IFN- γ) were detected. The obtained result is consistent with DC maturation and cytotoxicity studies. The obtained evidence suggested that mannan contributed an important key to elicit strong immune response.

4.2.4 Cellular internalization

4.2.4.1 Cellular uptake visualized by a confocal microscope

In addition to the aid of targeting molecule (e.g. mannan), the presence of magnetic nanoparticles can also play an important role in directing nanoparticles to a specific site. In this case, synthesized S-SPION-MN can be delivered to DCs under the induction of an external magnetic field. Figure 4.12 shows confocal images of cellular internalization at different times, 15 min and 3 h, with and without an external magnetic field. It can be observed that high amounts of S-SPION-MN particles can be clearly taken by DCs at 15 min under an induction of magnetic field, while only small amounts of particles can be internalized in the absence of magnetic field induction. This observation can be ascribed to the ability of magnetic nanocomposite in gathering nanoparticles to DCs surface, enabling them ready to be taken up by DCs. However, at 3 h study, it is likely that the benefit of presenting mannan as a targeting moiety surpass the advantage of magnetic induction in DCs targeting ability.

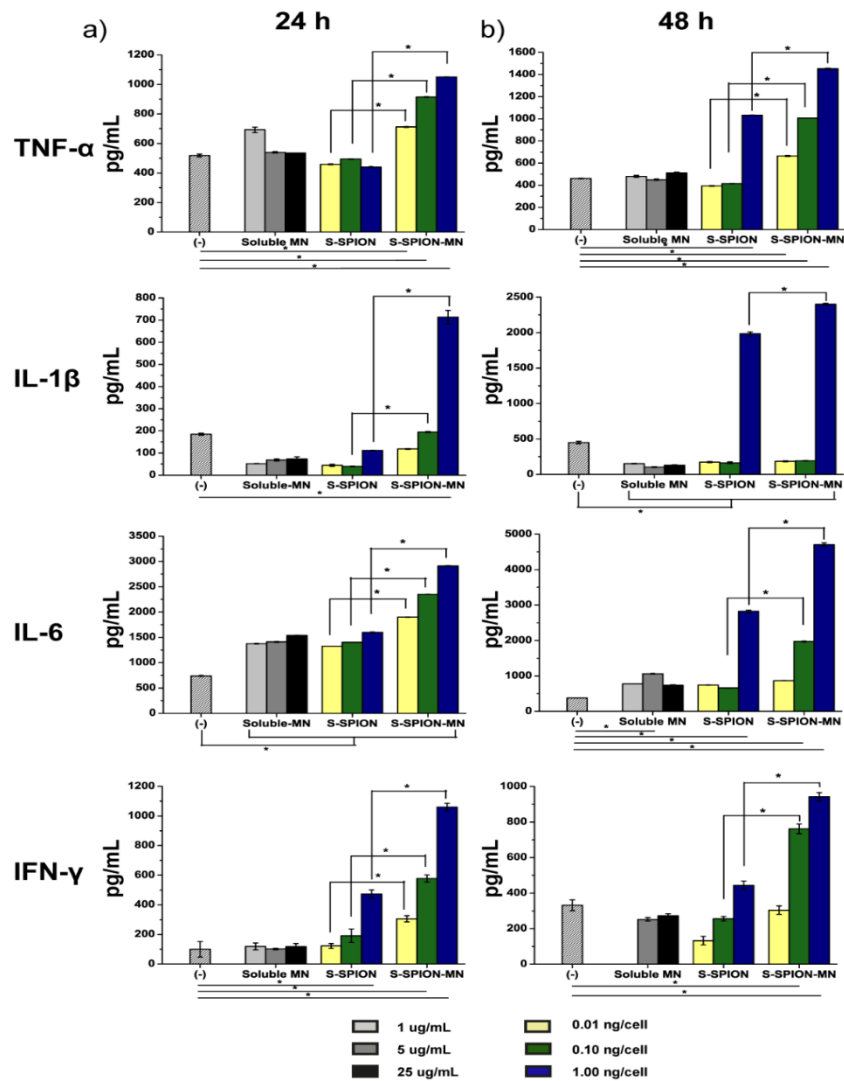


Figure 4.11 Cytokine production from stimulated BMDCs. BMDCs were incubated with the tested particles at different concentrations as indicated for (a) 24 h and (b) 48 h. Cytokine production was assessed by ELISA method. * indicates the statistically significant difference between the two samples, as determined by One-way ANOVA with Tukey HSD ($n = 3$) at $p < 0.05$.

To express the advantage of magnetic nanoparticles, obvious capability of presenting magnetic nanoparticles in directing nanoparticles to DCs can be seen in Figure 4.13. Uncoated magnetic nanoparticles, S-SPION, were used to demonstrate the effect of magnetism in delivery efficacy. Under an induction of magnetic field, at 15 min, it can be observed that there were plenty amounts of S-SPION nanoparticles gathering at DCs surface, while small amounts of nanoparticles were cellular internalized. Moreover, there were only small amounts of nanoparticles observed at DCs surface when no magnetic field is applied. Nevertheless, at 3 h study, higher amounts of nanoparticles were engulfed by DCs due to non-specific internalization of DCs. This finding emphasizes that magnetic nanoparticles played an important role in directing nanoparticles to DCs, but the nanoparticles did not help in cellular internalization. This speculation can be assured as many nanoparticles still maintained at DCs surface (indicated with yellow arrows) even though an induction of magnetic field at 3 h study was performed. In contrast, no particulate mannan (S-SPION-MN) can be observed at DCs outer membrane under the same condition. Therefore, the collaboration of magnetic nanoparticles and mannan as directing and targeting moieties, respectively, could greatly enhance the internalization and activation of DCs, making them as potential adjuvants.

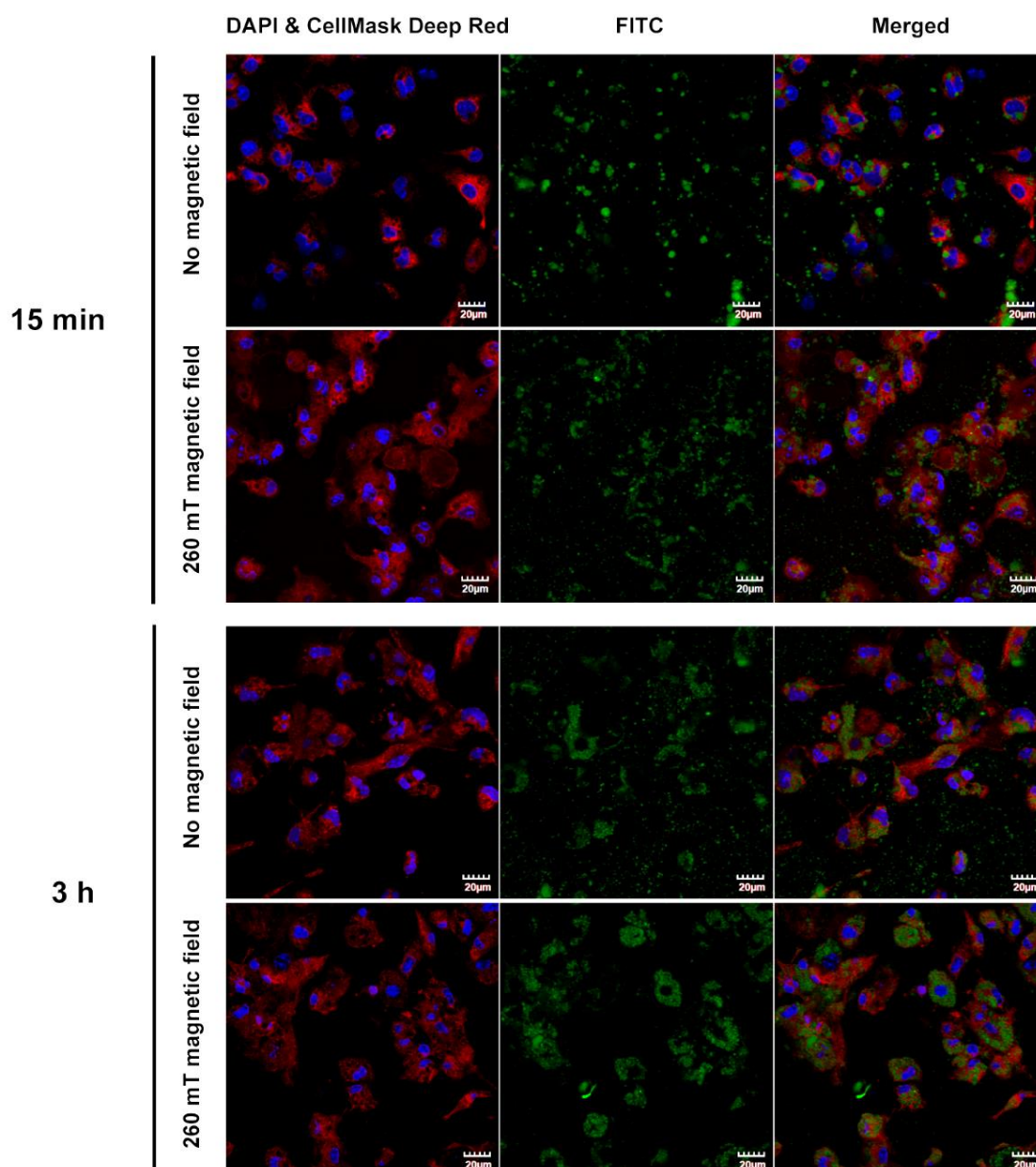


Figure 4.12 Internalization of particulate mannan by BMDCs. BMDCs were incubated with particulate mannan (S-SPION-MN) for 15 min and 3 h with and without a 260 mT magnetic field, and the internalization of the particles was observed under confocal microscopy. Representative confocal images of BMDCs (blue for nuclei and red for plasma membrane) and fluorescent S-SPION-MN particles (green) are displayed.

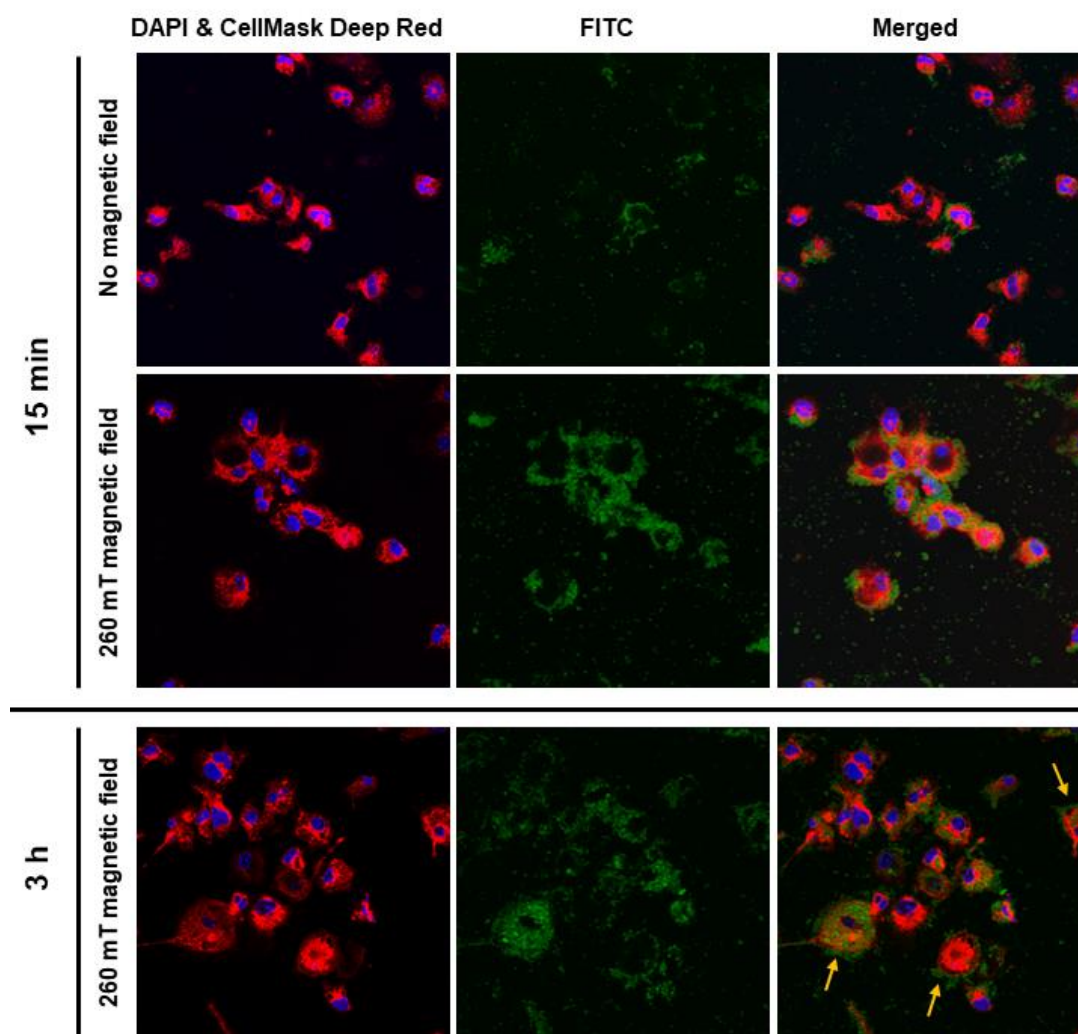


Figure 4.13 Internalization of S-SPION by BMDCs. BMDCs were incubated with particles for 15 min and 3 h with and without a 260 mT magnetic field, and the internalization of the particles was observed under confocal microscopy. Representative confocal images of BMDCs (blue for nuclei and red for plasma membrane) and fluorescent S-SPION particles (green) are displayed.

4.2.4.2 Cellular uptake assessed by flow cytometry

The quantitative assessment of cellular uptake of S-SPION-MN by BMDCs was also performed using flow cytometric analysis. The percentage of cellular uptake studied at different times (i.e. 15 min and 3 h) under the absence and presence of an external magnetic field is shown below in Figure 4.14. According to the graph

obtained from flow cytometric analysis, the result was consistent with the confocal images in Figure 4.12. At 15 min, the presence of a magnetic field significantly enhanced the engulfment of S-SPION-MN particles by DCs. The internalization of the particles by DCs was markedly increased at 3 h; however, no significant difference between the presence and absence of a magnetic field, which was consistent with the confocal images. This incident was attributed to the superiority of coated mannan as targeting molecules. Nevertheless, magnetic response can still be useful for directing nanoparticles to the desirable sites especially at the beginning phase of delivery.

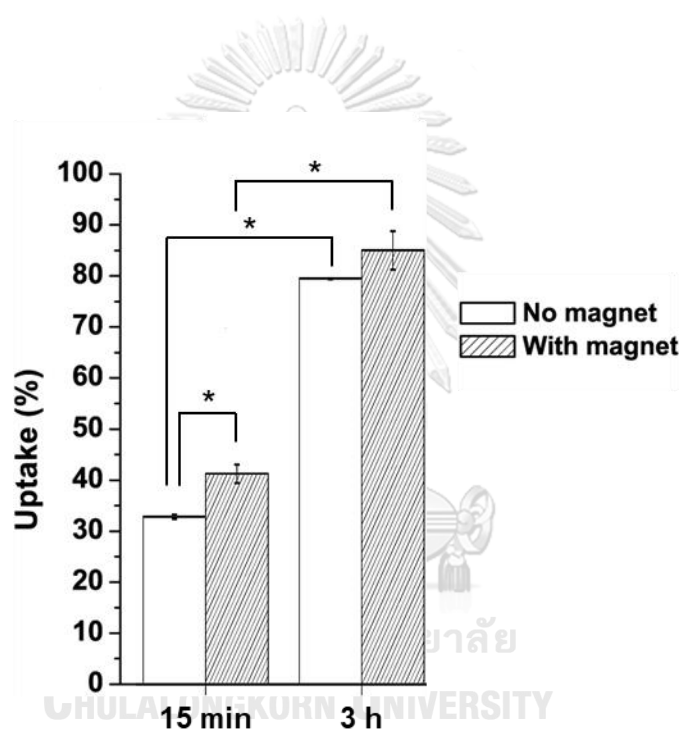


Figure 4.14 Flow cytometric analysis of BMDC internalization. BMDCs were incubated with particulate mannan (S-SPION-MN) for 15 min and 3 h with and without a 260 mT magnetic field. The percentage of cellular uptake was evaluated using histogram analysis. * indicates the statistically significant difference between the two samples, as determined by One-way ANOVA Tukey HSD ($n = 3$) at $p < 0.05$.

CHAPTER V

CONCLUSION

Vaccination has been widely accepted as an efficient way for treatment and protection our body from a variety of infectious diseases. However, current vaccine has still addressed some drawbacks, such as lacking strong immune response. Therefore, development of vaccine efficacy is of interest. One of the most important strategies to improve therapeutic effect of vaccination is the ability in targeting and activation of dendritic cells (DCs). Therefore, herein, the researchers focused in utilizing nanomaterials as a vaccine adjuvant for enhancing DCs targeting ability. In this work, nanocomposites of silica-magnetic nanoparticles and mannan were successfully synthesized. The fabricated nanocomposites have shown a potential as a vaccine adjuvant. The co-existence of superparamagnetic nanoparticles and mannan as a directing and targeting moieties, respectively, greatly improved the targeting and activation of DCs.

The produced uncoated (S-SPION) and mannan-coated (S-SPION-MN) magnetic nanocomposites were characterized using various techniques. FESEM and TEM were used for morphological characterization. For structural determination, XRD was applied. In addition, magnetic response was investigated by using VSM technique. The obtained S-SPION nanoparticles contained spherical shape with high amounts of magnetic nanoparticles distributed on nanoparticles' surface. The synthesized nanocomposite possessed superparamagnetic character according to VSM result. In the case of particulate mannan, S-SPION-MN, the successful attachment of mannan could be verified by an alteration of particle surface charge and hydrodynamic size of nanoparticles before and after surface modification. Moreover, the presence of carbohydrate and its content could also be detected and evaluated by colorimetric assay of sulfuric acid-phenol method. Although the nanocomposites were coated with mannan, superparamagnetic character remained.

Investigation of the synthesized nanocomposite in biological study was subsequently conducted. The toxicity of the materials incubated with DCs at

different times (i.e. 6 h, 12 h, 24 h, and 48 h) was performed by MTT assay. As a result, the reduction of cell viability stimulated with particulate mannan might be due to the capability of mannan in DCs stimulation. However, high percentage of cell viability stimulated by soluble mannan was observed. In addition, DC maturation and cytokine assessment were conducted by flow cytometry and ELISA method, respectively. The upregulation of mature DC's surface markers (i.e. CD80, CD86, and MHC class II) and released cytokines of TNF- α , IL1- β , IL-6, and IFN- γ confirmed that the presence of mannan could significantly enhance DC maturation and activation. In terms of targeting ability, confocal imaging and flow cytometry were used to investigate the cellular internalization. From the results, it was clearly observed that mannan-coated particles could be rapidly internalized compared to an uncoated counterpart. Remarkably, the accumulation of nanoparticles at DCs surface could be improved by the aid of magnetic nanoparticles. Therefore, the synergic effects of magnetic nanoparticles and mannan vastly impacted targeting ability, cellular activation and maturation of DCs. These primary results from *in vitro* studies offered a great possibility in developing nanomaterial-based vaccine adjuvants *in vivo*.

APPENDIX

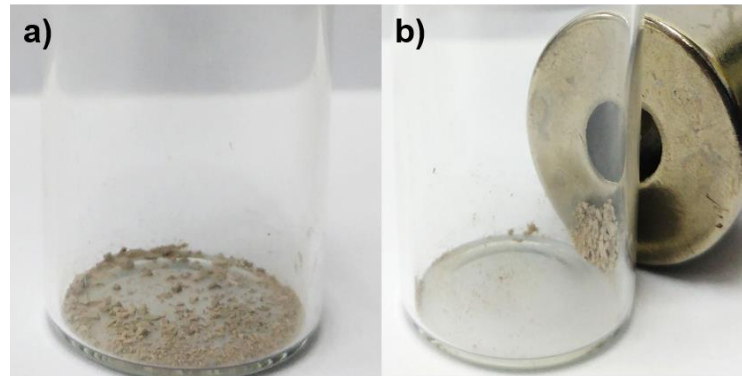


Figure A1 Picture demonstration of the synthesized S-SPION nanocomposite a) without and b) with an induction of an external magnetic field.

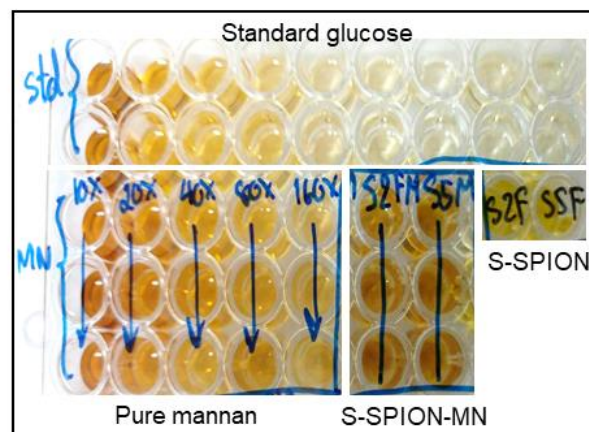


Figure A2 Colorimetric assay of sulfuric acid-phenol method confirming the presence of mannan in S-SPION nanocomposite.

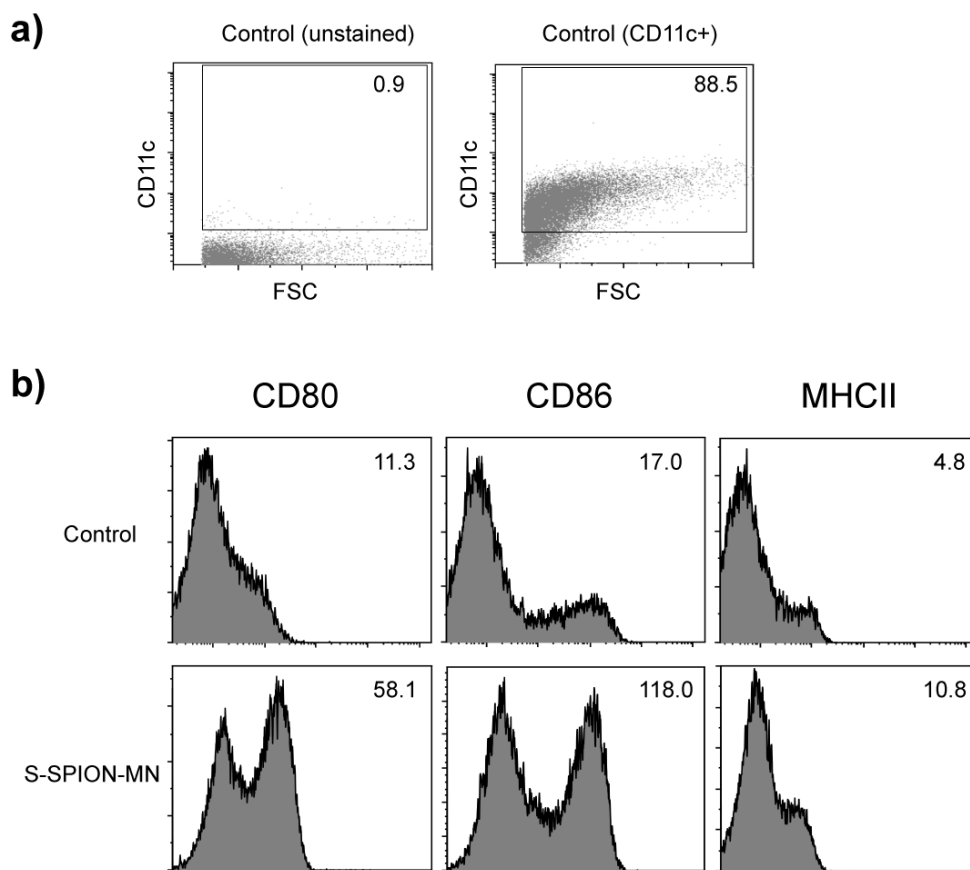


Figure A3 Flow cytometric analysis of DC maturation. BMDCs were stimulated with particulate mannan (S-SPION-MN). The dot plot analysis of BMDC was first shown using side scatter (SSC) and forward scatter (FSC), and the live cells were gated. (a) DCs were identified by gating on CD11c⁺ population. The left panel is the control staining, and the right panel is the control staining with anti-mouse CD11c mAb. The number shown in the panels represented the percentage of CD11c⁺ cells. (b) Histogram analysis of DCs markers (i.e. CD80, CD86 and MHC class II expression on CD11c⁺ cells). The numbers indicated the geometric mean fluorescence intensity (MFI).

REFERENCES

1. Zepp, F., *Principles of Vaccination*, in *Vaccine Design: Methods and Protocols: Volume 1: Vaccines for Human Diseases*, S. Thomas, Editor. 2016, Springer New York: New York, NY. p. 57-84.
2. Centers for Disease Control and Prevention. *Principles of Vaccination*. 2019 [cited 2019 20 Oct]; Available from: <https://www.cdc.gov/vaccines/pubs/pinkbook/prinvac.html>.
3. Vaccines. *Vaccine Types*. [cited 2019 20 Oct]; Available from: <https://www.vaccines.gov/basics/types>.
4. Keler, T., V. Ramakrishna, and M.W. Fanger, *Mannose receptor-targeted vaccines*. *Expert Opinion on Biological Therapy*, 2004. **4**(12): p. 1953-1962.
5. Gonçalves, C., et al., *Potential of mannan or dextrin nanogels as vaccine carrier/adjuvant systems*. *Journal of Bioactive and Compatible Polymers*, 2016. **31**(5): p. 453-466.
6. Sun, B. and T. Xia, *Nanomaterial-based vaccine adjuvants*. *Journal of Materials Chemistry B*, 2016. **4**(33): p. 5496-5509.
7. Plotkin, S.A., *Vaccines, Vaccination, and Vaccinology*. *The Journal of Infectious Diseases*, 2003. **187**(9): p. 1349-1359.
8. The History of Vaccines. *All Timelines Overview*. [cited 2019 22 Oct]; Available from: <https://www.historyofvaccines.org/timeline/all>.
9. Plotkin, S.A. and S.L. Plotkin, *The development of vaccines: how the past led to the future*. *Nature Reviews Microbiology*, 2011. **9**(12): p. 889-893.
10. The Immunisation Advisory Centre. *Types of vaccines*. 2017 [cited 2019 23 Oct]; Available from: <https://www.immune.org.nz/vaccines/vaccine-development/types-vaccines>.
11. Lauring, A.S., J.O. Jones, and R. Andino, *Rationalizing the development of live attenuated virus vaccines*. *Nature Biotechnology*, 2010. **28**(6): p. 573-579.
12. Innis, B.L., et al., *Protection Against Hepatitis A by an Inactivated Vaccine*. *JAMA*, 1994. **271**(17): p. 1328-1334.

13. Treanor, J.J., et al., *Safety and Immunogenicity of an Inactivated Subvirion Influenza A (H5N1) Vaccine*. 2006. **354**(13): p. 1343-1351.
14. Frerichs, G.N., et al., *Safety and efficacy of live and inactivated infectious bovine rhinotracheitis vaccines*. *Veterinary Record*, 1982. **111**(6): p. 116.
15. Rummyantsev, A.A., et al., *Comparison of live and inactivated tick-borne encephalitis virus vaccines for safety, immunogenicity and efficacy in rhesus monkeys*. *Vaccine*, 2006. **24**(2): p. 133-143.
16. Saint-Jean, S.R., J.J. Borrego, and S.I. Perez-Prieto, *Infectious Pancreatic Necrosis Virus: Biology, Pathogenesis, and Diagnostic Methods*, in *Advances in Virus Research*. 2003, Academic Press. p. 113-165.
17. Liljeqvist, S. and S. Ståhl, *Production of recombinant subunit vaccines: protein immunogens, live delivery systems and nucleic acid vaccines*. *Journal of Biotechnology*, 1999. **73**(1): p. 1-33.
18. Perrie, Y., et al., *Vaccine adjuvant systems: Enhancing the efficacy of sub-unit protein antigens*. *International Journal of Pharmaceutics*, 2008. **364**(2): p. 272-280.
19. Green, M.D. and N.H. Al-Humadi, *Chapter 27 - Preclinical Toxicology of Vaccines*¹¹*Disclaimer: The findings and conclusions in this chapter have not been formally disseminated by the Food and Drug Administration and should not be construed to represent any Agency determination or policy, in A Comprehensive Guide to Toxicology in Nonclinical Drug Development (Second Edition)*, A.S. Faqi, Editor. 2017, Academic Press: Boston. p. 709-735.
20. Coffman, R.L., A. Sher, and R.A. Seder, *Vaccine Adjuvants: Putting Innate Immunity to Work*. *Immunity*, 2010. **33**(4): p. 492-503.
21. Petrovsky, N. and J.C. Aguilar, *Vaccine adjuvants: Current state and future trends*. *Immunology And Cell Biology*, 2004. **82**: p. 488.
22. Lee, S. and M.T. Nguyen, *Recent advances of vaccine adjuvants for infectious diseases*. *Immune network*, 2015. **15**(2): p. 51-57.
23. Petrovsky, N. and P.D. Cooper, *Carbohydrate-based immune adjuvants*. *Expert Review of Vaccines*, 2011. **10**(4): p. 523-537.
24. van Dinther, D., et al., *Targeting C-type lectin receptors: a high-carbohydrate*

- diet for dendritic cells to improve cancer vaccines.* Journal of Leukocyte Biology, 2017. **102**(4): p. 1017-1034.
25. Sheng, K.-C., et al., *Mannan derivatives induce phenotypic and functional maturation of mouse dendritic cells.* Immunology, 2006. **118**(3): p. 372-383.
 26. Nguyen, T.N.Y., et al., *Cell wall mannan of Candida krusei mediates dendritic cell apoptosis and orchestrates Th17 polarization via TLR-2/MyD88-dependent pathway.* Scientific reports, 2018. **8**(1): p. 17123-17123.
 27. Elamanchili, P., et al., *“Pathogen-Mimicking” Nanoparticles for Vaccine Delivery to Dendritic Cells.* Journal of Immunotherapy, 2007. **30**(4): p. 378-395.
 28. Yu, W., et al., *Mannan-Modified Solid Lipid Nanoparticles for Targeted Gene Delivery to Alveolar Macrophages.* Pharmaceutical Research, 2010. **27**(8): p. 1584-1596.
 29. Azita, H., et al., *Immunoadjuvant activity of the nanoparticles’ surface modified with mannan.* Nanotechnology, 2014. **25**(35): p. 355101.
 30. Shi, G.-N., et al., *Enhanced antitumor immunity by targeting dendritic cells with tumor cell lysate-loaded chitosan nanoparticles vaccine.* Biomaterials, 2017. **113**: p. 191-202.
 31. Dranoff, G., *Cytokines in cancer pathogenesis and cancer therapy.* Nature Reviews Cancer, 2004. **4**(1): p. 11-22.
 32. Du, J., et al., *Nanoparticles for immune system targeting.* Drug Discovery Today, 2017. **22**(9): p. 1295-1301.
 33. Kumar, H., T. Kawai, and S. Akira, *Pathogen Recognition by the Innate Immune System.* International Reviews of Immunology, 2011. **30**(1): p. 16-34.
 34. Diercks, G.F.H. and P.M. Kluin, *Basic Principles of the Immune System and Autoimmunity*, in *Autoimmune Bullous Diseases: Text and Review*, M.F. Jonkman, Editor. 2016, Springer International Publishing: Cham. p. 3-12.
 35. Clark, R. and T. Kupper, *Old Meets New: The Interaction Between Innate and Adaptive Immunity.* Journal of Investigative Dermatology, 2005. **125**(4): p. 629-637.
 36. Vistica, D.T., et al., *Tetrazolium-based Assays for Cellular Viability: A Critical Examination of Selected Parameters Affecting Formazan Production.* Cancer

- Research, 1991. **51**(10): p. 2515.
37. abcam. *ELISA principle*. [cited 2019 03 Oct]; Available from: <https://www.abcam.com/kits/elisa-principle>.
 38. Leinco Technologies Inc. *Sandwich ELISA Protocol*. [cited 2019 03 Oct]; Available from: <https://www.leinco.com/sandwich-elisa-protocol/>.
 39. Creative Diagnostics. *Flow Cytometry Guide*. [cited 2019 03 Oct]; Available from: <https://www.creative-diagnostics.com/flow-cytometry-guide.htm>.
 40. Khan, H.A., et al., *14 - Nanoparticles for biomedical applications: An overview*, in *Nanobiomaterials*, R. Narayan, Editor. 2018, Woodhead Publishing. p. 357-384.
 41. Salk, J. and D. Salk, *Control of influenza and poliomyelitis with killed virus vaccines*. *Science*, 1977. **195**(4281): p. 834.
 42. Smith, D.M., J.K. Simon, and J.R. Baker Jr, *Applications of nanotechnology for immunology*. *Nature Reviews Immunology*, 2013. **13**: p. 592.
 43. Yoon, H.Y., et al., *Engineering nanoparticle strategies for effective cancer immunotherapy*. *Biomaterials*, 2018. **178**: p. 597-607.
 44. Rejinold, N.S., et al., *Evaluation of cell penetrating peptide coated Mn:ZnS nanoparticles for paclitaxel delivery to cancer cells*. *Scientific Reports*, 2018. **8**(1): p. 1899.
 45. Cha, B.G., J.H. Jeong, and J. Kim, *Extra-Large Pore Mesoporous Silica Nanoparticles Enabling Co-Delivery of High Amounts of Protein Antigen and Toll-like Receptor 9 Agonist for Enhanced Cancer Vaccine Efficacy*. *ACS Central Science*, 2018. **4**(4): p. 484-492.
 46. Peter, B., et al., *Interaction of Positively Charged Gold Nanoparticles with Cancer Cells Monitored by an in Situ Label-Free Optical Biosensor and Transmission Electron Microscopy*. *ACS Applied Materials & Interfaces*, 2018. **10**(32): p. 26841-26850.
 47. Liu, Z., et al., *Fabrication of red blood cell membrane-camouflaged Cu_{2-x}Se nanoparticles for phototherapy in the second near-infrared window*. *Chemical Communications*, 2019. **55**(46): p. 6523-6526.
 48. Tarn, D., et al., *Mesoporous Silica Nanoparticle Nanocarriers: Biofunctionality and Biocompatibility*. *Accounts of Chemical Research*, 2013. **46**(3): p. 792-801.

49. Liu, Y., et al., *Dual-functionalized Janus Mesoporous Silica Nanoparticles with Active Targeting and Charge Reversal for Synergistic Tumor Targeting Therapy*. ACS Applied Materials & Interfaces, 2019.
50. Stöber, W., A. Fink, and E. Bohn, *Controlled growth of monodisperse silica spheres in the micron size range*. Journal of Colloid and Interface Science, 1968. **26**(1): p. 62-69.
51. Korzeniowska, B., et al., *Silica nanoparticles for cell imaging and intracellular sensing*. Nanotechnology, 2013. **24**: p. 442002.
52. Kuchma, E., S. Kubrin, and A. Soldatov, *The Local Atomic Structure of Colloidal Superparamagnetic Iron Oxide Nanoparticles for Theranostics in Oncology*. 2018. **6**(3): p. 78.
53. Akbarzadeh, A., M. Samiei, and S. Davaran, *Magnetic nanoparticles: preparation, physical properties, and applications in biomedicine*. Nanoscale research letters, 2012. **7**(1): p. 144-144.
54. Mohammed, L., et al., *Magnetic nanoparticles for environmental and biomedical applications: A review*. Particuology, 2017. **30**: p. 1-14.
55. Ahn, T., et al., *Formation Pathways of Magnetite Nanoparticles by Coprecipitation Method*. The Journal of Physical Chemistry C, 2012. **116**(10): p. 6069-6076.
56. Okoli, C., et al., *Comparison and Functionalization Study of Microemulsion-Prepared Magnetic Iron Oxide Nanoparticles*. Langmuir, 2012. **28**(22): p. 8479-8485.
57. Park, J., et al., *Ultra-large-scale syntheses of monodisperse nanocrystals*. Nature Materials, 2004. **3**(12): p. 891-895.
58. Tartaj, P., et al., *The preparation of magnetic nanoparticles for applications in biomedicine*. Journal of Physics D: Applied Physics, 2003. **36**(13): p. R182-R197.
59. Hufschmid, R., et al., *Synthesis of phase-pure and monodisperse iron oxide nanoparticles by thermal decomposition*. Nanoscale, 2015. **7**(25): p. 11142-11154.
60. Patsula, V., et al., *Superparamagnetic Fe₃O₄ Nanoparticles: Synthesis by Thermal Decomposition of Iron(III) Glucuronate and Application in Magnetic*

- Resonance Imaging*. ACS Applied Materials & Interfaces, 2016. **8**(11): p. 7238-7247.
61. Cintolo, J.A., et al., *Dendritic cell-based vaccines: barriers and opportunities*. Future Oncology, 2012. **8**(10): p. 1273-1299.
 62. Hossain, M.K. and K.A. Wall, *Use of Dendritic Cell Receptors as Targets for Enhancing Anti-Cancer Immune Responses*. Cancers, 2019. **11**(3): p. 418.
 63. Yu, W., et al., *Mannan-Modified Solid Lipid Nanoparticles for Targeted Gene Delivery to Alveolar Macrophages*. 2010. **27**(8): p. 1584-1596.
 64. Ghotbi, Z., et al., *Active targeting of dendritic cells with mannan-decorated PLGA nanoparticles*. Journal of Drug Targeting, 2011. **19**(4): p. 281-292.
 65. Malvindi, M.A., et al., *SiO₂ nanoparticles biocompatibility and their potential for gene delivery and silencing*. Nanoscale, 2012. **4**(2): p. 486-495.
 66. Chiriaco, F., et al., *Epithelial cell biocompatibility of silica nanospheres for contrast-enhanced ultrasound molecular imaging*. 2013. **15**(7): p. 1779.
 67. Foglia, S., et al., *In vitro biocompatibility study of sub-5 nm silica-coated magnetic iron oxide fluorescent nanoparticles for potential biomedical application*. Scientific Reports, 2017. **7**.
 68. Hsiao, I.-L., et al., *Biocompatibility of Amine-Functionalized Silica Nanoparticles: The Role of Surface Coverage*. 2019. **15**(10): p. 1805400.
 69. Niemirowicz, K., et al., *Magnetic nanoparticles as new diagnostic tools in medicine*. Advances in Medical Sciences, 2012. **57**(2): p. 196-207.
 70. Yigit, M.V., A. Moore, and Z. Medarova, *Magnetic Nanoparticles for Cancer Diagnosis and Therapy*. Pharmaceutical Research, 2012. **29**(5): p. 1180-1188.
 71. Xianxian, Y., et al., *Graphene Quantum Dots-Capped Magnetic Mesoporous Silica Nanoparticles as a Multifunctional Platform for Controlled Drug Delivery, Magnetic Hyperthermia, and Photothermal Therapy*. Small, 2017. **13**(2): p. 1602225.
 72. Saengruengrit, C., et al., *The combined magnetic field and iron oxide-PLGA composite particles: Effective protein antigen delivery and immune stimulation in dendritic cells*. Journal of Colloid and Interface Science, 2018. **520**: p. 101-111.

73. Wu, W., Q. He, and C. Jiang, *Magnetic Iron Oxide Nanoparticles: Synthesis and Surface Functionalization Strategies*. *Nanoscale Research Letters*, 2008. **3**(11): p. 397-415.
74. Reddy, L.H., et al., *Magnetic Nanoparticles: Design and Characterization, Toxicity and Biocompatibility, Pharmaceutical and Biomedical Applications*. *Chemical Reviews*, 2012. **112**(11): p. 5818-5878.
75. Huang, Y., et al., *Superparamagnetic iron oxide nanoparticles conjugated with folic acid for dual target-specific drug delivery and MRI in cancer theranostics*. *Materials Science and Engineering: C*, 2017. **70**: p. 763-771.
76. Fang, Z.Z., et al., *Hyaluronic acid-modified mesoporous silica-coated superparamagnetic Fe₃O₄ nanoparticles for targeted drug delivery*. *International Journal of Nanomedicine*, 2019. **14**: p. 5785-5797.
77. Foged, C., et al., *Particle size and surface charge affect particle uptake by human dendritic cells in an in vitro model*. *International Journal of Pharmaceutics*, 2005. **298**(2): p. 315-322.
78. Halas, N.J., *Nanoscience under Glass: The Versatile Chemistry of Silica Nanostructures*. *ACS Nano*, 2008. **2**(2): p. 179-183.
79. Bitar, A., et al., *Silica-based nanoparticles for biomedical applications*. *Drug Discovery Today*, 2012. **17**(19): p. 1147-1154.
80. Kamegawa, R., M. Naito, and K. Miyata, *Functionalization of silica nanoparticles for nucleic acid delivery*. *Nano Research*, 2018. **11**(10): p. 5219-5239.
81. Moore, C.J., et al., *'Overloading' fluorescent silica nanoparticles with dyes to improve biosensor performance*. *Journal of Materials Chemistry B*, 2017. **5**(28): p. 5564-5572.
82. Nozawa, K., et al., *Smart Control of Monodisperse Stöber Silica Particles: Effect of Reactant Addition Rate on Growth Process*. *Langmuir*, 2005. **21**(4): p. 1516-1523.
83. Qu, H., et al., *Controllable in Situ Synthesis of Magnetite Coated Silica-Core Water-Dispersible Hybrid Nanomaterials*. *Langmuir*, 2013. **29**(33): p. 10573-10578.

84. Dean, N., *Asparagine-linked glycosylation in the yeast Golgi*. *Biochimica et Biophysica Acta (BBA) - General Subjects*, 1999. **1426**(2): p. 309-322.
85. Inaba, K., et al., *Isolation of Dendritic Cells*. 2009. **86**(1): p. 3.7.1-3.7.19.
86. Ding, L., et al., *Encapsulated Cd3P2 quantum dots emitting from the visible to the near infrared for bio-labelling applications*. *CrystEngComm*, 2014. **16**(41): p. 9622-9630.
87. Digigow, R.G., et al., *Preparation and characterization of functional silica hybrid magnetic nanoparticles*. *Journal of Magnetism and Magnetic Materials*, 2014. **362**: p. 72-79.
88. Walters, A.A., et al., *Assessment of the enhancement of PLGA nanoparticle uptake by dendritic cells through the addition of natural receptor ligands and monoclonal antibody*. *Vaccine*, 2015. **33**(48): p. 6588-6595.
89. Takeuchi, O. and S. Akira, *Pattern Recognition Receptors and Inflammation*. *Cell*, 2010. **140**(6): p. 805-820.
90. Kingeter, L.M. and X. Lin, *C-type lectin receptor-induced NF- κ B activation in innate immune and inflammatory responses*. *Cellular & Molecular Immunology*, 2012. **9**(2): p. 105-112.
91. Chen, P., et al., *Dendritic cell targeted vaccines: Recent progresses and challenges*. *Human Vaccines & Immunotherapeutics*, 2016. **12**(3): p. 612-622.
92. Burkholder, B., et al., *Tumor-induced perturbations of cytokines and immune cell networks*. *Biochimica et Biophysica Acta (BBA) - Reviews on Cancer*, 2014. **1845**(2): p. 182-201.



จุฬาลงกรณ์มหาวิทยาลัย
CHULALONGKORN UNIVERSITY

VITA

NAME Kamonlatth Rodponthukwaji

DATE OF BIRTH 16 October 1989

PLACE OF BIRTH Bangkok

INSTITUTIONS ATTENDED Khon Kaen University
Kasetsart University
Chulalongkorn University

HOME ADDRESS 171/2127 Phahon Yothin Road, Khlong Thanon, Sai Mai,
Bangkok 10220

PUBLICATION Rodponthukwaji K., Wattanakit C*, Yutthalekha T.,
Assavapanumat S., Warakulwit C., Wannapakdee W.,
Limtrakul J. “Catalytic upgrading of carboxylic acids as bio-
oil models over hierarchical ZSM-5 obtained via an
organosilane approach” RSC Advances 2017, 7, 35581-
35589.

Yutthalekha T., Warakulwit C., Wattanakit C.,
Wannapakdee W., Rodponthukwaji K., Witoon T., Limtrakul
J.* “Hierarchical FAU-type zeolite nanosheets as green
and sustainable catalysts for benzylolation of toluene”
Journal of cleaner production 2017, 142,1244-1251